LAWRENCE
LIVERMORE
NATIONAL
LABORATORY

LLNL-TR-676279

Progress Report on FY15 Crystalline Experiments M4FT-15LL0807052

M. Zavarin, P. Zhao, C. Joseph, J. Begg, Z. Dai, A. B. Kersting

August 13, 2015

Disclaimer

This work performed under the auspices of the U.S. Department of Energy by Lawrence Livermore National Laboratory under Contract DE-AC52-07NA27344.

July 15, 2015

Progress Report on FY15 Crystalline Experiments M4FT-15LL0807052

Mavrik Zavarin, Pihong Zhao, Claudia Joseph, James Begg, Zurong Dai, and Annie B. Kersting

Glenn T. Seaborg Institute, Physical & Life Sciences, Lawrence Livermore National Laboratory, 7000 East Avenue, Livermore, CA 94550, USA.

DISCLAIMER

Contents

1. INTRODUCTION

This progress report (M4FT-15LL0807052) summarizes research conducted at Lawrence Livermore National Laboratory (LLNL) as part of LLNL's crystalline generic repository effort within the Used Fuel Disposition (UFD) program (FT-15LL080705). It also includes international collaboration efforts (FT-15LL080706) and overlapping efforts with the argillite generic repository effort (FT-15LL080606). In the following sections, we summarize the results of three multi-year research efforts:

- Dissolution of plutonium intrinsic colloids in the presence of clay and as a function of temperature
- Long-term diffusion of U(VI) in bentonite: Dependence on density
- Plutonium sorption and desorption behavior on bentonite

The first two efforts are included herein as draft manuscripts prepared for journal submission later this fiscal year. The third effort was published earlier this fiscal year (Begg et al., 2015). These three efforts are focused on understanding the mechanisms controlling radionuclide transport in underground nuclear waste repositories. Transport of plutonium is likely to be limited to colloid-facilitated transport. Thus, the stability of Pu as an intrinsic colloid and as a pseudo-colloid was investigated. Radionuclide retardation in bentonite backfill material and in argillic repositories will likely be controlled by a combination of diffusion and sorption in clay. Thus, we investigated the diffusive behavior of U(VI). A unique aspect of our diffusion experiments is that these experiments were performed over a timescale of years rather than the more typical experimental timescale of weeks. As a result, we were able to capture long-term diffusive transport behavior and compare it to shorter timescale results from the literature. Long-term experiments are likely to yield diffusion results that are more representative of the repository performance timescales included in Performance Assessment models.

Our conceptual understanding of colloid-facilitated actinide transport has improved substantially over the past years. The next steps in our research will include (1) the parameterization of our conceptual model for use in reactive transport and Performance Assessment models and (2) the testing of our conceptual understanding under conditions that are representative of the generic repository scenarios proposed by the Used Fuel Disposition program. The result of these efforts will be a numerical model of colloid-facilitated transport that can be used to assess the impact of colloids on radionuclide migration and the associated performance of various repository scenarios.

2. DISSOLUTION OF PLUTONIUM INTRINSIC COLLOIDS IN THE PRESENCE OF CLAY AND AS A FUNCTION OF TEMPERATURE

2.1 Abstract

Colloid-facilitated plutonium transport is expected to be the dominant mechanism in its migration through the environment. The forms of Pu colloids (intrinsic versus pseudo-colloid) and their stabilities control temporal and spatial scales of Pu transport in the environment. In the present study, we examine the stability of Pu intrinsic colloids freshly prepared in alkaline solution relative to Pu-montmorillonite pseudo-colloids using a dialysis device and modeling approaches. Intrinsic colloids prepared under alkaline conditions were found to be unstable over a timescale of months. The kinetics of multiple processes, including hydrolysis/precipitation of Pu(IV), dissolution of intrinsic colloids in the absence and presence of the clay colloids, transport of dissolved Pu species across the dialysis membrane, and formation of pseudo-colloids were examined. The dissolution of intrinsic colloids was the rate-limiting process in most cases. The apparent intrinsic colloid dissolution rate constants range from 6×10^{-7} to 1×10^{-6} mol·m^{-2}·day^{-1} and 4×10^{-6} to 8×10^{-6} mol·m^{-2}·day^{-1} at 25 and 80°C, respectively, while the apparent diffusion rate constants for Pu ions crossing the dialysis membrane are >200 times higher. Elevated temperatures enhance dissolution of Pu colloids and the activation energy for the process is estimated to be 28 kJ mol^{-1}. The sorption of Pu to montmorillonite appears to be endothermic as the affinity of Pu for the clay increases with increasing temperature. Our results provide an in-depth understanding of how intrinsic and pseudo-colloids interact with each other kinetically. Although the fact that intrinsic colloids tend to dissolve in the presence of montmorillonite and transform into pseudo-colloids may limit the migration of intrinsic colloids, the thermodynamically more stable pseudo-colloids may play an important role in Pu transport in the environment over significant temporal and spatial scales.

2.2 Introduction

The large volumes of plutonium (Pu) designated for storage in high-level nuclear waste repositories are predicted to impact repository performance under certain scenarios (Kaszuba and Runde, 1999; Management, 2002). The dissolution of Pu in the waste forms will likely control the release of Pu to the environment as intrinsic or pseudo-colloids (Kersting, 2013; Walther and Denecke, 2013). Colloid facilitated Pu transport has been reported on the scale of kilometers at sites both in the US (Kersting et al., 1999; Santschi et al., 2002) and Russia (Novikov et al., 2006). Despite the recognized importance of colloid-facilitated Pu transport, geochemical and biochemical mechanisms controlling Pu colloid formation and stability over the range of concentrations expected in the environment have not been identified. In particular, kinetic information under environmental conditions is lacking. The temperature in the vicinity of radiological waste packages is expected to be elevated over an extended time period. Thus, understanding Pu behavior at elevated temperatures is necessary. The paucity of thermodynamic and kinetic data regarding temperature dependence limits the efficacy of current transport model predictions (Altmaier et al., 2013; Rao et al., 2011; Zavarin et al., 2014).

Pu can be associated with the colloidal fraction of groundwater in two forms. Pu can either form an intrinsic colloid or sorb to existing mineral, organic, or microbial colloids to form pseudo-colloids. At high concentrations where the solubility product is exceeded, Pu will precipitate and form Pu intrinsic colloids and precipitates (Neck et al., 2007c; Neck and Kim, 2001). Transport of Pu intrinsic colloids is controlled by its stability (both physical and chemical). At low concentrations, Pu will sorb onto inorganic or organic colloids, resulting in the formation of pseudo-colloids. Transport of Pu pseudo-colloids is determined by the Pu sorption/desorption kinetics. Both forms of Pu colloids may exist simultaneously under some subsurface conditions.

The identity of naturally occurring mineral colloids will be a function of the host rock mineralogy. Among the most ubiquitous mineral colloids are aluminosilicate clays that are commonly observed as mobile colloids due to their inherently small particle size and prevalence as alteration minerals from original host rock material (Kersting et al., 1999). Clays are known to sorb Pu (Begg et al., 2013; Bertetti et al., 1998; Keeney-Kennicutt and Morse, 1985; Kozai et al., 1996; Kozai et al., 1993; Lujaniene et al., 2007; Powell et al., 2004; Powell et al., 2005; Powell et al., 2008; Sabodina et al., 2006; Sanchez et al., 1985; Turner et al., 1998). The proposed use of bentonite within some engineered barrier system scenarios for high-level nuclear waste repositories provides additional importance to understanding Pu interaction with aluminosilicate clays (Sabodina et al., 2006). Aluminosilicate clays may represent a key phase that will control transport of Pu pseudo-colloids in repository near and far fields.

Batch sorption has been the most common method used to measure the affinity of a contaminant for a mineral surface. Data obtained from a conventional sorption experiment are the concentrations of the contaminant in the liquid phase before and after sorption. Filtration and/or centrifugation are used to separate solids from liquid after equilibrium is reached. The quantity sorbed is calculated based on the difference of the total and aqueous concentrations. However, if the contaminant is involved in multiple processes (i.e., sorption, colloids formation and/or precipitation), these individual processes cannot isolated or identified from the batch sorption data alone.

In order to distinguish between precipitated, colloidal, and sorbed species, we employed dialysis membranes to segregate intrinsic colloids from pseudo-colloids. Dialysis membranes are commonly used to separate suspended solutes or particles of different dimensions in a liquid mixture. Desirable size separation by dialysis can be achieved by selecting an appropriate membrane pore-size molecular weight cutoff (MWCO). Membrane pore sizes of ≤5 kilo Daltons (kDa) (approximately equivalent to ≤2 nm) can provide reasonable separation of aqueous and colloidal species. In the present study, we examined the stability of Pu intrinsic colloids relative to pseudo-colloids using a novel experimental design and modeling approaches. We employed dialysis membranes to segregate intrinsic colloids (2~5 nm) from montmorillonite colloids (>100 nm) and allow aqueous Pu to interact with both colloidal phases. Using the dialysis membrane approach, we monitored the dissolution of intrinsic colloids in the absence and presence of montmorillonite. The data provide new insights into the stability of intrinsic colloids in the presence of clay at 25 and 80°C.

2.3 Materials and Methods

2.3.1 Pu Stock and Intrinsic Colloid Preparation

All reagents were of analytical grade or better and used as received. De-ionized water from a Barnstead Milli‑Q (MQ) water purification system (18.2 MΩ cm) was used for all procedures and solution preparation. Pu stock solutions with two different Pu isotopic ratios were used. A relatively pure alpha-emitting ^{238}Pu stock solution was used in low and intermediate Pu concentration experiments. The ^{238}Pu, ^{239}Pu, ^{240}Pu, and ^{241}Pu mass percent in the stock was 76.8%, 21.0%, 2.0%, and 0.14%, respectively. The major isotope contributing to alpha activity in this stock was ^{238}Pu (~99.9% by activity). The second Pu stock solution, used in the high Pu concentration experiments, was a ^{242}Pu solution spiked with ~1% of the ^{238}Pu stock. The ^{238}Pu, ^{239}Pu, ^{240}Pu, ^{241}Pu, and ^{242}Pu mass percent in this stock was 0.75%, 0.21%, 0.13%, 0.04%, and 98.87%, respectively. The major isotopes contributing to alpha activity in this stock were ^{238}Pu (96.8%) and ^{242}Pu (2.9%). Both Pu stock solutions were purified using AG®1×8 100-200 mesh anion exchange resin from Bio-Rad Laboratories, and filtered through an Amicon Ultra 0.5 mL centrifugal filter with membrane MWCO of 3 kDa (EMD Millipore). The oxidation state of Pu(IV) was confirmed using both UV-Vis and solvent extraction. The aqueous Pu(IV) starting solution was prepared by spiking the acidic stock solution into a pH 8 buffer solution (5 mM NaCl/0.7 mM $NaHCO_3$) and gradually adding microliters of NaOH (1 N or 6 N) to readjust the pH to 8. The Pu intrinsic colloids were

prepared by neutralizing the aqueous Pu(IV) stocks using NaOH and adjusting solution to pH 9-10. After aging for more than a week, the intrinsic colloids were centrifuged at an RCF of 9168 for 1 h and the supernatant removed. The intrinsic colloid particle size cut-off based on centrifugation was 14 nm. However, the average particle size of the intrinsic colloids was 30 nm and composed of aggregated PuO_2 crystallites ranging in size from 2.5 to 4.5 nm (Figure 1). An intrinsic colloid stock solution was prepared by re-suspending the intrinsic colloids in MQ water. The intrinsic colloid starting solutions were prepared by spiking the intrinsic colloid stock solution into a pH 8 buffer solution without further pH adjustment. Pu concentrations in samples were analyzed by a PerkinElmer Tri-Carb 2900TR Liquid Scintillation Analyzer. The fraction of aqueous Pu in the intrinsic colloid stock solution, based on 3 kDa MWCO, was 1 to 3%.

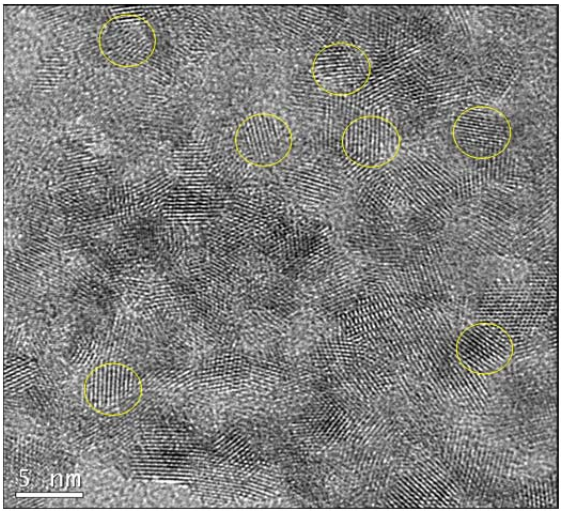

Figure 1. TEM image of PuO_2 intrinsic colloids. Several individual PuO_2 crystallites are highlighted by yellow circles. The measured average particle sizes was 3.5 nm with a range of 2.5-4.5 nm.

2.3.2 Montmorillonite

SWy-1 montmorillonite (Clay Minerals Society) was pre-treated using 1 mM HCl (to dissolve any carbonate minerals) followed by addition of 0.1% of H_2O_2 (to oxidize organic contaminants and reduced metals (e.g., Fe^{2+}). The pre-treated montmorillonite was centrifuged to remove excess liquid, and the wet paste was transferred to a 6 to 8 kDa MWCO dialysis tube suspended in 0.01 M NaCl solution to produce a homoionic Na-montmorillonite. The clay minerals were dialyzed for seven days, and the NaCl solution was changed at least once per day. The clay minerals were then suspended in MQ water and centrifuged to obtain particle sizes from 50 nm to 2 μm. The wet solids were dried at 40°C until a constant weight was obtained. A stock montmorillonite suspension was made by mixing 4 g of dried montmorillonite in 400 mL of pH 8 buffer solution (10 g L^{-1}). Quadrasorb SI surface area analyzer (QuantaChrome Instruments) was used for BET measurements. The surface area of montmorillonite measured by N_2(g)-BET was 31.5 ± 0.2 m^2 g^{-1}, which is comparable to the reported value of 31.8 m^2 g^{-1} (Clay Minerals Society).

2.3.3. Dissolution Experiments

Intrinsic colloid stability was evaluated using the experimental design shown in Figure 2. Briefly, intrinsic colloids are placed inside the dialysis bag, while the clay colloids are placed outside the dialysis

bag. Thus, the colloidal montmorillonite is isolated from the intrinsic colloids while exchange of truly aqueous (non-colloidal) ions between both solid phases is permitted. Pu detected outside the dialysis bag over time represents dissolved Pu species that diffused across the dialysis membrane. In the presence of montmorillonite, the dissolved Pu can either remain in solution or sorb to montmorillonite. The dissolution rate of intrinsic colloids is expected to be a function of its solubility, surface area, solution composition, pH and temperature. The sorption rate of Pu to montmorillonite is affected by similar processes.

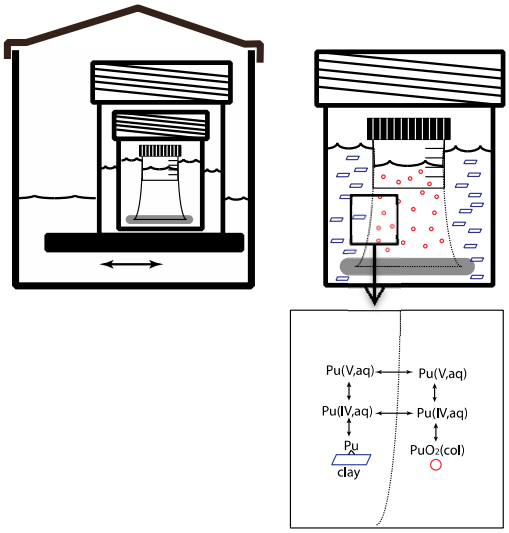

Figure 2. Experimental design using dialysis membrane to separate Pu intrinsic colloids (placed inside dialysis tubing) from mineral colloids (placed outside the tubing). For Pu-montmorillonite sorption to occur, intrinsic colloids must dissolve and diffuse through the membrane.

A total of 16 experiments (excluding a control blank) were performed to test the experimental design and quantify dissolution of intrinsic colloids in the presence of montmorillonite. The dialysis membrane used was Spectra/Por® 7 standard RC pre-treated dialysis tubing with a MWCO of 1 kDa (Spectrum Laboratories, Inc). The experiments were performed at two temperatures, 25°C (8 experiments) and 80°C (8 experiments) to evaluate the effect of temperature. At each temperature, Pu was added either as an aqueous species (to test simple diffusion and sorption of Pu) or as an intrinsic colloid (to test intrinsic colloid dissolution, diffusion and sorption of Pu). The initial Pu concentrations bracketed the PuO_2(am, hyd) solubility (~5×10^{-9} M) (Neck et al., 2007c). In addition, montmorillonite-free solutions (spiked blanks) with initial Pu concentrations below and near PuO_2(am, hyd) solubility were used to compare with sorption experiments and evaluate Pu loss to container walls and dialysis membranes.

All experiments were conducted in 450 mL Teflon jars with air-tight closures. 225 mL of pH 8 buffer solution was mixed with 25 mL of montmorillonite stock suspension to yield 250 mL of a 1 g L^{-1} montmorillonite suspension. A sealed dialysis tubing containing 30 mL of either aqueous Pu or intrinsic colloids was then placed in the 250 mL pH buffer solution with or without montmorillonite. The 450 mL Teflon jars were submerged in 1 L Teflon containers filled with MQ water to minimize evaporative losses and provide secondary containment to the radioactive samples. Over the course of the experiment, the 25°C samples were placed on a top-loading orbital shaker, and the 80°C samples were submerged in an

Innova 3100 water bath shaker (New Brunswick Scientific). All samples were shaken at an orbital speed of 100 rpm during experiments.

Each experiment was sampled as a function of time over a three-month period. At each sampling interval, aliquots of the montmorillonite suspension were collected, centrifuged and analyzed for total Pu, supernatant Pu, and solution pH. Alternatively, aqueous Pu was determined by measuring the filtrate Pu concentration after filtering the suspension through 3kDa MWCO centrifugal filters. The montmorillonite concentration in the suspension was also measured based on light scattering at a wavelength range of 300−500 nm using a Cary 500 Scan UV-Vis-NIR spectrophotometer (Varian). The pH of the clay suspension was monitored and maintained at pH 8 ± 0.5 at all times.

2.4 Results and Discussion

2.4.1 Kinetics

The formation of Pu-montmorillonite pseudo-colloids in this system involves a series of processes including intrinsic colloid dissolution, Pu(IV)/Pu(V) redox reactions, aqueous Pu diffusion, and sorption. Some of the processes are parallel and others are sequential. To simplify the kinetics comparison, we focus on the essential processes, which follow a sequential order: Pu intrinsic colloids dissolve to produce aqueous Pu inside the dialysis membrane (Eq. 1); the aqueous Pu is transported across the membrane (Eq. 2), and aqueous Pu sorbs onto clay that is placed outside of the dialysis membrane (Eq. 3)

$$PuO_2(s)\,|\,inside \xrightarrow{k_1} Pu(aq)\,|\,inside \quad (1)$$

$$Pu(aq)\,|\,inside \xrightarrow{k_2} Pu(aq)\,|\,outside \quad (2)$$

$$Pu(aq) + clay\,|\,outside \xrightleftharpoons{K,k_3,k_{-3}} Pu-clay\,|\,outside \quad (3)$$

where k_1 and k_2 represent apparent kinetic constants, $K = k_3/k_{-3}$ is the sorption equilibrium constant, and k_3 and k_{-3} are the sorption and desorption rate constants.

A pseudo 1st order reaction model was used for all three reactions (i.e. rate constant units of d^{-1}). As a result, kinetic rate constants can be compared directly to determine the rate limiting step. However, it should be noted that a true dissolution rate constant is typically normalized to surface area. Similarly, k_2 reflects the apparent diffusion coefficient of Pu under these experimental conditions, including the configuration/dimensions of the dialysis systems, the number of membrane pores and their sizes, and shaker speed used in the experiments. Thus, the apparent diffusion coefficient is not intended to reflect the true diffusivity in water. Aqueous Pu and intrinsic colloid experiments allow us to determine k_1 and k_2. By analyzing concentrations of total and aqueous Pu in the clay suspension, we can also obtain the equilibrium constant K.

2.4.2 Apparent Diffusion in the System

To determine the rates of apparent diffusion in our experiments, ^3H and aqueous Pu(V) were placed inside a dialysis bag and the solution outside dialysis bag was sampled as a function of time and monitored for Pu and ^3H (i.e. Eq. 2). The concentrations of ^3H or Pu inside the dialysis bag as a function of time can be described by

$$\frac{dC_{in}}{dt} = -k_2(C_{in} - C_{out}) \quad (4)$$

where C_{in} and C_{out} are ^{3}H or Pu concentrations (in mol L^{-1}) inside and outside of the dialysis bag, respectively, and k_2 is the rate constant for diffusion across the dialysis membrane. Assuming C_{out}=0 at t=0, the ^{3}H or Pu concentration outside of the dialysis bag can be described by

$$C_{out} = (C_{in}^{o} - C_{in}) * \frac{V_{in}}{V_{out}} \quad (5)$$

where V_{in} and V_{out} (L) are the solution volumes inside and outside of dialysis bag and C_{in}^{0} is the concentration (mol L^{-1}) inside the dialysis bag at time zero. Combining Eq. 4 and 5 and integrating leads to the following equation

$$C_{in} = C_{in}^{o}\left(\frac{V_{in}}{V_{in}+V_{out}}\right) + \mathrm{Ae}^{-k_2\left(\frac{V_{in}+V_{out}}{V_{out}}\right)t}. \quad (6)$$

Replacing C_{in} in Eq. 5 with Eq. 6, rearranging the terms, and assuming that C_{out}=0 at t=0 and C_{out} = $C_{in}\times V_{in}/(V_{in}+V_{out})$ at $t\rightarrow\infty$, we obtain:

$$C_{out} = \frac{V_{in}}{V_{out}+V_{in}} C_{in}^{o}\left[1 - e^{-k_2^{*}t}\right] \quad (7)$$

where k_2* is the apparent diffusion rate constant (d^{-1}).

The data obtained from diffusion experiments are plotted in Fig. 3. The fitted rate constant was 40 d^{-1} for tritium at both temperatures. The fitted rate constant for Pu(V) at 25°C was 25 day^{-1}. At 80°C, the short term (<0.1 d) Pu(V) data was fit to a rate constant of 30 d^{-1}. However, Pu concentrations decreased at later times. The decrease may reflect slow sorption to container walls, sorption to the dialysis membrane, and/or oxidation/reduction of Pu(V). All fitted rate constants are listed in Table 2. The fitted rate constants indicate that diffusion of aqueous species across the dialysis membrane will occur on time scale of <<1 day.

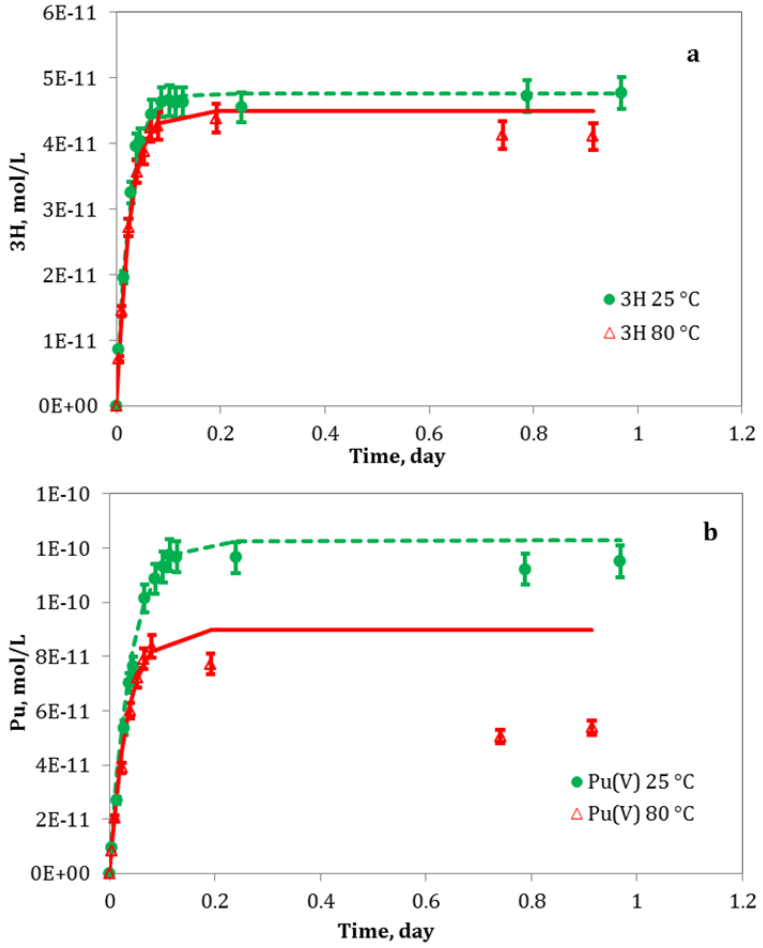

Figure 3. Diffusion of (a) ^{3}H and (b) Pu(V) as function of time at 25°C and 80°C and associated diffusion model fits.

Table 1. Experimental conditions and fitted apparent diffusion rate constants for Pu(V) and ^{3}H diffusion experiments.

Expt	T	Pu(V)	^{3}H	k_2
	°C	---- mol L^{-1} ---		d^{-1}
1	25	1.2E-9	4.4E-10	25,40*
2	80	1.2E-9	4.4E-10	30,40*

* Pu(V) and ^{3}H rate constants, respectively.
* V_{in} = 30 mL, V_{out} = 250 mL

2.4.3 Kinetics of Intrinsic Colloid Dissolution

In these experiments (Table 2), intrinsic Pu colloids were placed inside the dialysis bag, which was suspended in a clay suspension. The clay suspension was sampled as a function of time and the concentration of total and aqueous Pu was monitored. If the total Pu concentration in the clay suspension is used to evaluate the system (assuming Pu sorption to montmorillonite is an equilibrium process), then the system can be approximated by a simple chain reaction of first order rate laws. The rate law for mineral dissolution can be described by the following equation (Maher et al., 2006)

$$R = k_{dis} \cdot A \cdot \beta(a) \cdot f(\Delta G) \quad (8)$$

where k_{dis} is the rate constant in mol m^{-2} s^{-1}, A (in m^2) is the mineral surface area in contact with the aqueous solution. $\beta(a)$ is a function of various factors (e.g., pH, inhibitors or catalysts) that affect the dissolution. $f(\Delta G)$ is a dependence of rate on Gibbs free energy ΔG. In our experiments, the surface area A is proportional to PuO_2 colloids concentration in the dialysis bag: $A = C_{in}^0 V_{in} SSA$. The value of 4×10^4 m^2/mol used for the specific surface area (SSA) is calculated using an average particle size of 3.5 nm and density of 11.5 g/cm^3 for the PuO_2 colloids.

For the sake of simplicity and direct comparison between dissolution of PuO_2 colloids and diffusion of aqueous species, we used 1st order reactions for both Pu colloid dissolution and diffusion. If the kinetics can be described as two first order chain reactions, the Pu concentration in montmorillonite suspension is governed by the following equation (Lasaga, 1998):

$$C_{out} = \frac{V_{in}}{V_{out}+V_{in}} C_{in}^{o} \left[1 + \frac{k_1 \exp(-k_2 t) - k_2 \exp(-k_1 t)}{k_2 - k_1}\right] \quad (9)$$

where C_{out} in mol L^{-1} represents the total Pu concentration in clay suspension as a function of time (t, d), k_1 and k_2 (d^{-1}) are apparent rate constants of dissolution and diffusion processes, respectively. In the case where rate constants k_1 and k_2 differ by orders of magnitude, the rate-limiting process can be identified and the model further simplified to a first order rate model. The experimental data are plotted in Figure 4 and the fitted first order rate constants are summarized in Table 2. The first order rate constants for the dissolution of intrinsic colloids ranged from 0.025-0.40 d^{-1} at 25°C and 0.15-0.30 d^{-1} at 80°C, one to two orders of magnitude lower than the rate constants determined in the diffusion experiments. Thus, it appears that intrinsic colloid dissolution is the rate-limiting step.

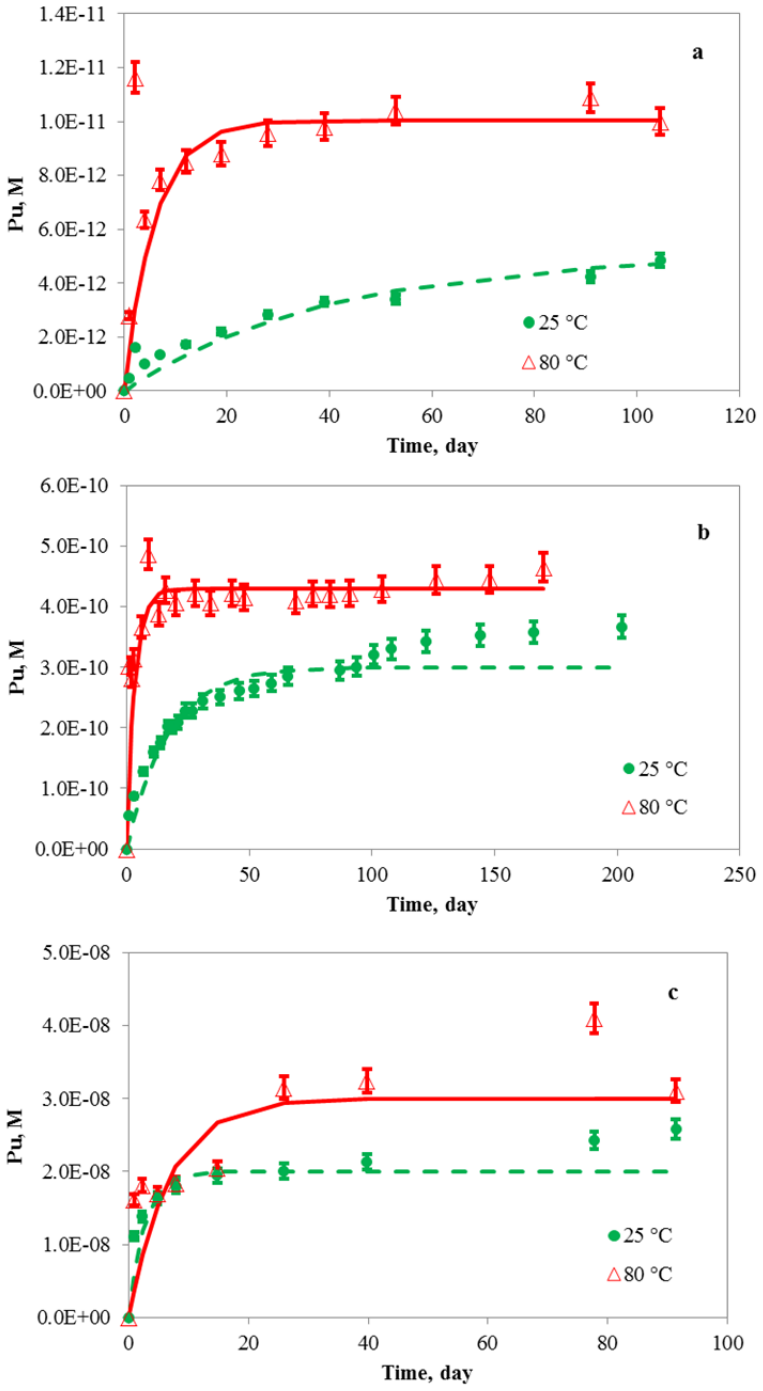

Figure 4. Dissolution and diffusion of Pu colloids in the presence of clay at 25 and 80°C. Lines are fitted curves using psuedo1st order reaction model. Initial Pu colloids concentrations were 1.1×10^{-10} mol L^{-1} (4a), 8.3×10^{-9} mol L^{-1} (4b), and 1.9×10^{-6} mol L^{-1} (4c).

Table 2. Experimental conditions and fitted apparent diffusion rate constants for Pu intrinsic colloid/montmorillonite experiments.

Expt	Temp	Pu coll.	k_1	k_s	Pu in clay
	°C	mol L^{-1}	d^{-1}	mol m^{-2} s^{-} $_1$	%
1	25	1.1E-10	0.025	7.2E-12	45
2		8.3E-9	0.06	1.7E-11	33
3		1.9E-6	0.4	1.1E-10	10
4	80	1.1E-10	0.17	4.9E-11	88
5		5.7E-9	0.3	8.6E-11	70
6		1.9E-6	0.15	4.3E-11	15

* Vin = 30 mL, Vout = 250 mL, 1 g/L montmorillonite

The surface area normalized dissolution rate constant, k_s (mol m^{-2} s^{-1}), can be calculated using the following equation:

$$k_s = \frac{k_1}{SSA} \quad (10)$$

Furthermore, the lifetime of PuO_2 colloids can be estimated using (Lasaga, 1998):

$$t_{lifetime} = \frac{r_o}{k_s \bar{V}} \quad (11)$$

where r_o is the initial average radius of PuO_2 (1.75 nm) and $\bar{V}$is the molar volume of the colloids. The logk_s (mol m^{-2} s^{-1}) values obtained in these experiments were -10 to -11 which results in a lifetime range of <1 to 4 months. The logk_s of montmorillonite is in the range of -14 to -18 (Golubev et al., 2006; Huertas et al., 2001; Rozalén et al., 2009; Rozalén et al., 2008). These lower dissolution rates combined with their much larger particle sizes, lead to much longer lifetimes (thousands to millions of years). However, the lifetime of Pu on these montmorillonite colloids is not known.

In a heterogeneous system and at constant pressure and temperature, the overall dissolution rate of a metal oxide can be described as the sum of the rates of proton-promoted, hydroxide-promoted, ligand-promoted and reductant or oxidant-promoted (if appropriate) dissolution. In other words, the dissolution rate is actually the sum of all the parallel dissolution rates of different metal centers (Afonso and Stumm, 1992; Hocsman et al., 2006; Kohler et al., 2003; Lasaga and Luttge, 2004; Stumm, 1997). We cannot distinguish between these processes here. However, the dissolution rate clearly increases with the intrinsic Pu colloid concentration, as would be expected for a surface-controlled dissolution process.

In the high intrinsic colloid concentration samples, the overall rates may have decreased significantly towards to the end of experiments as the system approached equilibrium (Lasaga, 1981; Lasaga and Luttge, 2004). The impact of solution saturation can explain the decrease in kinetic constant obtained in the highest Pu concentration experiment at 80°C (Table 2).

2.4.4 Sorption Kinetics in the Aqueous Pu(IV)-Montmorillonite System

Four experiments were performed using aqueous Pu(IV) in the presence of montmorillonite (Table 3). The purpose of these experiments was to investigate Pu speciation effects on diffusion. The experimental data are plotted along with fitting curves in Figure 5. The fast rates (30 d^{-1}) observed at 25°C suggest that these experiments were diffusion controlled. However, the rate constants obtained from the 80°C experiments were much lower (0.15-0.2 d^{-1}) and similar to those obtained from intrinsic colloid experiments. In fact, these rate constants are 200 times slower than that observed at 25°C. This suggests that aqueous Pu(IV) species hydrolyzed to form intrinsic Pu colloids or PuO_2 solids at 80°C. Once these intrinsic Pu colloids formed inside the dialysis bag, they slowly dissolved and diffused across the membrane. The intrinsic colloids dissolution was thermodynamically controlled. Hydrolysis of Pu(IV) is endothermic and, as a result, high temperatures will favor the formation of intrinsic Pu colloids (Cleveland, 1979). In addition, the ionization constant of water, K_w, increases with temperature which can lead to a 30 × increase in hydroxide concentration at pH 8 between 25 and 80°C. This will also enhance Pu(IV) hydrolysis. Endothermic hydrolysis behavior of aqueous Pu and other actinide species has been reported in numerous studies (Altmaier et al., 2013; Rao et al., 2004; Rao et al., 2011; Runde et al., 2002b).

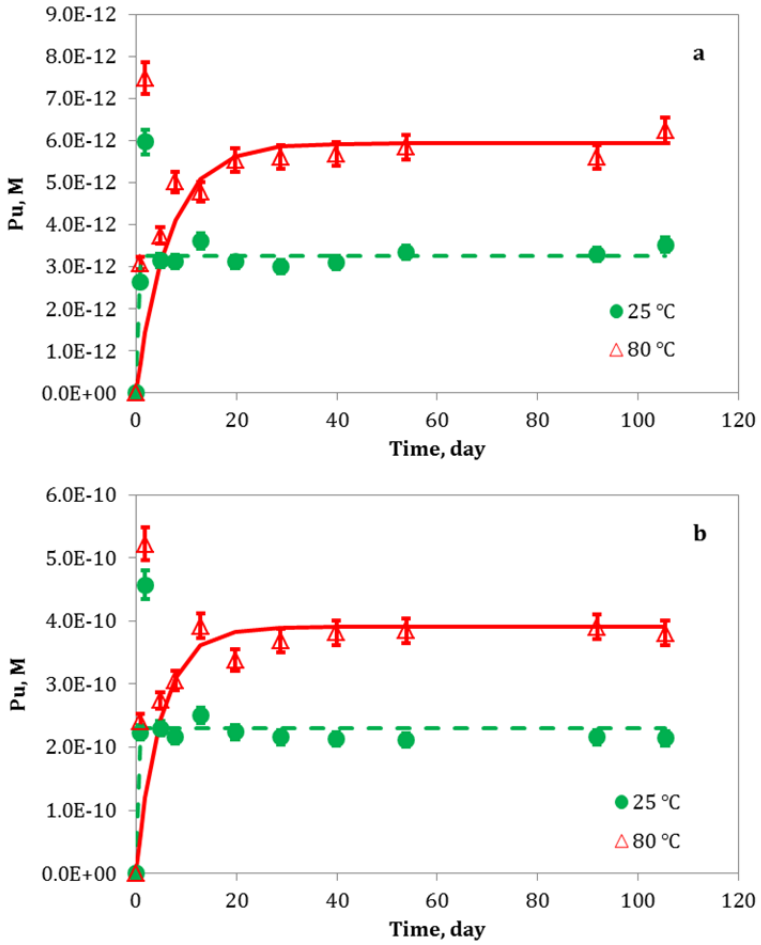

Figure 5. Kinetics of the aqueous Pu(IV)-montmorillonite system at 25 and 80°C. Lines are fitted curves using psuedo1st order kinetic model. Initial Pu concentrations of 5.5×10^{-11} mol L^{-1} (5a) and 5.8×10^{-9} mol L^{-1} (5b).

Table 3. Experimental conditions and fitted apparent diffusion rate constants for aqueous Pu(IV)-montmorillonite experiments.

Expt	Temp °C	Pu(IV),aq mol L^{-1}	k_1 d^{-1}	k_2 d^{-1}	k_s mol m^{-2} s^{-1}	Pu in clay %
1	25	5.5E-11		30		55
2		5.8E-9		30		37
3	80	5.5E-11	0.15		4.3E-11	100
4		5.8E-9	0.2		5.7E-11	63

* Vin = 30 mL, Vout = 250 mL, 1 g/L montmorillonite

2.4.5 Kinetics in the Absence of Montmorillonite

Four experiments using both intrinsic colloids and aqueous Pu(IV) were performed in the absence of montmorillonite. These experiments served as control experiments to evaluate the sorption of Pu to the

container walls, dialysis membrane and other materials. The experimental data are plotted along with fitting curves in Figure. 6. At 25°C, Pu concentrations in the solution outside of the dialysis bag were initially higher than at 80 °C, and then decreased over time, indicating there was significant sorption to the dialysis bag and/or container wall over time. To first order, the processes in this system can be described as a 1st order diffusion/dissolution reaction followed by a rate limited sorption reaction:

$$Pu \,|\, inside \xrightarrow{k} Pu \,|\, outside \quad (12)$$

$$Pu + memberane \,|\, outside \overset{K,\, k_3, k_{-3}}{\Longleftrightarrow} Pu - memberane \,|\, outside \quad (13)$$

The Pu concentration outside of the dialysis bag as a function of time is governed by (Lasaga, 1998):

$$C_{out} = \frac{V_{in}}{V_{out}} C_{in}^{o} \left[1 - \exp(-kt) - \frac{k_3}{k_3 + k_{-3}} \left(1 + \frac{k * \exp(-(k_3 + k_{-3})t) - (k_3 + k_{-3})\exp(-kt)}{k_3 + k_{-3} - k}\right)\right] \quad (14)$$

where k represents kinetic constant of either PuO_2 dissolution or aqueous Pu(aq) diffusion across the membrane; $K = k_3/k_{-3}$ is the sorption equilibrium constant, and k_3 and k_{-3} are the sorption and desorption rate constants.

Table 4 lists the curve fitting results and shows that rate constants are consistent with the ones obtained from dissolution or diffusion experiments depending upon Pu initial speciation and experimental temperatures. In the intrinsic colloid system, rate constants were 0.06 and 0.3 day^{-1} for experiments performed at 25 and 80°C, respectively. These values match k_1 values obtained in the intrinsic colloid-montmorillonite experiments, suggesting that kinetics were again governed by PuO_2 dissolution. In the aqueous Pu(IV) experiments, the rates constants were 30 and 0.3 d^{-1} in the 25 and 80°C experiments, respectively. The 30 d^{-1} rate constant matches aqueous Pu(IV) diffusion rate constants, indicating that the diffusion process was controlling the system. Thus, we can conclude that the presence of clay impacts neither diffusion rates of Pu species nor dissolution rates of intrinsic Pu colloids. At elevated temperature, the 0.3 day^{-1} rate constant matches those obtained from intrinsic Pu colloid dissolutions experiments with or without clay, suggesting that aqueous Pu(IV) underwent fast hydrolysis to form intrinsic Pu colloids, whose dissolution became a rate-limiting step governing the observed kinetics. Although the presence of clay doesn't affect the kinetics of these systems, it stabilizes Pu and increased the total amount of Pu on the outside of the dialysis membrane.

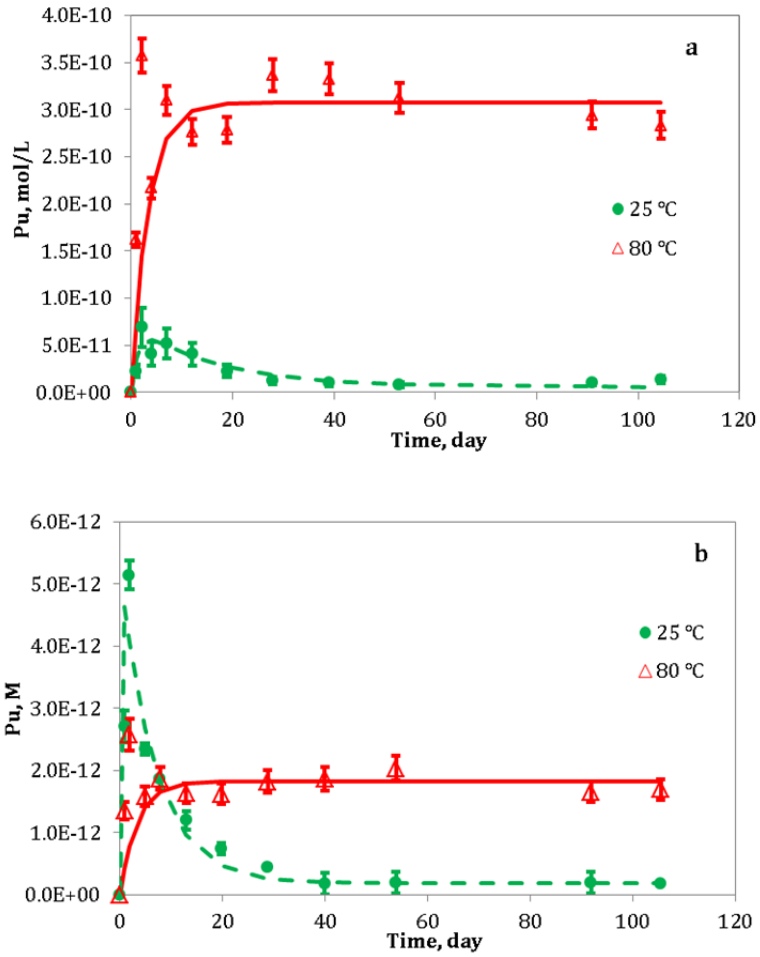

Figure 6. Pu concentrations outside the dialysis membrane for intrinsic colloid and aqueous Pu(IV) experiments in the absence of montmorillonite at 25 and 80°C. Lines are fitted curves using kinetics model pseudo 1st order dissolution/diffusion and rate-limited sorption/desorption. Intrinsic colloid (6a) and aqueous Pu(IV) (6b).

Table 4. Experimental conditions and fitted apparent diffusion rate constants for intrinsic colloids and aqueous Pu(IV) experiments in the absence of montmorillonite.

Temp	Pu intrinsic colloids	Pu(IV, aq)	k	k_3	k_{-3}	$K = k_3/k_{-3}$	Pu in clay suspension
°C	--- mol L^{-1} ---		-------- d^{-1} --------				%
25	7.8E-9		0.06	0.8	0.005	160	2
80	7.8E-9		0.3	20	0.8	25	35
25		5.5E-11	30	0.14	0.005	28	3
80		5.5E-11	0.3	0.002	0.03	0.007	28

* Vin = 30 mL, Vout = 225 mL.

2.4.6 Dependence on Temperature

High temperature can enhance Pu(IV) hydrolysis as the process is endothermic (Altmaier et al., 2013; Cleveland, 1979). In addition, a significant increase in water ionization due to a decrease in pK_w (~12.5) at 80°C also drives reaction towards Pu(IV) hydrolysis. As a result, the solubility of Pu colloids under our experimental conditions appeared to decrease at higher temperature. Pu(IV) solubility decreasing in J-13 and UE-25p #1 groundwaters in the vicinity of Yucca Mountain, NV at elevated temperatures has also been reported despite possible existence of higher oxidation states of Pu(V, VI) and/or multi solid phases controlling Pu solubility (Efurd et al., 1998; Nitsche et al., 1993; Nitsche et al., 1994; Runde et al., 2002b).

In general, the dissolution of a solid in an aqueous solution contains two essential steps: the chemical reactions occurring at the solid surface and the transport of dissolved species to and from the surface. The kinetics of the dissolution can be controlled by surface chemical reactions, transport of soluble species to and from the surface, or a combination of both processes (Berner, 1981). The values of the dissolution activation energy (E_a) not only provide important temperature dependence of the rates, but also offer important clues to the dissolution mechanisms. Transport-controlled processes in fluid media typically are associated with diffusion activation energies, whose E_a values are of <21 kJ mol^{-1}. The processes controlled by chemical reactions on solid surfaces would have values of E_a> 42 kJ mol^{-1} due to the involvement of breaking bonds in crystals (Lasaga, 1998). However, it has been observed that most of the activation energies (E_a) for wide variety of mineral dissolutions/alteration processes lie in the intermediate range 21-42 kJ mol^{-1}, suggesting that their dissolution was controlled by both mass transport and surface reactions (Hocsman et al., 2006). It is also possible that the catalytic effect of adsorption on surfaces or surface defects may reduce the activation energies to this intermediate energy range (Lasaga and Gibbs, 1990; Xiao and Lasaga, 1994).

The temperature dependence of rate constant is often assumed to follow the Arrhenius equation:

$$k_1 = \boldsymbol{A_{diss}}\, exp(-\frac{E_a}{RT}) \qquad (15)$$

The activation energy (*Ea*) can be calculated using rate constants at two different temperatures:

$$\ln\left[\frac{k_1(T_2)}{k_1(T_1)}\right] = -\frac{E_a}{R}(\frac{1}{T_2} - \frac{1}{T_1}) \qquad (16)$$

where A_{diss} is the pre-exponential factor, which is a constant for a given reaction, $k_1(T_1)$ and, $k_1(T_2)$ are the dissolution rate constant k_1 at absolute temperatures T_1 and T_2 in kelvin, respectively, E_a is the activation energy for the reaction in J mole^{-1}, and R = 8.314 J mol^{-1} K^{-1} is the gas constant.

We used k_1 values obtained from low Pu colloid concentration experiments, in which the systems were far from solution equilibrium, to calculate an apparent E_a. The average of apparent activation energy (E_a) for PuO_2 colloids dissolution process was 28 kJ mol^{-1}. This intermediate value may indicate that the dissolution process of intrinsic colloids is controlled by the combination of both surface reaction and mass transport at the surface (Hocsman et al., 2006). A theoretical generalization proposed by Berner (Berner, 1978; Berner, 1981) stated that dissolution of minerals with low solubility is more likely to be controlled by reactions at sites on the surface, whereas dissolutions of highly soluble minerals are controlled by material transport either from or to aqueous solution or through protective surface layers.

2.4.7 Temperature Dependence of Pu Sorption to Montmorillonite

The K_ds for Pu-montmorillonite can be calculated using the measured Pu activity on montmorillonite and in the supernatant. The resulting K_ds from various experiments are plotted in Figure 7. Many factors including Pu speciation, oxidation state, and temperature can impact K_ds. Generally, K_ds obtained from intrinsic colloid experiments tend to initially have lower values than those obtained from aqueous Pu(IV) experiments. However, K_ds from intrinsic colloid experiments tend to increase with time to approach values from aqueous Pu(IV) experiments. This phenomenon can be explained by the change in Pu oxidation states over time. Pu(V) is the predominant species formed as a result of intrinsic Pu colloid dissolution and this oxidation state exhibits a weaker sorption to clay relative to Pu(IV) (Altmaier et al., 2013; Begg et al., 2014; Neck et al., 2007a; Neck et al., 2007b). Over time, Pu(V) tends to reduce to Pu(IV) on the montmorillonite surface which leads to an increasing K_d (Begg et al., 2013). Figure 7 also shows that the K_d increases with increasing of temperature which implies that the sorption process is endothermic and that higher temperatures lead to greater Pu sorption to montmorillonite.

The van't Hoff equation as expressed in eq. 17 and Gibbs free energy as described in eq. 18 can be used to calculate the changes in enthalpy ($\Delta H°$, J mol^{-1}), entropy ($\Delta S°$, J mol^{-1} K^{-1}) and Gibbs free energy ($\Delta G°$, J mol^{-1}) of Pu-clay sorption at standard atmospheric pressure:

$$lnK_d = -\frac{\Delta H°}{RT} + \frac{\Delta S°}{R} \quad (17)$$

$$\Delta G° = \Delta H° - T\Delta S° \quad (18)$$

where T is the absolute temperature in kelvin and R = 8.314 J mol^{-1} K^{-1} is the gas constant.

The calculated thermodynamic parameters are summarized in Table 5. The positive value of $\Delta H°$ (38 kJ mol^{-1}) confirms the endothermic nature of the Pu-montmorillonite sorption, and negative values of $\Delta G°$ indicate that the sorption reaction is spontaneous. A more negative value of $\Delta G°$ obtained from elevated temperature confirms that the formed Pu pseudo-colloids are more stable at higher temperature. However, as described in the following paragraph, the thermodynamic parameters derived from these experiments are only approximate since redox conditions, pH, and Pu oxidation states were not strictly controlled.

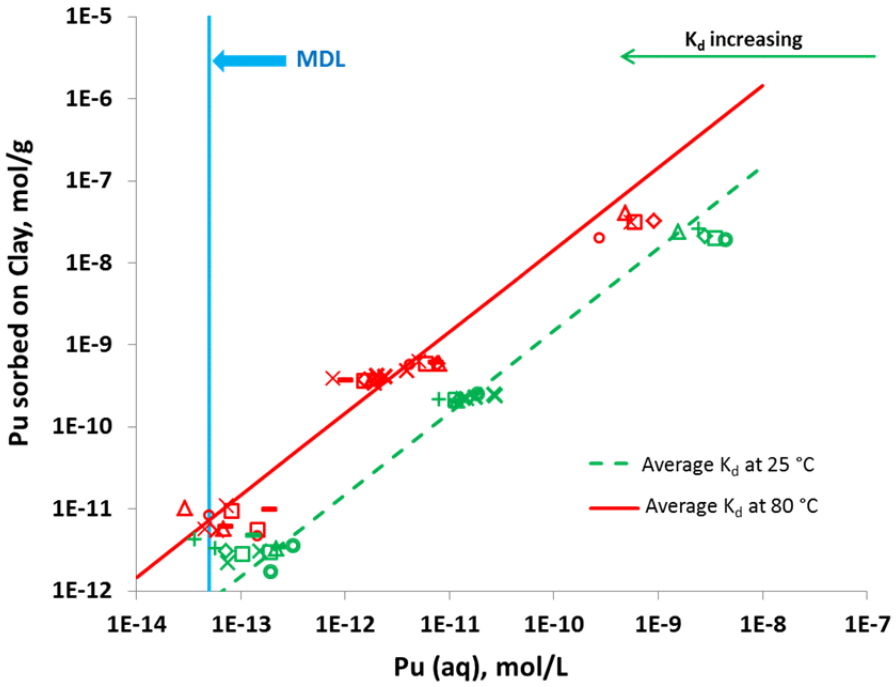

Figure 7. Pu-montmorillonite K_ds from intrinsic colloid and aqueous Pu(IV) experiments with montmorillonite at 25 and 80°C. Lines represent the average K_ds obtained from intrinsic colloid-montmorillonite and aqueous Pu(IV)-montmorillonite experiments.

At the termination of the experiments, Pu oxidation state distribution in the supernatants of both intrinsic colloid suspension and pseudo-colloid suspensions were analyzed using solvent extraction (Figure 8). We show that in the pseudo-colloid suspensions, higher oxidation states Pu(V) and Pu(VI) were the predominant aqueous species at 25°C, while Pu(IV) was more prevalent at 80°C (Figure 8a). This suggests that elevated temperatures led to more reducing solution conditions. This may, in part, explain the higher K_ds at 80°C. On the other hand, in the intrinsic colloid suspensions, Pu(IV) concentration was much higher at 25°C than that at 80°C. In the absence of clay, oxidizing Pu(IV) to higher oxidation states by oxygen in the air is enhanced at higher temperature. Although the Pu oxidation state distribution changed at different temperatures and colloidal solutions, and they made significant impact on the Pu sorption behavior, the processes controlling Pu speciation in solution or on mineral surface is not yet clear and requires further investigation.

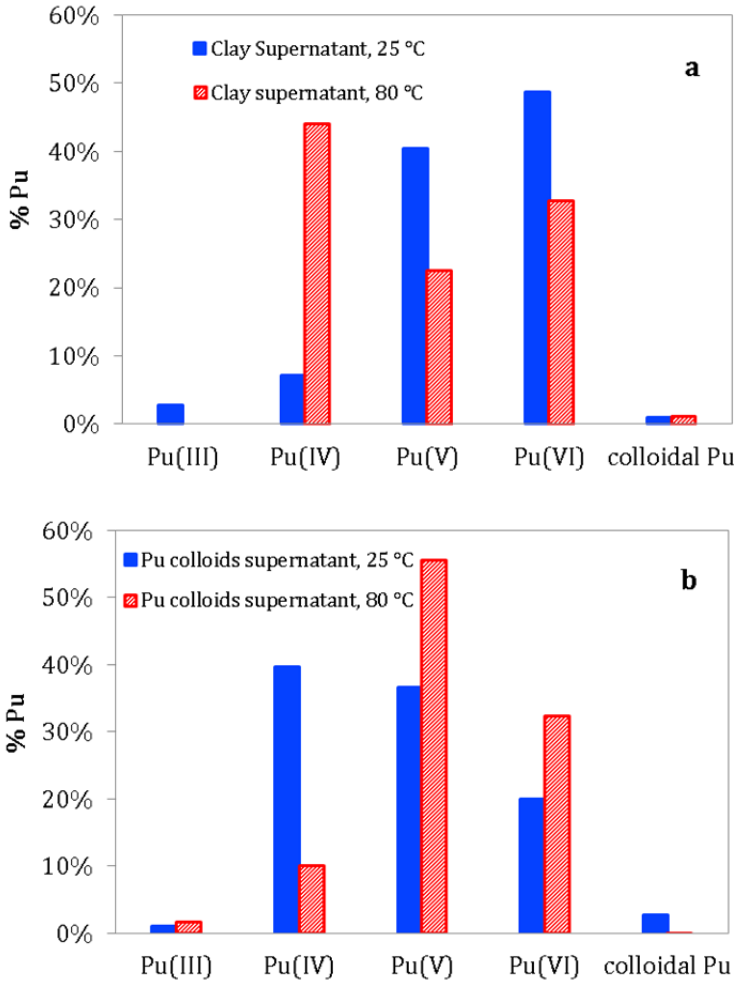

Figure 8. Pu oxidation state distributions in the aqueous phase at 25 and 80°C in montmorillonite suspensions (8a) and intrinsic colloid suspensions (8b).

Table 5. Thermodynamic parameters for sorption of Pu to montmorillonite at 25 and 80°C

Temp	Average K_d mL g^{-1}	T K	ΔH° kJ mol^{-1}	ΔS° kJ mol^{-1} K^{-1}	TΔS° kJ mol^{-1}	ΔG° kJ mol^{-1}
25 °C	1.50E+04	298.15	36.1	0.20	59.9	-23.8
80 °C	1.45E+05	353.15	36.1	0.20	71.1	-34.9

2.5 Conclusions

A study of the dissolution of intrinsic colloids in the presence of montmorillonite at different temperatures was successfully accomplished using a novel experimental setup containing a dialysis device. This device enables us to separate two solid phases. The kinetics of a series of processes including Pu intrinsic colloid dissolution were modeled using a series of 1st order reactions. We show that the kinetic constants for dissolution were one to two orders of magnitude lower than the apparent diffusion rates across the dialysis membranes. Therefore the dissolution process was the rate-limiting step. Although the presence of clay

changes neither the colloids dissolution nor diffusion rates, it can stabilize dissolved Pu species and drive intrinsic Pu colloid dissolution and the formation of more stable pseudo-colloids. Temperature enhances dissolution of intrinsic Pu colloids by overcoming a moderate activation energy (28 kJ mol^{-1}). Our thermodynamic study shows that the sorption of Pu to montmorillonite is endothermic as a positive change in enthalpy for the sorption has been obtained. The affinity of Pu for montmorillonite increases with increasing temperature and resulting in higher K_ds. Although the fact that intrinsic Pu colloids tend to dissolve in the presence of montmorillonite may limit the migration of intrinsic colloids, the subsequent formation of thermodynamically more stable pseudo-colloids can play important role in Pu transport in the environment over significant temporal and spatial scales.

2.6 Acknowledgements

P. Zhao would like to thank Dr. Yunwei Sun (LLNL) for very fruitful discussions. This work was performed with funding from the Department of Energy, Nuclear Energy Used Fuel Disposition Program, and under the auspices of the U.S. Department of Energy by Lawrence Livermore National Laboratory under Contract DE-AC52-07NA27344.

3. LONG-TERM DIFFUSION OF U(VI) IN BENTONITE: DEPENDENCE ON DENSITY

3.1 Introduction

High-level nuclear waste (HLW) mainly resulting from worldwide energy production by nuclear power plants presents a highly chemo- and radiotoxic risk to the environment. The main strategy of waste management is to place the waste in containers and to store them safely in deep geological formations such as salt domes, crystalline rock, and clay rock. The prevention of radionuclide entry to the ecosphere needs to be maintained until their radioactivity is decayed to the natural radiotoxicity level (about one million years). Independent of the chosen host rock in most of the nuclear waste repository designs currently under development, the clay rock bentonite is discussed as material used to backfill the drilled cavities after disposal of the waste containers. This bentonite will acquire different densities depending on the level of confinement (Keto et al., 2007). Typically, bentonite dry bulk densities between 1.5 and 1.8 g/cm^3 can be reached.

For risk assessment, it has to be known if the radionuclides can be mobilized within the repository and transported into the surrounding geo- and biosphere if there is sudden water ingress. For this, the respective retardation factors of the radionuclides migrating through, and interacting with, the different barriers in the system have to be determined under environmentally relevant conditions. Waste-released radionuclides can be retarded by the surrounding barriers (e.g., waste container, backfill material, host rock) in several ways such as sorption, surface precipitation, or molecular diffusion. In many cases it is not possible to attribute the retention of the radionuclide migration to only one interaction process. For instance, the interaction of U(VI) with the natural clay rock Opalinus Clay, which is discussed as potential host rock for a nuclear waste repository, was studied by batch sorption (Joseph et al., 2011) and diffusion experiments (Joseph et al., 2013b). Finally, molecular diffusion was identified as the decisive retardation process.

Many studies focus on the radionuclide diffusion through bentonite since this barrier interacts with the migrating radionuclides before the host rock. In particular, the influence of the bentonite density on the radionuclide diffusion was studied for tritiated water (HTO) (Brockmann, 2006; Sato et al., 1992), $^{90}Sr^{2+}$ (Kim et al., 1993; Sato et al., 1992), $^{99}TcO_4^-$ (Sato et al., 1992), $^{129}I^-$ (Sato et al., 1992), $^{137}Cs^+$ (Brockmann, 2006; Kim et al., 1993; Sato et al., 1992), $^{36}Cl^-$ (Kim et al., 1993; Van Loon et al., 2007b), $^{237}Np(V)$ (Kozai et al., 2001; Sato et al., 1992), and $^{241}Am(III)$ (Sato et al., 1992). The general observation of all studies was that the effective diffusion coefficient, D_e, decreases with increasing density.

Uranium, in particular the isotopes ^{238}U (half-life, $t_{1/2} = 4.468\times10^9$ a) and ^{235}U ($t_{1/2} = 7.038\times10^8$ a), represents the main fraction of disposed spent nuclear fuel rods and consequently, is the main radiologic component of HLW. In general, uranium is stored in the oxidation state IV in the form of UO_2, which is under repository-relevant conditions insoluble and immobile. However, several oxidation processes can occur and U(IV) can be partly transformed to U(VI) (Bruno et al., 2004), which forms mainly mobile species.

For the uranium diffusion through bentonite, several studies can be found in the literature (Table 6). Generally, the experiments are performed for less than one year, except the study of Ramebäck et al. (1998). There, the uranium release from spent UO_2 fuel and its following migration through compacted MX-80 bentonite was investigated for 74 months. Independent of the experimental time period applied, the diffusion results obtained by such studies shall be used to model the diffusion of radionuclides on a longer time frame with regard to safety assessment. This bears the question if the values obtained in short-

term experiments are also valid for longer time periods or if other factors may influence the diffusion with time.

Table 6. Literature selection of experimental conditions (t: time; ρ: dry bulk density) and corresponding diffusion parameters determined (D_a: apparent diffusion coefficient; K_d: distribution coefficient) for the uranium diffusion through compacted bentonite/montmorillonite.

t, days	ρ, g/cm^3	D_a, m^2/s	K_d, m^3/kg	Reference
62	2.0	3.4×10^{-12}; 6.4×10^{-13}; 2.7×10^{-13}	0.093	(Torstenfelt and Allard, 1986)
48; 85	0.9	$1.16 – 2.3\times10^{-12}$	0.047 – 0.310	(Wang et al., 2005)
90	1.6	$3\times10^{-15} – 6.6\times10^{-14}$	0.0013 – 0.0023	(Glaus and Van Loon, 2012)
29 – 121	0.8 – 1.8	$3.7\times10^{-12} – 3.1\times10^{-14}$	0.01 – 0.1	(Idemitsu et al., 1996)
279	1.65	$4\times10^{-14} – 1\times10^{-13}$	0.006 – 0.021	(Garcia-Gutierrez et al., 2004)
90 – 2220	2.0	$1.9\times10^{-13} – 1.6\times10^{-14}$	–	(Ramebäck et al., 1998)

Some of the studies presented in Table 6 were performed at lower bentonite densities than expected to be present in a repository (Wang et al., 2005). Often simple background electrolytes such as water (Garcia-Gutierrez et al., 2004; Idemitsu et al., 1996) or $NaClO_4$ (Wang et al., 2005) were used. In previous studies, the approach of Crank (1975) was applied to fit the uranium profiles and to determine the diffusion coefficients (Idemitsu et al., 1996; Wang et al., 2005). It describes the diffusion as a semi-infinite medium with the assumption that the upstream boundary reservoir is kept at a constant concentration. A variety of modeling software is available to describe more complex systems under variable boundary conditions and to determine respective diffusion parameters (Comsol, 2014; Steefel, 2011).

Besides the nature of the tracer (size, charge, oxidation state) and the composition of the solution (type of ions, level of salinity), the dry density of compacted bentonite affects the diffusion-accessible pore space or effective porosity, ε_{eff} [-], in diffusion experiments (Van Loon et al., 2007b). The effective porosity influences the effective diffusion coefficient of the diffusing species, D_e [m^2/s]. A common method to describe this relation and consequently to predict diffusion parameters in materials with known porosity is the application of an empirical formula analogous to Archie's law (Boving and Grathwohl, 2001):

$$D_e = \varepsilon_{eff}^m \cdot D_w \qquad (19)$$

where D_w [m^2/s] is the diffusion coefficient of the tracer in water and m [-] is an empirical constant also known as the cementation factor of sedimentary rocks. The constant m depends on the properties of the porous material and is not influenced by temperature or sorption of the tracer on the porous medium.

In the present study, the diffusion of HTO and U(VI) through compacted bentonite was investigated as a function of dry density (ρ = 1.3, 1.6, 1.9 g/cm^3) at room temperature under ambient conditions. Based on HTO diffusion experiments, values for ε_{eff} at the respective dry density were determined. In the case of the U(VI) diffusion, the experiments were conducted for six years. As background electrolyte, synthetic bentonite model pore water (Van Loon et al., 2007a) was used. Using such a complex salt system offers the opportunity to perform experiments under more realistic conditions, in particular, towards the present diffusing uranium species. Speciation modeling based on the present conditions in the reservoir solutions

was performed. The solutions were also analyzed for their biological contaminants, since microbial growth was observed over the duration of the experiment. To determine the diffusion parameters based on the collected experimental data the modeling codes CrunchFlow2011 (Steefel, 2011) and COMSOL Multiphysics® 5.0 (Comsol, 2014), and the parameter optimization software PEST (Doherty, 2003) were applied. The relation between the resulting fitting values of ε_{eff} (HTO) and D_e (HTO, U(VI)) were analyzed according to the Archie's law analog and empirical constants were determined.

3.2 Experimental

3.2.1 Materials and Solutions

In the diffusion experiments, natural Na-bentonite MX-80 from Wyoming, USA was used. Herbert and Moog (2002) determined its mineralogy as follows: ~90% montmorillonite, 4% quartz, 2% muscovite, 2% calcite, < 2% cristobalite, and < 1% pyrite. In this study, the bentonite was provided as granulate by Süd-Chemie AG (Munich, Germany). The N_2-BET specific surface area was 15.7 m^2/g (Coulter SA 3100, Beckman Coulter, Fullerton, USA). The bentonite was characterized using X-ray fluorescence (XRF; mod. Tiger S8, Bruker, Billerica, MA, USA). The results are shown in Table 7. The natural uranium content was measured by inductively coupled plasma–mass spectrometry (ICP–MS, Thermo Scientific™ iCAP™ Q, Thermo Electron Corp., Waltham, MA, USA) after digestion of bentonite samples with HNO_3, HCl, and HF on a hot plate. The uranium content amounted to 13 ± 0.1 ppm.

Table 7. Composition of the MX-80 batch used in the diffusion experiments determined by XRF (only compounds > 1 wt.% are shown; error = 2σ).

Compound	wt.%
SiO_2	63.0 ± 0.2
Al_2O_3	18.7 ± 0.1
Fe_2O_3	8.58 ± 0.01
CaO	4.36 ± 0.02
MgO	1.84 ± 0.04
SO_3	1.32 ± 0.02

Synthetic pore water was used in diffusion experiments (pH 8, I = 0.3 M, (Van Loon et al., 2007a)). Its composition was calculated at the Paul Scherrer Institute based on the inventory of the soluble salts of the bentonite, the cation loading of the surface, $\varepsilon_{eff}(Cl^-)$, and several saturation phases in the bentonite (Bradbury and Baeyens, 2003b). In this study, the bulk dry densities 1.3 g/cm^3, 1.6 g/cm^3, and 1.9 g/cm^3 were investigated. The modeled compositions of the respective pore waters with their ionic strength, I, are summarized in Table 8. The solutions were prepared under ambient conditions in Milli-Q water (18 MΩ; mod. Milli-RO/Milli-Q-System, Millipore, Schwalbach, Germany). The pH was measured using a laboratory pH meter (mod. inoLab pH 720, WTW, Weilheim, Germany) with a BlueLine 16 pH microelectrode (SI Analytics, Mainz, Germany), calibrated using standard buffers (WTW) at pH 7 and 9, and adjusted to pH 8 in the solutions using diluted NaOH (*p.a.*, Merck, Darmstadt, Germany) and HCl (*p.a.*, Merck).

Table 8. Composition of the model pore water in dependence on dry bulk density (Van Loon et al., 2007a).

ρ / g/cm^3	**1.3**	**1.6**	**1.9**
ε_{eff}(Cl^-)	**0.122**	**0.044**	**0.019**
$p(CO_2)$ / bar	-3.42	-3.47	-3.65
Na / M	1.83×10^{-1}	2.07×10^{-1}	2.54×10^{-1}
K / M	2.7×10^{-3}	3.1×10^{-3}	3.7×10^{-3}
Mg / M	1.0×10^{-2}	1.2×10^{-2}	1.5×10^{-2}
Ca / M	9.2×10^{-3}	9.8×10^{-3}	1.2×10^{-2}
Sr / M	8.1×10^{-5}	8.6×10^{-5}	1.1×10^{-4}
Cl / M	1.81×10^{-2}	6.18×10^{-2}	1.7×10^{-2}
SO_4 / M	1.02×10^{-1}	9.5×10^{-2}	7.1×10^{-2}
C_{inorg} / M	8.9×10^{-4}	8.0×10^{-4}	5.5×10^{-4}
F / M	2.2×10^{-4}	2.2×10^{-4}	1.9×10^{-4}
Si / M	1.8×10^{-4}	1.8×10^{-4}	1.8×10^{-4}
***I* / M**	**0.26**	**0.29**	**0.33**

A HTO solution (1.2 MBq/mL; Eckert & Ziegler, Valencia, CA, USA), and a depleted UO_2Cl_2 solution in 0.005 M HCl (5×10^{-4} M) were used as stock solutions to adjust the initial concentrations of C_0(HTO) = 500 Bq/mL (= 2.2×10^{-10} M) and C_0(U(VI)) = 1×10^{-6} M in the source reservoir solutions for the respective diffusion experiments.

3.2.2 Experimental Set-up

High-grade stainless steel diffusion cells (design described in detail in Van Loon et al. (2003)) were used in the diffusion experiments to resist the high swelling pressure of the bentonite. In total, four diffusion cells were filled with MX-80, one diffusion cell for each dry density studied (1.3, 1.6, 1.9 g/cm^3), and one blank cell (1.6 g/cm^3) to monitor the fraction of natural uranium leached out from the bentonite by contact with the background electrolyte. The required amount of MX-80 was compacted in a cylindrical sample holder between two stainless steel filter plates (316L, pore diameter: 0.01 mm; MOTT industrial division, Farmington, USA). The dimensions of the MX-80 samples and filters are shown in Table 9. The diffusion cells were closed by tightening the screws at the diffusion cell end plates. To compress the bentonite to dry densities of 1.6 and 1.9 g/cm^3 in the predefined volume of the sample holder, a uniaxial pressure testing machine (Amsler Prüfsysteme AG, Neftenbach, Switzerland) with a constant tension rate of 1 MPa/min was used. The cells containing bentonite at dry densities of 1.3 and 1.6 g/cm^3 were equipped with miniature ring load cells (mod. 8438, Burster Präzisionsmesstechnik GmbH & Co. KG, Gernsbach, Germany) to measure the swelling pressure in the compacted MX-80. Previous measurements showed that at 1.9 g/cm^3 the initial load on the load cell due to the compaction of MX-80 is too high for any additional load measurements (Brockmann, 2006) and thus, the respective diffusion cell was not equipped with a ring load cell. The measured signal of the load cells was converted to millivolts by a one-channel analog input/output module (mod. ADAM 4016, Advantech Corporation, Taipei, Taiwan). Prior to the filling with bentonite, calibration curves of the load cells up to a pressure of 30 MPa were recorded. For that, the empty diffusion cells were filled with water using a high-performance liquid chromatography (HPLC) pump (mod. K-501, Knauer, Berlin, Germany) and a flow rate of 0.05 mL/min.

Table 9. Dimensions of the filters and the MX-80 samples.

	Parameter	Value
Filters	Length	1.55×10^{-3} m
	Diameter	25.4×10^{-3} m
MX-80	Length	5.3×10^{-3} m
	Diameter	25.7×10^{-3} m
	Cross-sectional area	5.19×10^{-4} m^2

All experiments were performed under ambient conditions at room temperature. In the first instance, the respective synthetic pore water was pumped through the confined bentonite samples only at one end plate of the diffusion cells with a stepwise increase of the hydraulic pressure (cf. Appendix Table A.1) provided by the HPLC pump with a flow rate of 0.05 mL/min. After breakthrough of the pore water at the opposite end plate, the percolation was continued until several pore volumes had been exchanged. Then, the HPLC pump was disconnected and the diffusion cells were coupled with a peristaltic pump (mod. Ecoline, Ismatec, IDEX Health & Science, Glattbrugg, Switzerland) and a source and receiving reservoir, respectively, filled with the according synthetic pore water. This experimental set-up was described previously (Brockmann, 2006; Trepte, 2004).

The bentonite samples were conditioned by circulation of the respective background electrolyte through the end plates of the diffusion cells for three to four weeks. Subsequently, the solutions in the source and receiving reservoirs were replaced by fresh ones, whereby, the source reservoir solutions contained the tracer and the receiving reservoir solutions were tracer-free. Consequently, the tracer diffusion started. At first, HTO through- and out-diffusion experiments were performed as described by Brockmann (2006) in order to determine values for ε_{eff} of the MX-80 samples in dependence on dry density. After that, the U(VI) diffusion started. During the duration of the experiments, the pH in the reservoirs was not readjusted.

All diffusion experiments performed were designed at constant boundary conditions. In the case of the HTO diffusion experiments, the source and receiving reservoir solutions were collected in separate reservoirs after passing the end plate of the diffusion cells to prevent tracer solutions from recirculation. The receiving reservoir solutions were regularly exchanged and analyzed. In case of the U(VI) diffusion experiments, both the source and receiving reservoir solutions were recirculated. The U(VI) concentration in the solutions was regularly analyzed. The receiving reservoir solutions were replaced by fresh solution when their U(VI) concentration exceeded 1% of the initial U(VI) concentration in the source reservoir.

After 2457 days (~6 years), the U(VI) diffusion experiment was stopped and the clay samples were removed from the cells. For this, the cylindrical sample holders containing the MX-80 in different dry densities were shock frozen in liquid N_2. The bentonite samples were carefully extracted and placed on a 1 mm-thin bed of quartz sand (*p.a.*, Merck) each in a polytetrafluoroethylene (PTFE) cylinder manufactured at Helmholtz-Zentrum Dresden-Rossendorf (HZDR). Thereby, the bentonite side which was contacted with the source reservoir solution during the diffusion experiment faced the sand. The bentonite was dried in a drying cabinet overnight at 60°C. The next day, the bentonite samples were combined with a stainless steel drilling sample holder (made at HZDR) using a “water-clear” epoxy casting resin and hardener (ρ_S = 1.25 g/cm^3; R&G Faserverbundwerkstoffe GmbH, Waldenbuch, Germany; cf. Fig. 9). After hardening of the resin for one day the PTFE cylinder was opened with a saw. From the fixed bentonite samples the U(VI) diffusion profiles were determined with the help of the abrasive peeling technique (Van Loon and Eikenberg, 2005). The peeled layers were extracted for U(VI)

content by 1 M HNO_3 (*p.a.*, Roth, Karlsruhe, Germany) and analyzed. This method has been applied in a number of earlier experiments (Joseph et al., 2013b; Sachs et al., 2007).

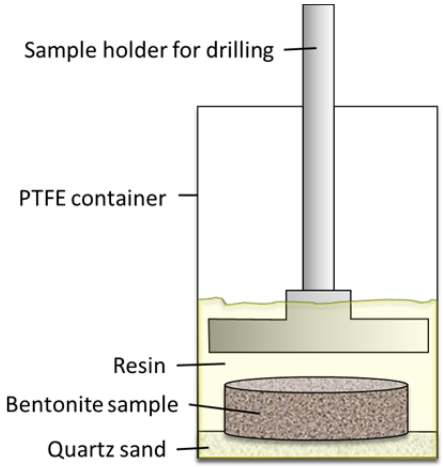

Figure 9. Set-up for combination of the bentonite sample with the stainless steel sample holder for drilling.

3.2.3 Characterization of the Reservoir Solutions

The composition of the solutions was analyzed with ICP–MS (mod. ELAN 6000, Perkin Elmer, Boston, USA), atomic absorption spectroscopy (AAS; mod. AAS-4100, Perkin Elmer), and ion chromatography (IC; mod. IC separation center 733, Metrohm, Herisau, Switzerland). The total inorganic carbon content was measured using a multi N/C 2100 analyzer (Analytik Jena, Jena, Germany) as difference of the total carbon (TC) and total organic carbon (TOC). The HTO activity was determined by liquid scintillation counting (LSC; mod. 1414 WIN Spectral Low-Level α/β, Perkin Elmer Wallac GmbH, Freiburg, Germany) using Ultima Gold™ (Perkin Elmer) as scintillation cocktail. The U(VI) concentration in the source and receiving reservoir solutions as well as in the extracts was measured with ICP–MS. In the evaluation of the experiment, the concentration values were decay corrected.

At the end of the diffusion experiment, the solutions were filtered (0.45-µm MF-Millipore membrane filter, EMD Millipore, Billerica, MA, USA; cf. Appendix Table A.2) for identification of the bacterial and eukaryotic inhabitants in selected reservoir solutions. The DNA of the filtered microorganisms was isolated using the RapidWater® DNA isolation kit (Mo Bio Laboratories Inc., Carlsbad, CA, USA) according to the manufacturer's recommendations. A 10-minute incubation step at 65 °C was added prior to bead beating to aid lysis of fungi and algae species present in solution. The PCR reaction mix contained one iQ™ supermix (Bio-Rad, Hercules, CA, USA), 0.2 µM of each of the following primers, and 4–20 ng genomic DNA as template. The universal bacterial primers GM3 (5´-AGAGTTTGATCMTGGC-3´) and GM4 (5´-TACCTTGTTACGACTT-3´) were used to amplify nearly the entire bacterial 16S rDNA gene (Muyzer et al., 1995). PCR conditions were: 5 min at 94 °C, 35 cycles of 1 min at 94 °C, 1 min at 42 °C, and 3 min at 72 °C, followed by a final elongation at 72 °C for 30 min. The universal eukaryotic primers NS1 (5'-GTAGTCATATGCTTGTCTC-3') and NS2 (5'-GGCTGCTGGCACCAGACTTGC-3') were used to amplify a region close to the 5' of the 18S rDNA gene; equivalent to a 555 bp fragment in *Saccharomyces cerevisiae* (White et al., 1990). The primers applied cover 52 of 59 phyla (White et al., 1990), no set of phyla was preferred. PCR conditions were: 5 min at 94 °C, 35 cycles of 1 min at 94 °C, 1 min at 44 °C, and 2 min at 72 °C, followed by a final elongation at 72 °C for 30 min.

Amplified rDNA was run on a 1% agarose gel electrophoresis in a 1X Tris-acetate-EDTA buffer. Bands were excised using a sterile razor, and DNA was purified using the NucleoSpin® PCR cleanup and gel extraction kit (Clontech Laboratories, Inc., Mountain View, CA, USA). Purified rDNA fragments were ligated into pCR®2.1-TOPO® vectors (Life Technologies, Grand Island, NY, USA) and transformed into Stellar™ chemically competent *Escherichia coli* (Clontech Laboratories, Inc.). Plasmid DNA extraction and sequencing were performed by Elim Biopharmaceuticals (Hayward, CA, USA). The rDNA sequences were taxonomically classified using SINA (Pruesse et al., 2012) with the minimal identity within query sequence set to 0.9 and default settings for all other parameters.

3.2.4 Theoretical Background

The species investigated, HTO and U(VI), were assumed to migrate via molecular diffusion through bentonite. The theoretical background of molecular diffusion is given in (Van Loon et al., 2003). The diffusion process through a porous medium is defined by Fick's first law:

$$J = -D_e \cdot \frac{\partial c}{\partial x} \tag{20}$$

where the diffusive flux J [mol/(m^2·s)] of a solute is equal to the effective diffusion coefficient times the negative concentration gradient (with c [mol/m^3] as tracer concentration in the mobile phase and x [m] as spatial coordinate). The change of concentration with time, t [s], is expressed by Fick's second law:

$$\frac{\partial c}{\partial t} = D_a \cdot \frac{\partial^2 c}{\partial x^2} \tag{21}$$

Thereby, D_a [m^2/s] denotes the apparent diffusion coefficient. Both diffusion coefficients are linked by the rock capacity factor α [–] according to:

$$D_a = \frac{D_e}{\alpha} \tag{22}$$

The rock capacity factor is defined as:

$$\alpha = \varepsilon_{eff} + \rho \cdot K_d \tag{23}$$

where ρ [kg/m^3] is the dry bulk density and K_d [m^3/kg] the sorption distribution coefficient. For non-sorbing tracers such as HTO with $K_d = 0$, it is assumed that α is equal to ε_{eff}. In contrast to D_e, D_a considers the tracer sorption on the clay. In addition, D_e is correlated to the diffusion coefficient of a species in water by:

$$D_e = \frac{\varepsilon \cdot \delta}{\tau^2} \cdot D_w \tag{24}$$

with δ constrictivity, which describes the relation between the size of the respective diffusing species and the present pore size, and τ as tortuosity, which describes to which degree the diffusion path is curved and twisted. In CrunchFlow2011 (Steefel, 2011), this relation is defined as:

$$D_e = \varepsilon_{eff} \cdot \tau \cdot D_w \tag{25}$$

with $\tau \leq 1$.

3.2.5 CrunchFlow2011 Implementation

From a chemical point of view, our CrunchFlow2011 simulations of U(VI) interaction with solid phases were reduced to simple K_d models. Only the following primary species were considered: HTO and UO_2^{2+}, as respective migrating species; Cl^- for charge balance; >SiOH and >FeOH, as generic surface species for U(VI) sorption onto clay and stainless steel filter plates, respectively, and no activity correction.

The HTO diffusion experiments were performed to determine ε_{eff}(HTO) diffusion as a function of clay bulk density. It was assumed that HTO does not interact with the clay and filter surfaces, thus, no HTO sorption was simulated. For modeling of the U(VI) diffusion, the pre-determined ε_{eff}(HTO) values were incorporated in the model assuming that these are equal to the ε_{eff}(U(VI)) values. Of course, the real ε_{eff}(U(VI)) values could be smaller based on the size of the U(VI) species molecule but cannot be determined by this experiment or by modeling. The K_d values for the U(VI) sorption on the bentonite samples were determined by fitting the binding site concentration of quartz, [>SiOH]. How these parameters are connected to each other can be seen in Eq. 26. A log *K* value for the UO_2^{2+} sorption onto quartz was fitted to achieve a K_d value for the sorption of $Ca_2UO_2(CO_3)_3$(aq) to opalinus clay of 0.0222 kg/m^3 (Joseph et al., 2011) assuming a specific surface area (SSA) of 100 m^2/g (montmorillonite; Payne et al., 2011) and a binding site density of 2.31 sites/nm^2 (= $3.8 \cdot 10^{-6}$ mol/m^2; (Pabalan et al., 1998)).

$$\log K = \log\left(\frac{[>\mathrm{SiOH}]}{K_d} \cdot \mathrm{SSA}\right) \qquad (26)$$

The U(VI) sorption on the stainless steel filter plates was determined after the stop of the diffusion experiment by acid extraction with 1 M HNO_3 for one week. With increasing clay bulk density and changes in the pore water composition the U(VI), sorption on the filters increased. The filter sorption was incorporated in the model by defining a log *K* (>$FeOHUO_2^{2+}$) and assuming a specific surface area of 50 m^2/g (goethite; Turner and Sassman, 1996) and a binding site density, [>FeOH], of 3.8×10^{-6} mol/m^2. The resulting K_d values measured and the log *K* values calculated are shown in the Appendix Table A.3.

For both, the HTO and U(VI) diffusion modeling, the CrunchFlow2011 model was composed of source reservoir, stainless steel filter, bentonite sample, stainless steel filter, and receiving reservoir. Each part was considered as homogeneous. In case of the HTO diffusion through bentonite a one-dimensional model was applied. The source reservoir was considered as exterior node and thus, not incorporated in the discretization. The two filter sections were separated in 10 nodes; each part had a length of 0.16×10^{-3} m. The clay section was composed of 200 nodes of 0.0265×10^{-3} m length. The receiving reservoir was described by only one node with a length of 0.15×10^{-3} m. Generally, the length of this last node is defined over the volume of the receiving reservoir solution (~200 mL in average). This would lead to a cell length of 0.39 m (considering the cross-sectional area given in Table 9). To reach a better continuity between the nodes during the modeling process the node length was artificially decreased to the length of the filter nodes. To compensate this size change the porosity of the receiving reservoir condition was artificially increased to 2600. Since the source reservoir was an exterior node, its porosity was set to 1.0.

During the performance of the U(VI) diffusion experiment ^{238}U was detected in the receiving reservoir solution. This was attributed to the continuous dissolution of natural uranium contained in the clay due to pore water contact. The receiving reservoir solution was regularly replaced by fresh pore water. In addition, there were several events where no circulation of solution through the diffusion cell end plates took place (e.g., tubing exchange, broken pump) during the six years the diffusion experiment was conducted. Both the number of solution replacements and the conservatively estimated total stops are summarized in Table 10.

Table 10. Amount of replacements of the receiving reservoir solutions and total duration of no solution circulation (conservative estimation) through the diffusion cell end plates for the U(VI) diffusion through MX-80 bentonite as a function of dry bulk density investigated.

ρ / g/cm^3	1.3	1.6	1.9
No. of replacements	35	20	20
Total stops / days	61	298	302

For modeling of the U(VI) diffusion in bentonite, a series of input files was used to take into account (i) the regular exchange of the receiving reservoir solution and (ii) unplanned stops of pore water circulation. Due to this and for reasons of consistency it was necessary to define a two-dimensional model (cf. Fig. 10). In the x-dimension, the discretization in this model was similar to that one used to model the HTO diffusion, except that the source reservoir was no longer an exterior node and that the clay section was discretized into 1060 nodes to effectively match the U sampling intervals. The volume of the pore water in the reservoirs was assumed to be 200 mL (source) and 50 mL (receiving), thus, their porosities were increased artificially to 2600 and 643 in the input files, respectively. In y-dimension three nodes with an equal length of 519×10^{-3} m were defined considering the cross-sectional area and assuming that each row of nodes represents the model of the whole experimental set-up.

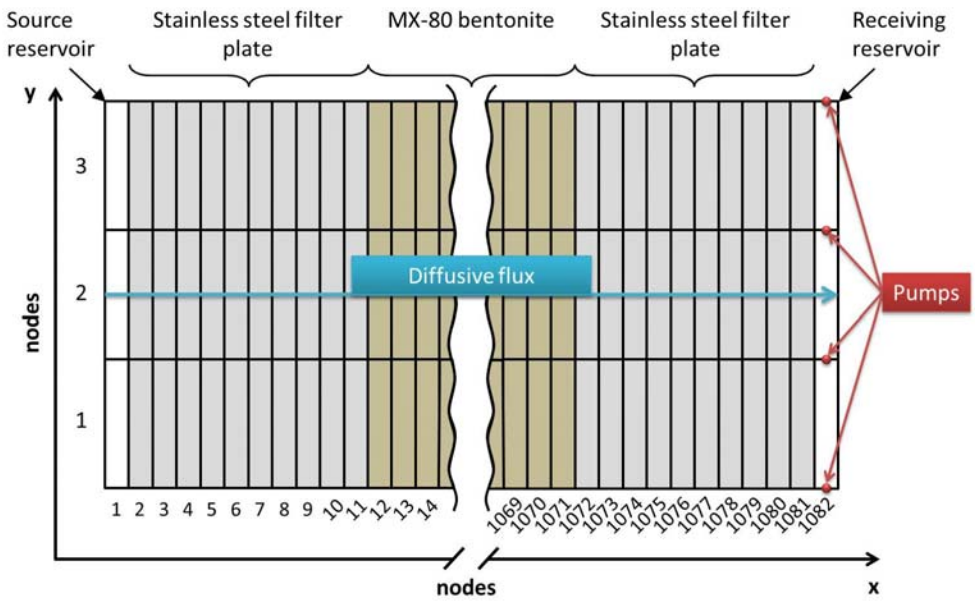

Figure 10. Conceptional description of the two-dimensional model used to simulate the U(VI) diffusion with CrunchFlow2011.

The exchange of the receiving reservoir solution was incorporated in the U(VI) diffusion model by virtual pumps which were placed on the exterior frame of the receiving reservoir nodes in y-dimension (cf. Fig. 10). At specified time points the pumps were switched on for a model time period of one day. Then, fresh receiving reservoir solution was pumped through the receiving reservoir nodes perpendicular to the direction of the diffusive flux to achieve a 6 pore volume exchange of the receiving reservoir.

In the case of the HTO and U(VI) modeling, constant conditions (Eq. 27) at the source reservoir boundary were assumed. For the receiving reservoir boundary, the increase of the HTO and U(VI) concentration with time in the respective receiving reservoir solutions were considered (Eq. 28).

$$c(x = 0, t > 0) = c_0 = \text{const.} \quad (27)$$

$$c(x = L, t > 0) = f_L(t) \quad (28)$$

whereby L [m] denotes the thickness of the system filter/clay/filter. During HTO diffusion modeling the filters, the bentonite and the receiving reservoir solution were regarded as initially free of tracer, whereas for U(VI) diffusion modeling, an initial uranium concentration, c_{initial}, was assumed.

As D_w(HTO) the value of Glaus et al. (2008) with $D_w = 2.2\times10^{-9}$ m^2/s and as D_w(U(VI)) the value published for $Ca_2UO_2(CO_3)_3$(aq) by Kerisit and Liu (2010) with $D_w = 4.6\times10^{-10}$ m^2/s were used. For each condition, a tortuosity was assigned. The tortuosities of the source and receiving reservoir solution (if part of discretization) were set to 1.0. The filter tortuosity was calculated based on Eq. 25. In the case of HTO, D_w(HTO), ε_{eff}(filter), and the D_e value for HTO diffusing through stainless steel filter plates ($D_f = 2.3\times10^{-10}$ m^2/s; (Glaus et al., 2008)) were used. In the case of U(VI), D_f was estimated by $D_f = D_w/10$ (Glaus et al., 2008). The clay tortuosity was in both model approaches a fitting parameter. A summary of the parameters kept constant in both models independent of the density investigated is shown in Table 11.

Table 11. Overview of the parameters used in the CrunchFlow2011 input files for modeling the HTO and U(VI) diffusion through bentonite independent of the dry bulk density investigated.

Condition	**Parameter**	**Value in the**	
		HTO model	**U(VI) model**
Overall	t / d	13.05	2457
	D_w / m^2/s	2.2×10^{-9}	4.6×10^{-10}
Source reservoir	ε_{eff}	1.0	2600
	τ	-	1.0
Stainless steel filter plates	ρ_S / g/cm^3	5.27	5.27
	ε_{eff}	0.3	0.3
	τ	0.35	0.33
MX-80 bentonite	ρ_S / g/cm^3	2.65	- [a]
Receiving reservoir	ε_{eff}	2600	643
	τ	1.0	1.0

[a] varied in dependence on ε(HTO) and ρ

For comparison with the experimental data, in case of the HTO diffusion, the HTO concentration in the node of the receiving reservoir on specified time points (the experimental sampling days) was determined. In the case of the U(VI) diffusion, two output files were relevant for comparison with the experimentally obtained profile and outflow data: (1) The uranium content in the clay as a function of distance at the end of the diffusion experiment and (2) the U(VI) concentration in the receiving reservoir at the time points where the solution was replaced.

3.2.6 PEST Estimation

The PEST estimation code (Doherty, 2003) was used to minimize the differences between the data of the CrunchFlow2011 output files and the experimental diffusion data by changing pre-defined CrunchFlow2011 input parameters. Crucial for reaching convergence in the fitting routine was the definition of the weighting factors for the experimental data. For fitting the HTO diffusion the weighting factor was $1/\Delta c$, where Δc [M] describes the uncertainty of the measured HTO concentration. For the U(VI) profile fit the weighting factor was $1/d$, where d denotes the distance to the clay edge [mm]. For the fit of the U(VI) outflow in the receiving reservoir solution, $1/c$ was used as the weighting factor, where c denotes the U(VI) concentration in the receiving reservoir at the time points of the solution replacement. The relevant diffusion parameters and their fitting equivalents for HTO and U(VI) diffusion modeling are shown in Table 12, whereby $c(\mathrm{U(VI)})_{BG}$ denotes the background U(VI) concentration in the clay.

Table 12. Overview of the diffusion parameters and their fitting equivalents varied in the MX-80 bentonite in the CrunchFlow2011 input files using the PEST optimization code.

Model	**HTO outflow**		**U(VI) profile**			**U(VI) outflow** [a]
Diffusion parameter	D_e	ε_{eff}	K_d	-	D_e, D_a	D_e, D_a
Fitting equivalent	τ	ε_{eff}	[>SiOH]	$c(\mathrm{U(VI)})_{BG}\tau$		τ

[a] Only one parameter was fitted due to the strong correlation between τ, [>SiOH], and $c(\mathrm{U(VI)})_{BG}$.

3.2.7 COMSOL Multiphysics® 5.0

To confirm the parameter fitting obtained by CrunchFlow2011 and PEST, COMSOL Multiphysics® 5.0 (Comsol, 2014) was used. Here, a one-dimensional model consisting of source reservoir, filter, clay, filter, and receiving reservoir was defined using an extremely fine mesh (maximum element size: 8.4×10^{-5} m) to simulate both the HTO and U(VI) diffusion. Thereby, the same input parameters as for the CrunchFlow2011 modeling were used, except that the already optimized values for the diffusion-relevant parameters were incorporated. No chemical species had to be defined, since the molecular diffusion through a porous medium was investigated from the physical point of view only. The regular replacements of the receiving reservoir solution and the irregular pump stops were not considered in the model. Again, the time evolution of the HTO flux and the accumulated concentration of HTO and U(VI) in the receiving reservoir solution as well as the U(VI) profile in the clay at the end of the diffusion experiment were extracted from the model and compared with the respective experimental data.

3.2.8 Experimental Uncertainties

The experimental uncertainties of the values for the diffusive HTO flux and the accumulated diffused HTO activity in the receiving reservoir solution resulted from the uncertainty of the parameters required to calculate these values (cf. (Van Loon and Soler, 2004)). In the case of U(VI) diffusion profiles, the experimental uncertainty of the diffusion depth is given by the average of the individual distance measurement at four points of the clay sample. The uncertainties of the diffusion parameters resulted from the uncertainties of their fitting equivalents (cf. Table 12), which were provided by PEST after the fitting procedure in the form of 95% confidence limits. The impact of the drying procedure to prepare the samples for abrasive peeling on the samples' dimensions and dry densities and consequently, on the diffusion parameters were investigated by CrunchFlow2011 modeling. It was assumed that the dry bulk

density decreases by 10% and the diameter of the sample increases or decreases by 10%. No significant influence on the resulting diffusion parameters was observed.

3.3 Results and Discussion

3.3.1 Swelling Behavior of Bentonite

In the beginning of the experiments the bentonite samples were conditioned with pore water (cf. Table 8). The associated load cells measured the swelling pressure of the MX-80 samples as a function of time during this saturation process. The results for the diffusion cells with ρ of 1.3 and 1.6 g/cm^3 are shown in Figure 11.

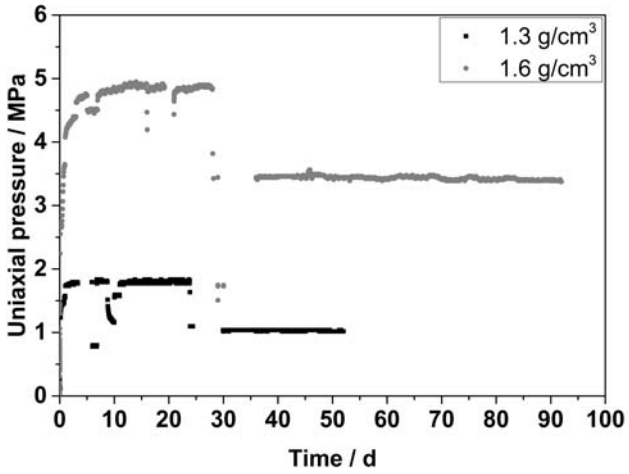

Figure 11. Swelling pressure measured for the diffusion cells with ρ = 1.3 and 1.6 g/cm^3 as a function of time.

At 1.3 g/cm^3 and 1.6 g/cm^3, swelling pressure reached equilibrium within 30 days at about 1 MPa and within 35 days at about 3.5 MPa, respectively. The intense drops of pressure before equilibrium establishment can be attributed to changes in the hydraulic pressure of the HPLC pump (cf. Appendix Table A.1). Lee et al. (2012) investigated the swelling pressure of Ca-bentonite as a function of dry density, ionic strength, and time. Under comparable conditions as used in this study they observed that the steady state region was reached after 20 days which agrees well with the present results. It was assumed that after the respective time periods the bentonite samples were fully saturated with pore water and the HTO and U(VI) diffusion experiments were started.

3.3.2 Aqueous U(VI) Speciation

Table 13 summarizes the composition of the experimentally prepared pore water in the source reservoir in the first and the last year of the diffusion experiment for all three dry bulk densities investigated.

Table 13. Composition of the source reservoir solutions in the first and the last year of the U(VI) diffusion experiment as well as the main aqueous U(VI) species calculated for the listed conditions.

	1.3 g/cm^3		**1.6 g/cm^3**		**1.9 g/cm^3**	
	***t* = 191 d**	***t* = 2401 d**	***t* = 191 d**	***t* = 2401 d**	***t* = 191 d**	***t* = 2401 d**
***c* / M**						
U [a]	1.1×10^{-6}	1.1×10^{-6}	1.1×10^{-6}	1.1×10^{-6}	1.1×10^{-6}	1.2×10^{-6}
Na [a]	2.0×10^{-1}	2.2×10^{-1}	2.2×10^{-1}	2.8×10^{-1}	2.7×10^{-1}	3.2×10^{-1}
K [a]	3.2×10^{-3}	3.2×10^{-3}	3.6×10^{-3}	4.0×10^{-3}	4.4×10^{-3}	4.6×10^{-3}
Mg [b]	1.1×10^{-2}	1.2×10^{-2}	1.2×10^{-2}	1.5×10^{-2}	1.6×10^{-2}	1.8×10^{-2}
Ca [b]	9.2×10^{-3}	1.1×10^{-2}	8.9×10^{-3}	1.4×10^{-2}	1.2×10^{-2}	1.5×10^{-2}
Sr [a]	8.6×10^{-5}	9.5×10^{-5}	8.2×10^{-5}	1.1×10^{-4}	1.1×10^{-4}	1.3×10^{-4}
Si [a]	n.d. [e]	5.3×10^{-4}	n.d.	3.9×10^{-4}	n.d.	3.7×10^{-4}
Cl^- [c]	1.9×10^{-2}	2.1×10^{-2}	6.4×10^{-2}	7.8×10^{-2}	1.7×10^{-1}	2.1×10^{-1}
SO_4^{2-} [c]	1.1×10^{-1}	1.2×10^{-1}	1.1×10^{-1}	1.2×10^{-1}	6.7×10^{-2}	8.8×10^{-2}
C_{inorg} [d]	9.7×10^{-4}	9.7×10^{-4}	8.7×10^{-4}	6.0×10^{-4}	5.2×10^{-4}	6.2×10^{-4}
F^- [c]	2.3×10^{-4}	2.5×10^{-4}	2.3×10^{-4}	3.5×10^{-4}	2.0×10^{-4}	2.6×10^{-4}
I	0.28	0.31	0.30	0.37	0.32	0.41
Aqueous U(VI) species distribution / % [f]						
$Ca_2UO_2(CO_3)_3(aq)$	85.5	87.5	83.7	89.1	89.9	90.4
$UO_2(CO_3)_3^{4-}$	9.4	8.2	10.6	7.3	5.4	6.1
$MgUO_2(CO_3)_3^{2-}$	3.2	2.4	3.9	2.4	3.1	2.6
$CaUO_2(CO_3)_3^{2-}$	1.2	1.1	1.2			

[a] ICP–MS (error: ±10%)
[b] AAS (error: ±2%)
[c] IC (error: ±3-10%)
[d] TC – TOC (error: ±3%)
[e] n.d. = not determined
[f] only species ≥ 1% shown

The comparison of the composition and ionic strength of the solutions shows that their salinity increased with time. This can be attributed partly to water evaporation over the long time period the experiment was conducted. Within this time the source reservoir solutions were never exchanged. However, all reservoir solutions were replaced by fresh ones at t = 2401 days. The experiment was stopped at t = 2457 days. The composition of these solutions is summarized in Table A.4.

To interpret the diffusion results it has to be known which U(VI) species dominates the solution. Based on the composition of the source reservoir solutions, U(VI) speciation was calculated using the speciation code "The Geochemist's Workbench® 8.0" (Bethke and Yeakel, 2010) and the thermodynamic data compiled in Guillaumont et al. (2003b) including the data for the alkaline earth tricarbonato complexes with U(VI) (Bernhard et al., 2001; Dong and Brooks, 2006). The speciation results are presented in Table 13. The $Ca_2UO_2(CO_3)_3(aq)$ complex dominates the speciation in all solutions and consequently, can be assumed to be the main diffusing U(VI) compound under the present conditions.

Since the $Ca_2UO_2(CO_3)_3(aq)$ complex is a neutral species, it will be not repulsed by the negatively charged clay surface and the main part of the interparticle space would be accessible. Bernhart et al. (2001) investigated this complex by extended X-ray absorption fine-structure spectroscopy. Based on their results an average diameter between 10-11 Å for the non-hydrated complex can be assumed taking into account the radii of calcium and oxygen. The question arises if this complex also has access to the interlayers of the montmorillonite fraction of MX-80, which can have distances from 2 to 10 Å (Bradbury and Baeyens, 2002; Keren and Shainberg, 1975) depending on how many water layers are present. In this study, ε_{eff} of HTO is used in the U(VI) diffusion model, although one can expect that ε_{eff} of U(VI) is smaller than HTO regarding the size of $Ca_2UO_2(CO_3)_3(aq)$ which leads to higher steric hindrance. However, as previously discussed (Joseph et al., 2013b), the used value of ε_{eff} has no significant impact on the modeled U(VI) diffusion parameters, since the U(VI) sorption onto the clay is dominating (cf. Eq. 23).

3.3.3 Biological Contaminants

Despite the presence of NaF ($c \approx 2\times10^{-4}$ M) and the oligotrophic nature of the reservoir solutions, contaminating eukaryotic and prokaryotic microorganisms were detected within each reservoir, including those tracered with 1×10^{-6} M U(VI). To identify the most abundant contaminating microorganisms and determine whether the presence of U(VI) influenced the diversity of microbial contaminants, a subset of 16S and 18S rDNA was sequenced from all source reservoir solutions and one receiving reservoir (cell 1.9 g/cm^3). Surprisingly, the majority of bacteria were heterotrophs (cf. Appendix Table A.5), despite the low levels of dissolved organic carbon. Exceptions include the green sulfur family *Chlorobiales* that are photoautotrophs.

The comparison of the prokaryotic diversity in the source and receiving reservoir solution of cell 1.9 g/cm^3 shows that bacteria from the *Planctomyces* genus and *Rhodospirillales* order can be found in both solutions. The *Planctomyces* genus even dominates the diversity in both samples. Otherwise, there are also prokaryotic families only present in the source or receiving reservoir solution. That leads to the conclusion that the solutions should be regarded as independent. Their prokaryotic diversity cannot be attributed to spores or microorganisms that were originally contained in the bentonite clay sample since all diffusion cells contained compacted MX-80 from the same batch.

The prokaryotic diversity of the blank cell solution differs from those of the solutions tracered with U(VI). Although members of the family *Planctomycetaceae* represent the largest fraction of bacterial contaminants in the blank cell solution and can be found in the source reservoir solutions of the cells 1.6 and 1.9 g/cm^3, there is an interesting difference at the genus level. The *pir4 lineage* dominates in the

blank cell solution, but is not found in the solution containing U(VI). There, the *Planctomyces* genus dominates in the solutions. There are also several members of the phylum *Actinobacteria* that are only present in the blank solution (e.g., *Ilumatobacter*, *Nocardioidaceae*, *Gaiellales*). Thus, the presence of U(VI) may have selected against growth of some bacterial species.

Of particular note, six of seven 16S rDNA clone sequences of the phylum *Actinobacteria*, identified in the 1.6 g/cm^3 cell source reservoir solution, have 99% sequence similarity to an uncultured isolate (WC2_55) that was found in a low-level radioactive waste site at the Idaho National Laboratory (Field et al., 2010). Furthermore, isolates with the highest sequence similarity to the additional seventh clone were identified in environments contaminated by heavy metals and mining operations (These sequences have been deposited in the GenBank but not included in a publication to date.).

The phyla from *Proteobacteria*, *Chloroflexi*, *Actinobacteria*, *Acidobacteria*, *Chlorobium*, and *Planctomycetes* identified in this study were also found in subsurface sediments from uranium-contaminated sites in Tennessee (Akob et al., 2007; Barns et al., 2007) and Colorado (Barns et al., 2007). Amongst others, representatives of the *Proteobacteria* and *Acidobacteria* phylum were identified in uranium and heavy metal-contaminated soils and mine waste piles at former uranium mining and milling sites in Bulgaria (Radeva et al., 2013) and in samples from several uranium mining wastes in Germany and the United States (Radeva and Selenska-Pobell, 2005). *Proteobacteria* were found in the pore water of Opalinus Clay samples (Stroes-Gascoyne et al., 2011). At longer times scales, i.e. after ten years of interaction, *Actinobacteria* and *Proteobacteria* were identified at the iron/clay interface between re-compacted argillite and steel coupons (Urios et al., 2013). These studies show the ubiquitous presence of the identified prokaryotic species at uranium contaminated soils, hence, also in this experiment.

In the case of the eukaryotic diversity in all reservoir solutions investigated, fungi species (*Ascomycota* phylum) were identified (cf. Appendix Table A.6). In particular, between the source and receiving reservoir solutions of cell 1.9 g/cm^3 no additional similarities could be found.

The eukaryotic diversity at relatively high U(VI) concentrations differs from that with background level U(VI) concentrations. In all three source reservoir solutions tracered with U(VI), representatives of the green algae phylum *Chlorophyta* were the largest or second largest fraction in the analyzed plasmids. Only at lower U(VI) concentrations were representatives of the *Stramenopiles* phylum identified and these represented the dominant fraction, suggesting that this phylum may not have an appropriate defense mechanism towards relatively high levels of uranium.

Algae are particularly well known for excretion of organic compounds that can seed heterotrophic growth. Intriguingly, reservoirs with a high abundance of algae (i.e., source and receiving reservoir cell 1.9 g/cm^3, blank cell) also have high levels of *Planctomyces*, which could suggest a potential synthrophic relationship as previously described (Pizzetti et al., 2011). Jasrotia et al. (2014) found *Ascomycota* in a subsurface environment contaminated with uranium at the watershed scale at Oak Ridge, Tennessee. Amongst others, *Amoebae*, *Fungi*, and *Stramenopiles* taxes were identified in the eukaryotic community in biofilms formed in an acid mine drainage in the underground uranium mine Königstein (Saxony, Germany) (Zirnstein et al., 2012). These species seem to have a well-performing survival mechanism to overcome the chemotoxic effect of the present uranium. For *Stramenopiles* this finding stands in contrast to the conclusion in the present study. Probably, the difference in pH ((Zirnstein et al., 2012): pH 2.86 ± 0.05; this study: pH 8) has an impact on its survival mechanism.

In this study it is assumed that the various prokaryotic and eukaryotic species present in the reservoir solutions have no impact on the uranium diffusion path. The solutions were regularly filtered. In addition, the tubing between the solutions and the diffusion cells was regularly exchanged to guarantee the

unhindered flow of the solutions through the endplates of the diffusion cells. The filtered solutions showed still a U(VI) concentration of about 1×10^{-6} M. Thus, a biotransformation of the U(VI) to insoluble uranium species can be excluded. However, it cannot be ruled out that the detected microorganisms release organic compounds to the pore water solutions, which can affect the U(VI) speciation. The TOC levels were determined for each solution (cf. Appendix Tables A.5 and A.6), but the organic compounds were not analyzed in more detail.

3.3.4 HTO Diffusion Through MX-80 as a Function of Clay Bulk Density

Before the U(VI) diffusion experiments were started a HTO diffusion experiment was conducted to determine the HTO transport porosity and to determine if the applied experimental set-up delivers parameter values which are comparable to literature data. Table 14 summarizes the HTO diffusion parameters used in, and obtained by, fitting of the experimental results for the three investigated dry bulk densities.

As expected, ε_{eff} and τ decrease with increasing MX-80 dry density since the diffusion available pore space becomes smaller as well as the diffusion path more curved with increasing clay compaction in the diffusion cell. Both parameters contribute to the decrease of D_e with increasing density. The unusual high porosity at ρ = 1.6 g/cm^3 seems to be an outlier. Probably, it can be attributed to phase heterogeneities in the clay sample caused by the HPLC pump during the saturation process. The comparison of the results with literature values shows a quite good agreement, in particular with the values from (Glaus et al., 2010) obtained for ρ = 1.9 g/cm^3. Figure 12 shows the relation between the values of D_e and ε_{eff} obtained in this study. The data were fitted using Archie's law analog (Eq. 19) with D_w(HTO) (Table 14).

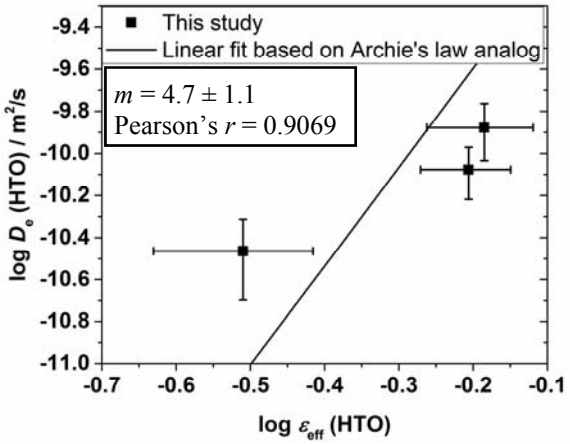

Figure 12. Relation between D_e and ε_{eff} for the HTO diffusion through MX-80 bentonite.

Table 14. Parameter values of the HTO diffusion through bentonite obtained in this study and found in literature as a function of dry bulk density.

ρ / g/cm^3	1.3	1.6	1.9
Parameter			
c_0 / M	2.25×10^{-10}	2.24×10^{-10}	2.20×10^{-10}
ε_{eff} / –	0.65 ± 0.11	0.62 ± 0.09	0.31 ± 0.08
τ / $\times10^{-2}$	9.2 ± 1.4	6.1 ± 0.7	4.8 ± 0.9
D_e / $\times10^{-11}$ m^2/s	13.2 ± 4.1	8.4 ± 2.2	3.4 ± 1.4
ε_{eff} / – [a]	0.38 ± 0.05 / 0.41 ± 0.06		
D_e / $\times10^{-11}$ m^2/s [a]	1.7 ± 0.2 / 1.9 ± 0.2		
ε_{eff} / – [b]	0.44 ± 0.02	0.40 ± 0.02 / 0.35 ± 0.02	
D_e / $\times10^{-11}$ m^2/s [b]	11.2 ± 0.6	5.9 ± 0.3 / 5.2 ± 0.4	

[a] Values from (Glaus et al., 2010) obtained for compacted Na-montmorillonite at I = 0.1 M and 1 M $NaClO_4$.
[b] Values from (Wu et al., 2012) obtained for GMZ bentonite at dry densities of 1.6, 1.8, and 2.0 g/cm^3.

The empirical constant resulting from the linear fit agrees well with the cementation factor of 4.5 ± 1.0 determined by Wu et al. (2012) for the HTO diffusion through GMZ bentonite using D_w(HTO) of 2.3×10^{-9} m^2/s. Instead of using D_w(HTO), Glaus et al. (2010) defined this factor as fitting parameter called A in their investigation of the HTO diffusion through compacted Na-montmorillonite. They obtained values of $A = 9.8\times10^{-11}$ m^2/s and m = 1.81. If such a free fit is applied to the data in the present study, values of $A = (2.1 \pm 0.8)\times10^{-10}$ m^2/s and $m = 1.6 \pm 0.6$ result. The cementation factor can be confirmed. The discrepancy in A can be attributed to the outlier at 1.6 g/cm^3. The agreement with literature values proves the applicability of the present experimental set-up. Thus, the diffusion studies were continued with U(VI).

3.3.5 U(VI) Diffusion in MX-80 as a Function of Clay Bulk Density

In Figure 13, the uranium depth profiles for the U(VI) diffusion into MX-80 as a function of dry density are presented together with the best fit curves of the CrunchFlow modeling. In addition, the uranium profile of the blank diffusion cell is depicted. Its maximal uranium concentration is used as guidance for the natural uranium level in all MX-80 samples investigated. Based on this comparison it can be seen that the added uranium diffuses about 2 mm, 1 mm, and 0.7 mm into the clay at ρ = 1.3, 1.6, and 1.9 g/cm^3, respectively.

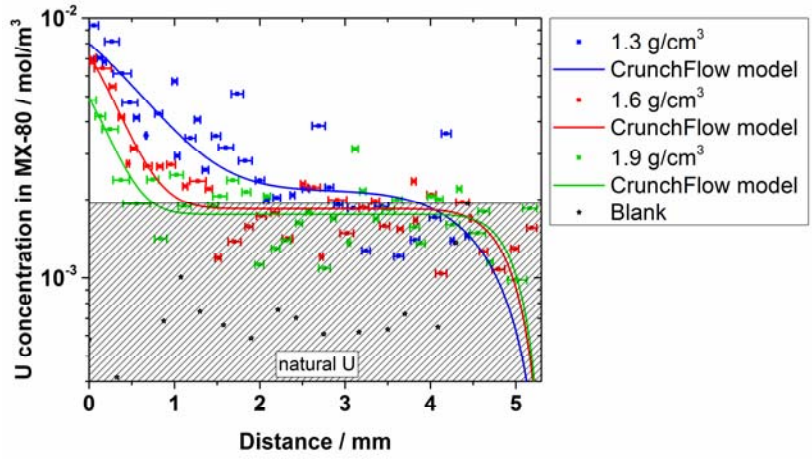

Figure 13. Concentration depth profile of uranium in MX-80 as a function of clay dry density.

The drop of the modeled uranium concentration in MX-80 at a depth of about 5 mm results from the leaching of natural uranium from the clay rock and its transport to the adjacent receiving reservoir solution, which was considered in the model. For example, the experimentally determined U(VI) concentration in the receiving reservoir solution of cell 1.6 g/cm^3 is presented in Figure 14 which also highlights the time points of solution replacement. For consistency, the data of the U(VI) outflow of the blank cell are also shown. Since both sets of data points are in the same order of magnitude, the measured U(VI) in the receiving reservoir of cell 1.6 g/cm^3 can be clearly attributed to natural uranium leached out of MX-80 and not to the diffused, experimentally added U(VI) tracer. Obviously, the CrunchFlow model using the profile fit parameters does not fit the experimental observations (straight lines in the model curves are the considered time periods of no solution circulation (cf. Table 10)).

In a second fit approach, instead of the uranium profile, the experimentally determined U(VI) outflow was fitted for each dry density. A quite good agreement between experiment and model data was achieved (cf. Fig. 14). Consequently, the corresponding U(VI) model profiles are no longer in agreement with the experimental data (cf. Appendix Fig. A1). This discrepancy shows that the in- and outflow of U(VI) in MX-80 has to be regarded independently in this study.

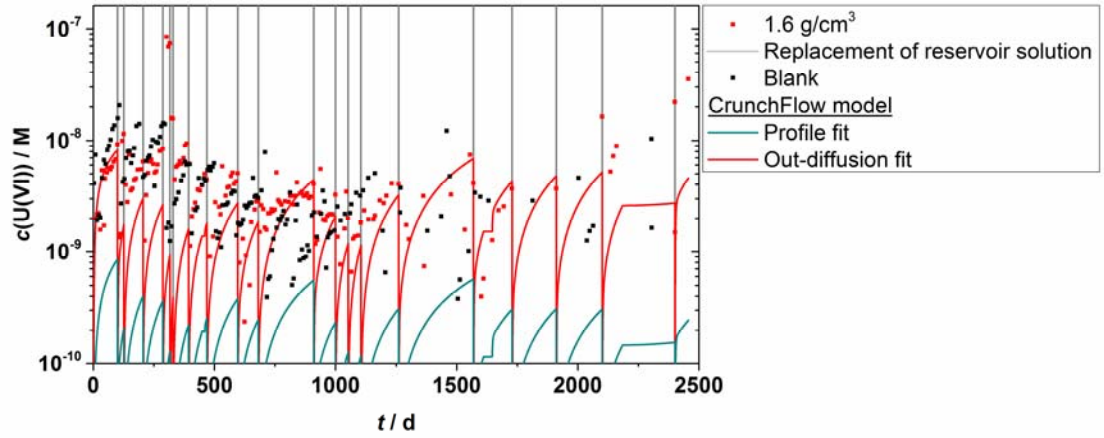

Figure 14. U(VI) concentration in the receiving reservoir solution of diffusion cell 1.6 g/cm^3 as a function of time. CrunchFlow model data obtained by fitting the uranium depth profile in MX-80 and the uranium out-diffusion in the receiving reservoir.

Table 15 summarizes the diffusion parameter values used in and obtained by modeling and fitting of the U(VI) diffusion depth profiles and the U(VI) concentration evolutions in the receiving reservoir solutions as a function of the dry density. The K_d values obtained are very low. This can be explained by the present U(VI) speciation (cf. Table 13). The neutral $Ca_2UO_2(CO_3)_3(aq)$ complex is dominating the source reservoir solutions and is known to sorb only weakly onto clay (Joseph et al., 2011). In addition, $UO_2(CO_3)_3^{4-}$, the second dominant species in solution, is regarded as non-sorbing species (Joseph et al., 2013a; Křepelová et al., 2006) since it will be repulsed by the negatively charged clay surface. The obtained K_d values are all in the same order of magnitude (vary by a factor of two) and tend to lower values with increasing ρ. The K_d variance may be attributed to small changes in the composition of the pore waters used in the three diffusion experiments. Due to the decreases in K_d and ε_{eff}, α decreases with increasing ρ (cf. Eq. 23). The low Kd values suggest that U(VI) reduction to U(IV) was negligible in these experiments.

Table 15. Parameter values of the U(VI) diffusion in MX-80 based on modeling the uranium depth profile in the clay and the uranium out-diffusion in the receiving reservoir as a function of dry bulk density.

ρ / g/cm^3	1.3		1.6		1.9	
Fit of	**profile**	**out-diffusion**	**profile**	**out-diffusion**	**profile**	**out-diffusion**
Parameter						
ρ_S / g/cm^3	3.75		4.24		2.75	
ε_{eff} / –	0.65 ± 0.11		0.62 ± 0.09		0.31 ± 0.08	
$c(U(VI))_{initial}$ / M [a]	3.87×10^{-10}		4.2×10^{-12}		4.2×10^{-12}	
$c(U(VI))_{BG}$ / ×10^{-7} M	3 ± 1		2.4 ± 0.3		3.4 ± 1.0	
[>SiOH] / ×10^{-7} mol/m^2	10 ± 1		7.5 ± 0.4		4.4 ± 1.4	
K_d / ×10^{-3} m^3/kg	5.8 ± 0.6		4.4 ± 0.2		2.6 ± 0.8	
α / –			8.2 ± 0.8	7.6 ± 0.4	5.2 ± 1.5	
τ / ×10^{-5}	5.4 ± 3.4		340 ± 80	1.6 ± 0.4		77 ± 25
	1.5 ± 1.6	59 ± 20				
D_e / ×10^{-15} m^2/s	16 ± 10		1030 ± 240		4.5 ± 1.2	
	220 ± 70		2.1 ± 2.3	83 ± 28		
D_a / ×10^{-16} m^2/s	20 ± 11		1200 ± 300		5.9 ± 1.2	
	290 ± 90		4.0 ± 3.5	160 ± 50		

[a] Initial uranium concentration assumed in the filters and the receiving reservoir based on the minimal uranium concentration measured in the respective receiving reservoir.

Table 16 shows a multitude of published K_d values for U(VI) sorption onto bentonite and montmorillonite which can be explained by the different conditions used in the respective experiments. The K_d values from the present study differ from the values obtained by diffusion experiments published by (Wang et al., 2005) by about one order of magnitude. They studied U(VI) diffusion through MX-80 as a function of U(VI) concentration and time under a slightly lower pH and ionic strength than used in the present study which leads to a different U(VI) speciation and sorption behavior. Probably, $(UO_2)_2CO_3(OH)_3^-$ is the dominant U(VI) species in solution which is known to sorb more strongly on clay than $Ca_2UO_2(CO_3)_3(aq)$ (Joseph et al., 2013a; Křepelová et al., 2006) and thus higher K_d values were obtained. (Glaus and Van Loon, 2012) investigated U(VI) diffusion through compacted montmorillonite in $NaClO_4$ in the presence of calcium and carbonate ions as a function of the $NaClO_4$ ionic strength. In this case, besides the $Ca_2UO_2(CO_3)_3(aq)$ complex, a relatively large fraction of the different negatively charged uranyl carbonato complexes are present in solution, which, as mentioned before, sorb even less than the $Ca_2UO_2(CO_3)_3(aq)$ complex. Thus, slightly smaller K_d values are obtained. However, the values differ from the K_d values presented in this study only by a factor of three which can be regarded as in very good agreement.

Table 16. Selection of K_d values from the literature obtained by diffusion as well as batch sorption experiments.

	Clay type	Background electrolyte	pH	[U(VI)] M	K_d $\times 10^{-3}$ m^3/kg	Reference
Obtained by diffusion experiments [a] **ρ / g/cm^3**						
0.953	MX-80	0.1 M $NaClO_4$	7	1×10^{-6}	92	[b]
0.996	MX-80	0.1 M $NaClO_4$	7	1×10^{-6}	51	[b]
1.6	mont [c]	0.1; 0.5 M [d]	8.6-9	6×10^{-5}	1.3; 1.6	[e]
Obtained by batch sorption experiments [a] **S/L ratio / g/L [f]**						
2.5	MX-80	1.3 pore water 1.6 pore water 1.9 pore water	8	1×10^{-6}	13 ± 1.5 39 ± 1 39 ± 0.9	[g]
10	MX-80	synthetic ground-water (0.008 M)	8.2	2.1×10^{-7}	93	[h]
0.32-13.5	MX-80	model pore water (0.7 M)	7.6	1×10^{-6}-3×10^{-8}	28 (average)	[i]

[a] If more than one K_d is published in a literature source, these K_d values are taken whose experimental conditions are most similar to the conditions used in the present study.
[b] (Wang et al., 2005)
[c] mont = montmorillonite
[d] varying $NaClO_4$ + 1×10^{-2} M CHES buffer + 1×10^{-3} M C_{inorg} + 1×10^{-4} M Ca^{2+}
[e] (Glaus and Van Loon, 2012)
[f] S/L ratio = solid-to-liquid ratio
[g] (Nebelung and Brendler, 2009)
[h] (Allard et al., 1982)
[i] (Bradbury and Baeyens, 2011)

Bradbury and Baeyens (2003a) suggested that a comparison between K_d data from intact and dispersed systems is only meaningful when the same water conditions are present. Thus, the batch sorption K_d values published by Nebelung and Brandler (2009) provide the best comparison with the K_d values obtained by diffusion experiments in this study, since the same MX-80 batch, pore waters, and initial U(VI) concentration were used. Their K_d values are about one order of magnitude higher than the K_d values obtained by diffusion. The reason could be that more binding sites are accessible for U(VI) during a batch sorption experiment, where the powder clay is mixed with the U(VI) solution, than in a diffusion experiment, where the only binding sites accessible for U(VI) interaction are those on the source reservoir side of the compacted clay cylinder and those that surround the individual diffusion path. In addition, since a much smaller S/L ratio was applied in the batch sorption experiments than in the diffusion experiments, possibly, the pore water is not in equilibrium with the small amount of solid and minerals can precipitate on the micromolar level. U(VI) can be either incorporated in these precipitates or can sorb on the newly formed mineral phases(Allard et al., 1982; Bradbury and Baeyens, 2011; Pabalan and Turner, 1997)(Allard et al., 1982; Bradbury and Baeyens, 2011; Pabalan and Turner, 1997)(Allard et al., 1982; Bradbury and Baeyens, 2011; Pabalan and Turner, 1997)(Allard et al., 1982; Bradbury and Baeyens, 2011; Pabalan and Turner, 1997)(Allard et al., 1982; Bradbury and Baeyens, 2011; Pabalan and

Turner, 1997)(Allard et al., 1982; Bradbury and Baeyens, 2011; Pabalan and Turner, 1997)(Allard et al., 1982; Bradbury and Baeyens, 2011; Pabalan and Turner, 1997)(Allard et al., 1982; Bradbury and Baeyens, 2011; Pabalan and Turner, 1997). The dependence of K_d on the S/L ratio was already described in previous studies for the U(VI) sorption onto clay (Joseph et al., 2011) and soils (Zheng et al., 2003), where it was attributed to the calcium carbonate content in the solid. (Zheng et al., 2003) defined a formula to calculate the appropriate S/L ratio for sorption experiments with calcareous soils. If this formula is applied to the present conditions a S/L ratio of at least 7.5 g/L results. In the case of Allard et al. (1982) and Bradbury and Baeyens (2011) an appropriate high S/L ratio was used, but the batch sorption experiments were conducted with different background electrolytes (ionic strength, composition) than applied in the present experiments which has an impact the U(VI) sorption behavior.

By fitting the uranium profile in the clay, about two orders of magnitude lower tortuosities were obtained than by fitting the uranium outflow in the receiving reservoir solution. These lead to two orders of magnitude lower D_e and D_a values which points to a slower U(VI) in-diffusion than out-diffusion in the investigated system. The comparison with literature D_a values (cf. Fig. 15) reveals that the profile fit results are about two orders of magnitude smaller than any reported D_a value for the U(VI) diffusion through bentonite so far, but the outflow fit results agree quite well with the values reported by Idemitsu et al. (1996) and Gaus and Van Loon (2012).

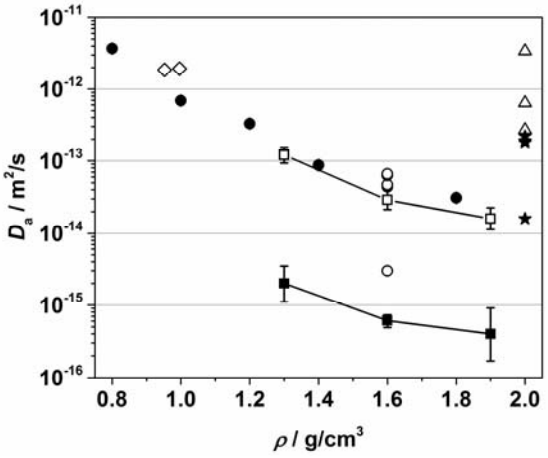

Figure 15. Comparison of D_a values obtained in this study by fitting of the uranium profiles in the MX-80 (■) and the uranium out-diffusion into the receiving reservoir solutions (□) with literature values as a function of dry density: (Δ) (Torstenfelt and Allard, 1986); (●) (Idemitsu et al., 1996); (★) (Ramebäck et al., 1998); (◊) (Wang et al., 2005); (○) (Glaus and Van Loon, 2012). Lines were drawn for visual reasons.

Idemitsu et al. (1996) investigated the uranium diffusion through two bentonite clays (Kunigel V1, Kunipia F) as a function of dry density at pH 8-10 in deionized water for 29-121 days. In Figure 15 only the diffusion results for Kunipia F are shown because its composition is similar to that of MX-80. Glaus and Van Loon (2012) investigated the diffusion through compacted montmorillonite as a function of ionic strength using ^{233}U(VI) as diffusing tracer. The smallest D_a value was obtained at I = 0.1 M $NaClO_4$ and lies close to the profile fit results in the present study. Glaus and Van Loon (2012) interpreted the uranium diffusion behavior under their conditions as “anion-like”. They observed a change in the profile from a sharp decline with strong tailing to a profile with a smaller decrease without tailing with increasing ionic strength which is characteristic for an increase of D_a. The uranium profiles in the present study are

influenced by the natural ^{238}U background. Thus, no clear statement concerning a tailing or rather any "anion-like" diffusion behavior can be made.

Torstenfelt and Allard (1986) studied the U(VI) diffusion through MX-80 for 62 days (artificial groundwater, pH 8.8-9, I = 0.035 M). They also observed a tailing of the ^{233}U profile at higher diffusion distances. They assumed that there are three different U(VI) fractions or species diffusing through the clay and defined a respective D_a value for each species. However, each of their species showed at least a one order of magnitude higher D_a value at 2 g/cm^3 than resulted in the present study at lower dry densities. This difference could be due to a different uranium speciation with a larger fraction of anionic U(VI) species in solution or the applied diffusion set-up.

Rameback et al. (1998) performed a complex long-term diffusion experiment using spent UO_2 fuel as uranium source material. Unfortunately, the temperature was not monitored during the experiment. Although it can be expected that it is elevated due to radioactive decay of the radionuclides present. This would directly affect the U(VI) migration behavior and significantly increase the resulting D_e values. However, their diffusion cells were stopped and the profiles were analyzed at different time points. The first D_a value determined after 3 months of diffusion lies close to one of the D_a values of Torstenfelt and Allard (1986). The longest time period investigated amounted to 74 months (~6 years) which is close to the duration of the diffusion experiment which was conducted in the present study. Rameback et al. (1998) observed that the D_a values decreased with time by about one order of magnitude (cf. Fig. 12) and concluded that the system at shorter time scales may not be in equilibrium. This behavior of diffusing U(VI) could be reflected by the results in the present study. The two orders of magnitude big difference to the D_a values of Rameback et al. (1998) could be a temperature effect. Wang et al. (2005) also performed time-dependent diffusion experiments but at times shorter than a year (maximal 85 days). No decrease of the D_a values was observed. This is an additional indication that the change of D_a with time becomes obvious only in long-term experiments.

The question arises as to what causes this retardation of U(VI) migration within the MX-80. Rameback et al. (1998) proposed consideration of sorption kinetics with regard to surface redox reactions, leading on the longer time scale to surface precipitation of UO_2 and thus to an immobilization of the diffusing tracer. Although in this study the diffusion experiments were conducted under aerobic conditions, a redox reaction within the clay core, for instance, with the Fe(II) species, cannot be ruled out and thus is regarded as one possible retardation scenario. However, we would expect that the reduction of U(VI) to U(IV) would lead to a higher apparent Kd which was not observed in our simulations. Thus, reduction of U(VI) to U(IV) appears to be an unlikely explanation for the lower apparent diffusivities observed here.

Xiong et al. (2014) created a meso-scale model to describe the diffusion of species through porous media and investigated $Ca_2UO_2(CO_3)_3(aq)$ diffusion through bentonite. They obtained similar D_a values as published by Wang et al. (2005). However, they pointed out that the pore space connectivity is dependent on the size and sorption properties of a diffusing species and showed that with progression of the diffusion process, the pore connectivity decreases due to sorption of the diffusing species onto throat walls. In the long-term, as sorption proceeds, this leads to a decrease of the D_a values. Compared to Wang et al. (2005), one order of magnitude smaller K_d values were obtained in this study (cf. Tables 10 and 11), thus the sorption and subsequent blocking of diffusion paths may have a smaller contribution to the retardation process observed in the present study. The work of Singer et al. (2014) confirms experimentally the blocking of pores by sorption. They investigated U(VI) batch sorption and diffusion kinetics in meso-porous silica as a function of time, initial U(VI) concentration, and solution composition (pH, calcium and carbonate presence) and found that the kinetics were strongly concentration-dependent. At c_0(U(VI)) = 1×10^{-5} M, after a particular time point they observed precipitation of a uranium-bearing phase within the silica pores and assumed that the initial diffusion and sorption was thermodynamically

controlled by the aqueous U(VI) speciation, but the subsequent precipitation was kinetically controlled by continuous sorption of the respective U(VI) species near the pore openings which led to a so-called bottle-neck effect. However, at $c_0(U(VI)) = 1\times10^{-6}$ M, the U(VI) concentration also used in the present diffusion study, no precipitation was observed. But does this mean that the formation of a uranium-containing precipitate in the MX-80 pores may not occur? The experiment of Singer et al. (2014) was conducted for 336 h (two weeks) and not for about six years as in the present study. If it is a precipitation reaction with relatively slow kinetics, a blocking of pores would become obvious only in long-term experiments. Thus, it cannot be excluded for the U(VI) diffusion through MX-80 bentonite.

Keller et al. (2015) investigated the evolution of the interparticle pore space of MX-80 used in a long-term (over two years) part-time heated (about one year) experiment. They found that due to the filling of the pore space with a so-called clay-gel or colloidal gel the interparticle porosity of the clay decreased below the percolation threshold for gas. Consequently, the pore connectivity decreased substantially. Thus, gas transport through the interparticle pore space was excluded. However, such a change in porosity and pore connectivity may not only be relevant for gas transport. It also could significantly affect the molecular diffusion of slow-migrating tracers like U(VI).

In the long term, all scenarios described would hinder or even stop the U(VI) diffusion through MX-80 bentonite. Thus, they can be responsible, or at least contribute, to the observed retardation of the U(VI) migration. However, in all cases the leaching or out-diffusion of natural U(VI) would not be affected.

Since the investigation of the in-diffusion of U(VI) delivered diffusion parameter values which are obviously biased by retarding effects, for determination of the Archie's law constants, only the data obtained by fitting the U(VI) out-diffusion were used. In Fig. 16 the relation between D_e(U(VI)) and ε_{eff}(HTO) is plotted and fitted by Archie's law analog using D_w(U(VI)) (cf. Table 6). An empirical constant of 9.7 ± 2.5 for the U(VI) diffusion out of MX-80 bentonite was determined. To the best of the author's knowledge, this is the first time an Archie's law analog constant for the U(VI) / bentonite system is reported.

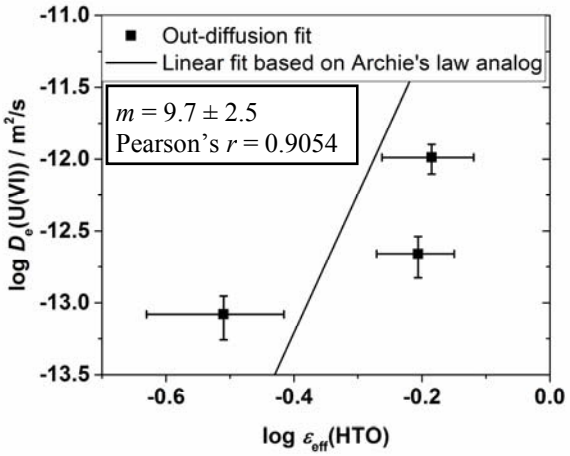

Figure 16. Relation between D_e and ε_{eff} for the U(VI) out-diffusion from MX-80 into the receiving reservoir solution.

Recently, Van Loon (2014) discussed the limits of Archie's law analog by collecting and comparing D_e and respective ε_{eff} values for several diffusing tracers. He found that for $\varepsilon_{eff} \leq 0.1$, the Archie's law analog is not able to describe appropriately the relation between D_e and ε_{eff} for various sedimentary rocks. He

proposed a small variation of Archie's law analog, the so-called extended Archie's law (cf. Eq.29), to reproduce the data and consequently, to predict D_e values also for systems with smaller porosities.

$$D_e = \varepsilon_{eff}^{m1} \cdot D_w + \varepsilon_{eff}^{m2} \cdot B \quad (29)$$

where B, $m1$, $m2$ are empirical factors.

Van Loon (2014) used Eq. (29) to estimate D_e values for various tracers, host rocks, and compacted bentonite. For bentonite a total porosity of 0.36 was assumed, which is close to the ε_{eff} of the MX-80 dry density 1.9 g/cm^3 investigated in this study. The Archie's parameters were defined with $m1 = 2.4$, $m2 = 1.0$ and $B = 1\times10^{-11}$ m^2/s. For U(IV+VI), a neutral diffusing species was assumed, meaning the whole total porosity was accessible for diffusion. Using a D_w value of 7.5×10^{-10} m^2/s, slightly higher than in this study, a D_e value of 6.8×10^{-11} m^2/s was estimated (upper boundary: 1.8×10^{-10} m^2/s; lower boundary: 3.8×10^{-11} m^2/s). This value is over one order of magnitude higher than any D_e value obtained in the current study for the out-diffusion of U(VI). Thus, the extended Archie's law significantly overestimates U(VI) diffusion through compacted bentonite. Either ε_{eff} for U(VI) is substantially smaller, or the extended Archie's law in this form is not applicable to the U(VI) / MX-80 system.

3.4 Conclusions

For a time period of six years, U(VI) diffusion through compacted MX-80 bentonite was investigated as a function of clay dry bulk density (ρ =1.3, 1.6, 1.9 g/cm^3). Speciation calculations revealed that independent of pore water type and water sampling time the $Ca_2UO_2(CO_3)_3$(aq) complex was always the dominant U(VI) species in solution (83-90%). This neutral complex was assumed to be the main diffusing U(VI) species in the system. As effective transport porosity, ε_{eff}, the value for HTO was assumed in the U(VI) diffusion model, although one can expect that ε_{eff}(U(VI)) is smaller than ε_{eff}(HTO) regarding to the size of the molecules and their respective access to the clay interlayers. However, the used value of ε_{eff} has no significant impact on the modeled U(VI) diffusion parameters, since the U(VI) sorption onto the clay is dominating.

Under consideration of the natural uranium background in MX-80 it was estimated that U(VI) diffused about 2 mm, 1 mm, and 0.7 mm deep in the clay at ρ = 1.3, 1.6, and 1.9 g/cm^3, respectively. The distribution coefficients modeled are very low (K_d = 5.8-2.6×10^{-3} m^3/kg). This can be attributed to $Ca_2UO_2(CO_3)_3$(aq) which is known to sorb only weakly onto clay. For the same system, batch sorption experiments were performed using a solid-to-liquid ratio of 2.5 g/L (Nebelung and Brendler, 2009). The K_d values obtained were about one order of magnitude higher than the K_d values of the present study. Probably, the S/L ratio was too small. Such a dependence of K_d on the S/L ratio was previously described for U(VI) sorption onto clay (Joseph et al., 2011). However, the K_d values of the present study differ only by a factor of three from the K_d values published by Glaus and Van Loon (2012) for U(VI) diffusion through compacted montmorillonite in calcareous $NaClO_4$ solutions for I = 0.1 M, 0.5 M, which can be regarded as in very good agreement.

For determination of the apparent U(VI) diffusion coefficient, D_a, two fitting approaches were applied. 1) Fitting of the uranium depth profiles: about two orders of magnitude lower D_a values were obtained than any published D_a value so far, in particular, for "short-term" diffusion studies conducted for less than one year. 2) Fitting of the out-diffusion of natural uranium into the receiving reservoir solution: D_a values are in very good agreement with literature data (Glaus and Van Loon, 2012; Idemitsu et al., 1996). This discrepancy shows that the in- and out-diffusion of U(VI) in MX-80 has to be regarded independently in this study.

The reason for these substantial different results could be a reduction of clay porosity far below the percolation threshold by formation of a clay-gel in the pores after longer time scales as just recently reported for MX-80 (Keller et al., 2015), which leads to a decrease in pore connectivity and would hinder or even stop the through-diffusion of U(VI). However, the out-diffusion or leaching of U(VI) from the clay would still be possible. The experiments show the value of long-term diffusion experiments, since migration determining processes may occur or be visible only at longer time frames. In addition, it shows the excellent retention capacity of bentonite for weakly sorbing U(VI) species.

3.5 Acknowledgements

The authors would like to thank Dirk Falkenberg for manufacturing of the diffusion cells and additives needed for performance of abrasive peeling, Dr. Sina Brockmann for helpful discussions concerning the experimental set-up of the diffusion experiment, Ursula Schaefer, Aline Ritter, Carola Eckardt, and Rachel Lindvall for cation and anion analysis and total organic carbon measurements, Garry Eppich for XRF analysis, Dr. Manja Vogel for plating of the biological contaminants, Carl Steefel from LBNL for helpful advice concerning CrunchFlow modeling, and Peter Rieke from PNNL for setting up the optimization of the COMSOL files. The manuscript was prepared by LLNL under Contract DE-AC52-07NA27344. This work was supported by the Used Fuel Disposition Campaign of the Department of Energy's Nuclear Energy Program and the U. S. DOE Office of Biological & Environmental Sciences, Subsurface Biogeochemistry Research Program. The Helmholtz-Zentrum Dresden-Rossendorf thanks the European Commission (Project NF-PRO under contract C2-ST-C-01) for funding the experiment.

3.6 Appendix

Table A.1. Steps of hydraulic pressure exerted on the MX-80 in the diffusion cells during saturation process.

1.3 g/cm^3		**1.6 g/cm^3**		**1.9 g/cm^3**	
Time period / d	***p* / MPa**	**Time period / d**	***p* / MPa**	**Time period / d**	***p* / MPa**
1	0.4-0.5	1	0.9-1.0	1	0.9-1.0
7	0.7-0.8	2	1.9-2.0	1	1.9-2.0
		21	2.4-2.5	4	2.4-2.5
				0.25	2.9-3.0
				29	3.4-3.5

Table A.2. Filtered volumes of the reservoir solutions for microbial analysis at t = 2401 d..

1.3 g/cm^3	**1.6 g/cm^3**	**1.9 g/cm^3**		**Blank**
source / mL	**source / mL**	**source / mL**	**receiving / mL**	**source / mL**
175 + 125 [a]	200	265	17 [b]	10 [b]

[a] For 18S RNA and 16S RNA analysis, respectively.
[b] Entire solution remaining at the end of the diffusion experiment.

Table A.3. Experimentally determined K_d values for the U(VI) sorption on the stainless steel filter plates, the according log K values for the respective UO_2^{2+} surface complex formed on the filters assumed in the model database, and the resulting capacity factor, α, as a function of clay dry bulk density.

ρ / kg/m^3	**K_d(filter) / m^3/kg**	**log K (>FeOHUO$_2^{2+}$)**	**α (filter)**
1300	0.0008	-0.600915605	3.08
1600	0.0024	-1.096735999	8.99
1900	0.0048	-1.401759154	17.85

Table A.4. Composition of the source reservoir solutions at t = 2401 d (fresh solution) and t = 2457 d of the U(VI) diffusion experiment as well as the main aqueous U(VI) species calculated for the listed conditions.

	1.3 g/cm^3		**1.6 g/cm^3**		**1.9 g/cm^3**	
	***t* = 2401 d**	***t* = 2457 d**	***t* = 2401 d**	***t* = 2457 d**	***t* = 2401 d**	***t* = 2457 d**
***c* / M**						
U [a]	1.3×10^{-6}	1.1×10^{-6}	1.1×10^{-6}	7.8×10^{-7}	1.1×10^{-6}	9.2×10^{-7}
Na [a]	1.8×10^{-1}	1.4×10^{-1}	2.1×10^{-1}	1.6×10^{-1}	2.6×10^{-1}	1.9×10^{-1}
K [a]	2.6×10^{-3}	2.0×10^{-3}	2.9×10^{-3}	2.3×10^{-3}	3.4×10^{-3}	2.7×10^{-3}
Mg [b]	9.6×10^{-3}	7.4×10^{-3}	1.2×10^{-2}	8.9×10^{-3}	1.5×10^{-2}	1.1×10^{-2}
Ca [b]	9.3×10^{-3}	6.9×10^{-3}	9.4×10^{-3}	7.5×10^{-3}	1.2×10^{-2}	8.8×10^{-3}
Sr [a]	7.8×10^{-5}	6.0×10^{-5}	8.3×10^{-5}	6.3×10^{-5}	1.0×10^{-4}	7.8×10^{-5}
Si [a]	1.2×10^{-5}	4.6×10^{-5}	9.5×10^{-6}	4.0×10^{-5}	9.7×10^{-6}	2.2×10^{-5}
Cl^- [c]	1.8×10^{-2}	n.d. [e]	5.9×10^{-2}	n.d.	1.7×10^{-1}	n.d.
SO_4^{2-} [c]	1.0×10^{-1}	n.d.	9.6×10^{-2}	n.d.	7.0×10^{-2}	n.d.
C_{inorg} [d]	8.7×10^{-4}	n.d.	7.4×10^{-4}	n.d.	5.0×10^{-4}	n.d.
F^- [c]	1.9×10^{-4}	n.d.	2.1×10^{-4}	n.d.	1.7×10^{-4}	n.d.
I	0.26	n.d.	0.29	n.d.	0.33	n.d.
Aqueous U(VI) species distribution / % [f]						
$Ca_2UO_2(CO_3)_3$(aq)	87.3	-	86.0	-	89.6	-
$UO_2(CO_3)_3^{4-}$	8.1	-	8.6	-	6.0	-
$MgUO_2(CO_3)_3^{2-}$	2.7	-	3.3	-	2.9	-
$CaUO_2(CO_3)_3^{2-}$	1.1	-	1.1	-		

[a] ICP–MS (error: ±10%)
[b] AAS (error: ±2%)
[c] IC (error: ±3-10%)
[d] TC – TOC (error: ±3%)
[e] n.d. = not determined
[f] only species ≥ 1% shown

Table A.5: Classification of the extracted subsets of 16S rDNA in some of the reservoir solutions at t = 2401 d.

Sequence number	SINA alignment score	Identity [a]	Gene base pairs [b]	Taxonomic classification
Source reservoir 1.3 g/cm^3 (TOC: 30.4 mg/L)				
1	0.995275	99.6617	1478	Bacteria; Actinobacteria; Actinobacteria; Micrococcales; Microbacteriaceae; Microbacterium;
2	0.991891	96.3583	1474	Bacteria; Chlorobi; Chlorobia; Chlorobiales; SJA-28;
3	0.996122	96.2912	1453	Bacteria; Chloroflexi; Anaerolineae; Anaerolineales; Anaerolineaceae; uncultured;
4	0.988642	99.1435	1444	Bacteria; Proteobacteria; Alphaproteobacteria; Rhizobiales; Rhizobiaceae; Rhizobium;
5	0.993977	98.6343	1421	Bacteria; Proteobacteria; Alphaproteobacteria; Caulobacterales; Caulobacteraceae; Brevundimonas;
6	0.916514	84.318	1456	Bacteria; Proteobacteria; Alphaproteobacteria; Rhodospirillales; Rhodospirillaceae; uncultured;
7	0.994048	98.2001	1447	Bacteria; Proteobacteria; Alphaproteobacteria; Sphingomonadales; Sphingomonadaceae; Sphingobium;
Source reservoir 1.6 g/cm^3 (TOC: 71.2 mg/L)				
1	0.994832	96.2888	1480	Bacteria; Acidobacteria; Acidobacteria; Subgroup 4; Family Incertae Sedis; Blastocatella;
2	0.995184	97.1705	1481	Bacteria; Actinobacteria; Actinobacteria; Micrococcales; Microbacteriaceae;
3	0.989163	97.9914	697	Bacteria; Actinobacteria; Actinobacteria; Micrococcales; Microbacteriaceae;
4	0.994939	97.2414	1482	Bacteria; Actinobacteria; Actinobacteria; Micrococcales; Microbacteriaceae;
5	0.99941	97.4465	1481	Bacteria; Actinobacteria; Actinobacteria; Micrococcales; Microbacteriaceae;
6	0.998331	97.3775	1481	Bacteria; Actinobacteria; Actinobacteria; Micrococcales; Microbacteriaceae;
7	0.999058	97.4144	1481	Bacteria; Actinobacteria; Actinobacteria; Micrococcales; Microbacteriaceae;
8	0.99941	97.5155	1481	Bacteria; Actinobacteria; Actinobacteria; Micrococcales; Microbacteriaceae;
9	0.957789	85.9422	1483	Bacteria; Planctomycetes; Planctomycetacia; Planctomycetales; Planctomycetaceae; Planctomyces;
10	0.958302	85.8425	1483	Bacteria; Planctomycetes; Planctomycetacia; Planctomycetales; Planctomycetaceae; Planctomyces;
11	0.959896	85.9422	1483	Bacteria; Planctomycetes; Planctomycetacia; Planctomycetales; Planctomycetaceae; Planctomyces;
12	0.998232	99.2409	1448	Bacteria; Proteobacteria; Alphaproteobacteria; Rhodospirillales;
13	0.996117	94.3515	1442	Bacteria; Proteobacteria; Alphaproteobacteria; Caulobacterales; Caulobacteraceae; Phenylobacterium;

Table A.5 (continued): Classification of the extracted subsets of 16S rDNA in some of the reservoir solutions at t = 2401 d.

Sequence number	SINA alignment score	Identity [a]	Gene base pairs [b]	Taxonomic classification
Source reservoir 1.9 g/cm^3 (TOC: 13.8 mg/L)				
1	0.956615	85.9422	1483	Bacteria; Planctomycetes; Planctomycetacia; Planctomycetales; Planctomycetaceae; Planctomyces;
2	0.978713	96.0358	861	Bacteria; Planctomycetes; Planctomycetacia; Planctomycetales; Planctomycetaceae; Planctomyces;
3	0.959648	85.9422	1483	Bacteria; Planctomycetes; Planctomycetacia; Planctomycetales; Planctomycetaceae; Planctomyces;
4	0.994544	99.1426	1482	Bacteria; Planctomycetes; Planctomycetacia; Planctomycetales; Planctomycetaceae; uncultured;
5	0.987073	97.2678	1478	Bacteria; Planctomycetes; Planctomycetacia; Planctomycetales; Planctomycetaceae; Planctomyces;
6	0.985868	97.1897	1540	Bacteria; Planctomycetes; Planctomycetacia; Planctomycetales; Planctomycetaceae; Planctomyces;
7	0.985091	97.1116	1478	Bacteria; Planctomycetes; Planctomycetacia; Planctomycetales; Planctomycetaceae; Planctomyces;
8	0.996453	99.3103	1448	Bacteria; Proteobacteria; Alphaproteobacteria; Rhodospirillales;
9	0.990316	98.3425	1446	Bacteria; Proteobacteria; Alphaproteobacteria; Rhizobiales; Methylobacteriaceae; uncultured;
10	0.995982	95.7547	861	Bacteria; Proteobacteria; Deltaproteobacteria; Sh765B-TzT-29;
11	0.996177	96.6465	1521	Bacteria; Proteobacteria; Deltaproteobacteria; Sh765B-TzT-29;
12	0.993285	96.3783	1521	Bacteria; Proteobacteria; Deltaproteobacteria; Sh765B-TzT-29;
13	0.992335	96.2441	1528	Bacteria; Proteobacteria; Deltaproteobacteria; Sh765B-TzT-29;
14	0.996864	96.6465	1521	Bacteria; Proteobacteria; Deltaproteobacteria; Sh765B-TzT-29;
15	0.994749	96.5795	1520	Bacteria; Proteobacteria; Deltaproteobacteria; Sh765B-TzT-29;
Receiving reservoir 1.9 g/cm^3 (TOC: 12.4 mg/L)				
1	0.994984	96.4936	1481	Bacteria; Acidobacteria; Acidobacteria; Subgroup 4; Family Incertae Sedis; Blastocatella;
2	0.997053	96.4912	1480	Bacteria; Acidobacteria; Acidobacteria; Subgroup 4; Family Incertae Sedis; Blastocatella;
3	0.991193	96.3583	1474	Bacteria; Chlorobi; Chlorobia; Chlorobiales; SJA-28;
4	0.989999	96.1398	1474	Bacteria; Chlorobi; Chlorobia; Chlorobiales; SJA-28;
5	0.992331	96.4312	1474	Bacteria; Chlorobi; Chlorobia; Chlorobiales; SJA-28;
6	0.987478	97.2678	1478	Bacteria; Planctomycetes; Planctomycetacia; Planctomycetales; Planctomycetaceae; Planctomyces;
7	0.957186	85.9422	1483	Bacteria; Planctomycetes; Planctomycetacia; Planctomycetales; Planctomycetaceae; Planctomyces;

Table A.5 (continued): Classification of the extracted subsets of 16S rDNA in some of the reservoir solutions at t = 2401 d.

Sequence number	SINA alignment score	Identity [a]	Gene base pairs [b]	Taxonomic classification
8	0.988288	97.2678	1416	Bacteria; Planctomycetes; Planctomycetacia; Planctomycetales; Planctomycetaceae; Planctomyces;
9	0.988669	97.3458	1478	Bacteria; Planctomycetes; Planctomycetacia; Planctomycetales; Planctomycetaceae; Planctomyces;
10	0.97735	88.563	1450	Bacteria; Planctomycetes; Phycisphaerae; Phycisphaerales; Phycisphaeraceae; SM1A02;
11	0.984449	97.1116	1478	Bacteria; Planctomycetes; Planctomycetacia; Planctomycetales; Planctomycetaceae; Planctomyces;
12	0.983618	97.1116	1478	Bacteria; Planctomycetes; Planctomycetacia; Planctomycetales; Planctomycetaceae; Planctomyces;
13	0.98784	97.3458	1478	Bacteria; Planctomycetes; Planctomycetacia; Planctomycetales; Planctomycetaceae; Planctomyces;
14	0.998198	99.0997	1444	Bacteria; Proteobacteria; Alphaproteobacteria; Rhodospirillales; Rhodospirillaceae; Ferrovibrio;
15	0.993439	94.8052	1459	Bacteria; Proteobacteria; Alphaproteobacteria; Rhodospirillales; Rhodospirillaceae; uncultured;
Source reservoir blank (TOC: 9.46 mg/L)				
1	0.973816	88.817	1505	Bacteria; Actinobacteria; Thermoleophilia; Gaiellales; uncultured;
7	0.992813	96.9466	1477	Bacteria; Actinobacteria; Acidimicrobiia; Acidimicrobiales; Acidimicrobiaceae; Ilumatobacter;
2	0.979708	97.1066	1477	Bacteria; Actinobacteria; Actinobacteria; Corynebacteriales; Mycobacteriaceae; Mycobacterium;
9	0.985871	96.1273	1474	Bacteria; Actinobacteria; Actinobacteria; Propionibacteriales; Nocardioidaceae;
4	0.991824	96.6019	1461	Bacteria; Chloroflexi; Caldilineae; Caldilineales; Caldilineaceae; uncultured;
3	0.96176	85.8425	1482	Bacteria; Planctomycetes; Planctomycetacia; Planctomycetales; Planctomycetaceae; Planctomyces;
5	0.976667	95.9533	1480	Bacteria; Planctomycetes; Planctomycetacia; Planctomycetales; Planctomycetaceae; Pir4 lineage;
6	0.968724	92.8287	1498	Bacteria; Planctomycetes; Planctomycetacia; Planctomycetales; Planctomycetaceae; Pir4 lineage;
8	0.982095	93.6255	1498	Bacteria; Planctomycetes; Planctomycetacia; Planctomycetales; Planctomycetaceae; Pir4 lineage;
10	0.969645	93.1206	1498	Bacteria; Planctomycetes; Planctomycetacia; Planctomycetales; Planctomycetaceae; Pir4 lineage;

[a] The highest identity the aligned sequence has with any sequence in the alignment seed.

[b] The number of base pairs within the small subunit.

Table A.6. Classification of the extracted subsets of 18S rDNA in some of the reservoir solutions at t = 2401 d.

Sequence number	SINA alignment score	Identity [a]	Gene base pairs [b]	Taxonomic classification
Source reservoir 1.3 g/cm^3 (TOC: 30.4 mg/L)				
1	0.990453	99.3559	621	Eukaryota; Amoebozoa; Discosea; Longamoebia; Centramoebida; Acanthamoeba;
2	0.995935	99.6779	620	Eukaryota; Amoebozoa; Discosea; Longamoebia; Centramoebida; Acanthamoeba;
3	0.976368	96.4093	555	Eukaryota; Archaeplastida; Chloroplastida; Chlorophyta; Trebouxiophyceae;
4	0.970769	96.0503	555	Eukaryota; Archaeplastida; Chloroplastida; Chlorophyta; Trebouxiophyceae;
5	0.976368	96.4093	555	Eukaryota; Archaeplastida; Chloroplastida; Chlorophyta; Trebouxiophyceae;
6	0.881533	79.4816	459	Eukaryota; Excavata; Malawimonas;
7	0.99265	97.2763	549	Eukaryota; Opisthokonta; Nucletmycea; Fungi; Dikarya; Ascomycota; Pezizomycotina; Eurotiomycetes;
8	0.99265	97.2763	549	Eukaryota; Opisthokonta; Nucletmycea; Fungi; Dikarya; Ascomycota; Pezizomycotina; Eurotiomycetes;
9	0.992668	97.0817	549	Eukaryota; Opisthokonta; Nucletmycea; Fungi; Dikarya; Ascomycota; Pezizomycotina; Eurotiomycetes;
10	0.989928	97.4708	549	Eukaryota; Opisthokonta; Nucletmycea; Fungi; Dikarya; Ascomycota; Pezizomycotina; Eurotiomycetes;
11	0.989928	97.4708	549	Eukaryota; Opisthokonta; Nucletmycea; Fungi; Dikarya; Ascomycota; Pezizomycotina; Eurotiomycetes;
12	0.989928	97.4708	549	Eukaryota; Opisthokonta; Nucletmycea; Fungi; Dikarya; Ascomycota; Pezizomycotina; Eurotiomycetes;
13	0.989925	97.2763	549	Eukaryota; Opisthokonta; Nucletmycea; Fungi; Dikarya; Ascomycota; Pezizomycotina; Eurotiomycetes;
14	0.972734	96.7245	549	Eukaryota; Opisthokonta; Nucletmycea; Fungi; Dikarya; Ascomycota; Pezizomycotina; Sordariomycetes; Hypocreomycetidae; Hypocreales;
15	0.99256	98.9796	552	Eukaryota; Opisthokonta; Nucletmycea; Fungi; Dikarya; Ascomycota; Pezizomycotina; Leotiomycetes; Leotiomycetidae;
Source reservoir 1.6 g/cm^3 (TOC: 71.2 mg/L)				
1	0.957817	93.8959	555	Eukaryota; Archaeplastida; Chloroplastida; Chlorophyta; Trebouxiophyceae;
2	0.976368	96.4093	555	Eukaryota; Archaeplastida; Chloroplastida; Chlorophyta; Trebouxiophyceae;
3	0.998402	98.5428	549	Eukaryota; Opisthokonta; Nucletmycea; Fungi; Dikarya; Ascomycota; Pezizomycotina; Eurotiomycetes; Chaetothyriomycetidae; Chaetothyriales;

Table A.6 (continued). Classification of the extracted subsets of 18S rDNA in some of the reservoir solutions at t = 2401 d.

Sequence number	SINA alignment score	Identity [a]	Gene base pairs [b]	Taxonomic classification
5	0.995577	98.1785	549	Eukaryota; Opisthokonta; Nucletmycea; Fungi; Dikarya; Ascomycota; Pezizomycotina; Eurotiomycetes; Chaetothyriomycetidae; Chaetothyriales;
6	0.998402	98.5428	549	Eukaryota; Opisthokonta; Nucletmycea; Fungi; Dikarya; Ascomycota; Pezizomycotina; Eurotiomycetes; Chaetothyriomycetidae; Chaetothyriales;
7	0.992764	98.1785	549	Eukaryota; Opisthokonta; Nucletmycea; Fungi; Dikarya; Ascomycota; Pezizomycotina; Eurotiomycetes; Chaetothyriomycetidae; Chaetothyriales;
8	0.995555	98.5428	549	Eukaryota; Opisthokonta; Nucletmycea; Fungi; Dikarya; Ascomycota; Pezizomycotina; Eurotiomycetes; Chaetothyriomycetidae; Chaetothyriales;
9	0.998402	98.5428	549	Eukaryota; Opisthokonta; Nucletmycea; Fungi; Dikarya; Ascomycota; Pezizomycotina; Eurotiomycetes; Chaetothyriomycetidae; Chaetothyriales;
10	0.98797	97.4708	549	Eukaryota; Opisthokonta; Nucletmycea; Fungi; Dikarya; Ascomycota; Pezizomycotina; Eurotiomycetes;
11	0.998402	98.5428	549	Eukaryota; Opisthokonta; Nucletmycea; Fungi; Dikarya; Ascomycota; Pezizomycotina; Eurotiomycetes; Chaetothyriomycetidae; Chaetothyriales;
12	0.99624	98.3607	549	Eukaryota; Opisthokonta; Nucletmycea; Fungi; Dikarya; Ascomycota; Pezizomycotina; Eurotiomycetes; Chaetothyriomycetidae; Chaetothyriales;
13	0.983933	95.1087	549	Eukaryota; Opisthokonta; Nucletmycea; Fungi; Dikarya; Ascomycota; Pezizomycotina; Sordariomycetes; Hypocreomycetidae; Hypocreales;
14	0.990089	97.8221	550	Eukaryota; Opisthokonta; Nucletmycea; Fungi; Dikarya; Ascomycota; Pezizomycotina; Sordariomycetes; Hypocreomycetidae; Hypocreales;
Source reservoir 1.9 g/cm^3 (TOC: 13.8 mg/L)				
1	0.976368	96.4093	555	Eukaryota; Archaeplastida; Chloroplastida; Chlorophyta; Trebouxiophyceae;
2	0.976368	96.4093	555	Eukaryota; Archaeplastida; Chloroplastida; Chlorophyta; Trebouxiophyceae;
3	0.976368	96.4093	555	Eukaryota; Archaeplastida; Chloroplastida; Chlorophyta; Trebouxiophyceae;
4	0.976368	96.4093	555	Eukaryota; Archaeplastida; Chloroplastida; Chlorophyta; Trebouxiophyceae;

Table A.6 (continued). Classification of the extracted subsets of 18S rDNA in some of the reservoir solutions at t = 2401 d.

Sequence number	SINA alignment score	Identity [a]	Gene base pairs [b]	Taxonomic classification
5	0.973758	96.2298	555	Eukaryota; Archaeplastida; Chloroplastida; Chlorophyta; Trebouxiophyceae;
6	0.97075	96.0503	555	Eukaryota; Archaeplastida; Chloroplastida; Chlorophyta; Trebouxiophyceae;
7	0.973527	96.2298	555	Eukaryota; Archaeplastida; Chloroplastida; Chlorophyta; Trebouxiophyceae;
8	0.976368	96.4093	555	Eukaryota; Archaeplastida; Chloroplastida; Chlorophyta; Trebouxiophyceae;
9	0.987091	97.2763	549	Eukaryota; Opisthokonta; Nucletmycea; Fungi; Dikarya; Ascomycota; Pezizomycotina; Eurotiomycetes;
10	0.993291	98.0072	550	Eukaryota; Opisthokonta; Nucletmycea; Fungi; Dikarya; Basidiomycota; Ustilaginomycotina; Exobasidiomycetes; Exobasidiomycetidae;
11	0.984719	96.036	552	Eukaryota; Opisthokonta; Nucletmycea; Fungi; Dikarya; Basidiomycota;
Receiving reservoir 1.9 g/cm^3 (TOC: 12.4 mg/L)				
1	0.989928	97.4708	549	Eukaryota; Opisthokonta; Nucletmycea; Fungi; Dikarya; Ascomycota; Pezizomycotina; Eurotiomycetes;
2	0.98424	97.0817	549	Eukaryota; Opisthokonta; Nucletmycea; Fungi; Dikarya; Ascomycota; Pezizomycotina; Eurotiomycetes;
3	0.989928	97.4708	549	Eukaryota; Opisthokonta; Nucletmycea; Fungi; Dikarya; Ascomycota; Pezizomycotina; Eurotiomycetes;
4	0.989928	97.4708	549	Eukaryota; Opisthokonta; Nucletmycea; Fungi; Dikarya; Ascomycota; Pezizomycotina; Eurotiomycetes;
5	0.970755	93.4702	553	Eukaryota; SAR; Stramenopiles;
6	0.96952	94.0298	553	Eukaryota; SAR; Stramenopiles;
7	0.970755	93.4702	553	Eukaryota; SAR; Stramenopiles;
8	0.967364	92.7374	553	Eukaryota; SAR; Stramenopiles;
9	0.970755	93.4702	553	Eukaryota; SAR; Stramenopiles;
10	0.970755	93.4702	553	Eukaryota; SAR; Stramenopiles;
11	0.970345	93.8433	553	Eukaryota; SAR; Stramenopiles; Chrysophyceae;
Source reservoir blank (TOC: 9.46 mg/L)				
1	0.951908	95.9742	608	Eukaryota; Amoebozoa; Discosea; Longamoebia; Centramoebida; Acanthamoeba;
2	0 100	621	Eukaryota; Amoebozoa; Discosea; Longamoebia; Centramoebida; Acanthamoeba;	
3	0 100	621	Eukaryota; Amoebozoa; Discosea; Longamoebia; Centramoebida; Acanthamoeba;	

Table A.6 (continued). Classification of the extracted subsets of 18S rDNA in some of the reservoir solutions at t = 2401 d.

Sequence number	SINA alignment score	Identity [a]	Gene base pairs [b]	Taxonomic classification
4	0 100	621	Eukaryota; Amoebozoa; Discosea; Longamoebia; Centramoebida; Acanthamoeba;	
5	0.973563	96.2298	555	Eukaryota; Archaeplastida; Chloroplastida; Chlorophyta; Trebouxiophyceae;
6	0.984804	96.1315	551	Eukaryota; Opisthokonta; Nucletmycea; Fungi; Dikarya; Ascomycota; Pezizomycotina; Eurotiomycetes;
7	0.970213	92.9236	553	Eukaryota; SAR; Stramenopiles;
8	0.970755	93.4702	553	Eukaryota; SAR; Stramenopiles;
9	0.970755	93.4702	553	Eukaryota; SAR; Stramenopiles;
10	0.967749	93.2836	553	Eukaryota; SAR; Stramenopiles;
11	0.970755	93.4702	553	Eukaryota; SAR; Stramenopiles;

[a] The highest identity the aligned sequence has with any sequence in the alignment seed.

[b] The number of base pairs within the small subunit.

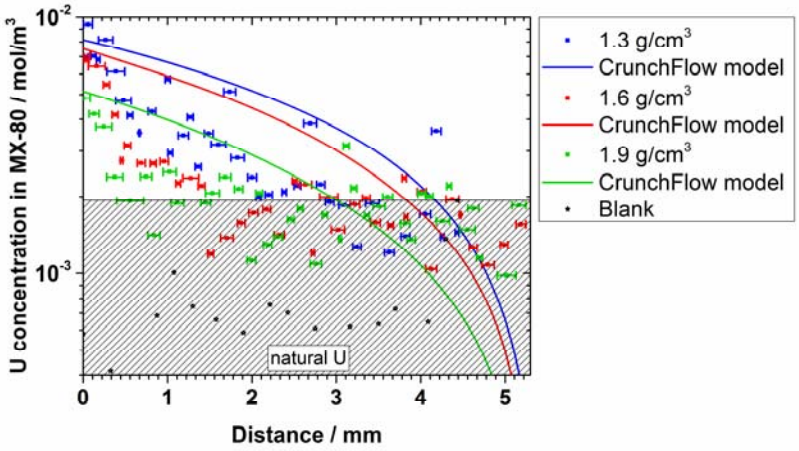

Figure A1. Concentration depth profile of uranium in MX-80 as a function of clay dry density. CrunchFlow model data obtained by fitting the uranium outflow in the receiving reservoir.

4. SORPTION AND DESORPTION OF PLUTONIUM BY BENTONITE

Note: This chapter was originally published in the Journal of Environmental Radioactivity 141 (2015). 106-114.

4.1 Abstract

Understanding plutonium (Pu) sorption to, and desorption from, mineral phases is key to understanding its subsurface transport. In this work we study Pu(IV) sorption to industrial grade FEBEX bentonite over the concentration range 10^{-7}–10^{-16} M to determine if sorption at typical environmental concentrations ($\leq 10^{-12}$ M) is equal to sorption at Pu concentrations used in most laboratory experiments (10^{-7}–10^{-11} M). Pu(IV) sorption was broadly linear over the 10^{-7}–10^{-16} M concentration range during the 120 d experimental period; however, it took up to 100 d to reach sorption equilibrium. At concentrations $\geq 10^{-8}$ M, sorption was likely affected by additional Pu(IV) precipitation/polymerization reactions. The extent of sorption was similar to that previously reported for Pu(IV) sorption to SWy-1 Na-montmorillonite over a narrower range of Pu concentrations (10^{-11}–10^{-7} M). Sorption experiments with FEBEX bentonite and Pu(V) were also performed across a concentration range of 10^{-11}–10^{-7} M and over a 10 month period which allowed us to constrain the slow apparent rates of Pu(V) reduction on a smectite-rich clay. Finally, a flow cell experiment with Pu(IV) loaded on FEBEX bentonite demonstrated continued desorption of Pu over a 12 day flow period. Comparison with a desorption experiment performed with SWy-1 montmorillonite showed a strong similarity and suggested the importance of montorillonite phases in controlling Pu sorption/desorption reactions on FEBEX bentonite.

4.2 Introduction

Permanent interment in a deep geological repository is seen as the most viable option for radioactive waste disposal in many countries with a civilian nuclear fuel program (Iaea, 1995). Conceptually, the repository scenario comprises a geological barrier (host rock) combined with engineering barriers that aim to contain the radionuclides until they have decayed below harmful levels. The waste itself will likely be contained in steel canisters surrounded by a layer of compacted clay. The efficacy of this disposal option is related to its capacity to confine radioactivity and isolate it from the biosphere (Dozol et al., 1993).

Due to its swelling properties, plasticity, ion exchange and sorption behavior, and sealing capability, bentonite is considered a good candidate for backfill material (Guven, 1990). Traditionally, the term bentonite refers to aluminum phyllosilicate clays derived from the devitrification and chemical alteration of glassy volcanic ash or tuff (Ross and Shannon, 1926). However, the term has been used to describe smectite-rich materials, regardless of origin (Grim, 1968). The smectite mineral group includes a number of 2:1 layer silicates, the most common of which is montmorillonite. Montmorillonites constitute a large proportion of bentonite mineralogy (65-90 wt %) with the result that the two names are often used synonymously, although the former is a clay mineral and the latter a clay rock (Grauer, 1986). Montmorillonite can display significant morphological and chemical differences depending on its provenance (Guven, 1988).

ENRESA, the body responsible for the management of Spanish radioactive waste, has proposed FEBEX bentonite from Cortijo de Archidona in Almeria, Spain for use in its repositories. As a result, the physiochemical properties of this clay rock have been well studied, particularly in an

extensive experimental program performed at the National Cooperative for the Disposal of Radioactive Waste's (Nagra) Grimsel Test Site in Switzerland. The FEBEX bentonite has a high smectite content (93 ± 2 %) with quartz (2 ± 1%), plagioclase (3 ± 1 %), cristobalite (2 ± 1 %), potassium feldspar, calcite and tridymite as accessory minerals (Missana et al., 2004). The less than 2 μm fraction (after Ca homoionization) of this bentonite is composed of >99% smectite with the structural formula: $(Si_{7.78}Al_{0.22})(Al_{2.78}Fe^{3+}_{0.33}Fe^{2+}_{0.02}Ti_{0.02}Mg_{0.81})O_{20}(OH)_4(Ca_{0.50}Na_{0.08}K_{0.11})$ (Fernandez et al., 2004).

Due to their long half-lives and toxicity, the isotopes ^{239}Pu (2.41×10^4 y) and ^{240}Pu (6.56×10^3 y) are expected to contribute significantly to the total hazardous inventory in a waste repository scenario (Schwenk-Ferrero, 2013). Despite several decades of study, our understanding of how Pu migrates in subsurface environments is far from complete due to the wide array of factors which can significantly influence its mobility. These include Pu redox processes (Choppin, 1991; Sanchez et al., 1985), colloid-facilitated transport processes (Kersting et al., 1999; Novikov et al., 2006), solubility effects (Efurd et al., 1998; Neck et al., 2007c), sorption/desorption rates and affinities for natural mineral surfaces (Powell et al., 2004; Zavarin et al., 2012), and interactions with natural organic matter (including bacteria) (Icopini et al., 2009; Zhao et al., 2011). Pu exhibits a complex redox chemistry in natural waters with four oxidation states (VI, V, IV, III) potentially stable and with each oxidation state displaying a unique solubility (Neck et al., 2007c) and mineral sorption affinity (Begg et al., 2013; Keeney-Kennicutt and Morse, 1985; Sanchez et al., 1985; Silva and Nitsche, 1995). Pu(IV) and Pu(V) are the more common species under mildly oxic environmental conditions and also represent the oxidation states with the lowest (Pu(V)) and highest (Pu(IV)) affinities for mineral surfaces (Choppin, 2007; Kaplan et al., 2007; Silva and Nitsche, 1995).

Mineral-colloid facilitated transport is thought to be a significant contributor to Pu migration in the subsurface (Kersting et al., 1999; Novikov et al., 2006; Santschi et al., 2002). One of the concerns with the use of bentonite as a backfill material in a repository is that it can form colloids, which may enhance the migration of radionuclide species that are sorbed to them (Geckeis et al., 2004). As a result, attention has been focused on the interaction between Pu and bentonite colloids (Huber et al., 2011; Missana et al., 2008). Previous work on FEBEX bentonite has shown that colloids with a hydrodynamic size of 250 ± 50 nm have an XRD pattern consistent with an aluminum-rich dioctahedral smectite with no significant impurities (Missana et al., 2004).

The sorption of Pu species to Khakassiya bentonite and SWy-1 montmorillonite has been found to exhibit pH and ionic strength dependency, indicating that both ion-exchange and surface complexation processes are occurring (Sabodina et al., 2006; Zavarin et al., 2012). However, surface complexation processes will dominate at neutral to alkaline pHs. Smectite minerals have been shown to have a high sorption affinity for Pu. For example, Pu(V) partitioning to Yucca Mountain tuffs found a ubiquitous and preferential association of Pu with smectite minerals (Vaniman et al., 1995). Further, Pu(IV) K_d values from 10,000 to 40,000 mL g^{-1} have been reported for smectite-rich sediments from Lithuania in the pH range 5 to 12 (Lujaniene et al., 2007). Missana et al. (2008) studied the sorption of Pu(IV) to FEBEX bentonite *colloids* (>99% smectite) at pH 9.5 and reported log K_d values of 5.37 ± 0.18. Pu(IV) sorption to FEBEX bentonite *colloids* under anaerobic conditions at pH 9.6, resulted in log R_d values (a term equivalent to K_d but without the assumption of equilibrium) of 5 and 5.9 after one and three weeks of sorption time, respectively (Nagra, 2006). The increase in R_d values with time was attributed to the presence of a small amount (~ 5 %) of Pu(VI) in the spike solution which was slowly reduced to Pu(IV) on the mineral surface (Nagra, 2006).

In a recent study, we examined the long term sorption behavior of Pu(IV) and Pu(V) on SWy-1 Na-montmorillonite under aerobic conditions. After 30 d equilibration, calculated log K_d values for Pu(IV) and Pu(V) were 4.25 ± 0.15 and 3.57 ± 0.18, respectively (Begg et al., 2013). However, following one year of equilibration, calculated log K_d values in the Pu(V) experiments had increased to 4.32 ± 0.15, similar to those calculated for Pu(IV) after 30 d. The convergence of K_d values for Pu(IV) and Pu(V) was attributed to the slow reduction of Pu(V) on the montmorillonite surface causing increased uptake of Pu(V). This finding highlights the need to ensure that experimental studies used to inform predictive transport models accurately encapsulate long term environmental behaviors.

Several recent studies have indicated that actinide concentration can affect their sorption to mineral surfaces (Hixon and Powell, 2014; Missana et al., 2008; Snow et al., 2013). In the case of Pu(IV), its low solubility at circumneutral pH means that sorption may demonstrate an apparent concentration dependence as solubility limits are reached. For example, the study of Pu(IV) sorption to bentonite colloids (>99% smectite) observed that sorption was linear for initial Pu concentrations of $1 \times 10^{-8} – 1 \times 10^{-7}$ M but at higher concentrations precipitation of Pu was evidenced by a sharp increase in the isotherm slope (Missana et al., 2008). Concentration dependent sorption behavior may also be observed at low actinide concentrations: work with goethite and Np(V) found that K_d values differed by an order of magnitude at solution concentrations below 10^{-11} M compared to higher concentrations. This behavior was attributed to the existence of different adsorption sites on the mineral with different adsorption affinities for Np (Snow et al., 2013). These examples of concentration dependent behavior of actinides indicate that there may be a difference between the sorption behavior of Pu at the concentrations found in contaminated subsurface waters (10^{-12}–10^{-20} M) (Dai et al., 2005; Kersting et al., 1999; Novikov et al., 2006; Penrose et al., 1990) and concentrations typically used in laboratory experiments (10^{-7}–10^{-11} M Pu). Although a primary assumption of reactive transport models, the validity of extrapolating Pu-mineral sorption behavior from relatively high concentration laboratory experiments to the low concentrations found in many field settings has not been widely tested.

Pu desorption reactions have been far less well studied than sorption reactions. This is problematic because application of thermodynamic equilibrium parameters in field transport models which incorrectly represent desorption processes are likely to be flawed (Artinger et al., 2002). One of the pertinent issues for Pu, especially given the evidence that its mobility may be enhanced by mineral-colloid facilitated transport, is whether there is equality in sorption and desorption behavior (Kersting et al., 1999). Differences in behavior may be caused by aging processes, hysteresis effects, and irreversible sorption, amongst others (Tinnacher et al., 2011). A study of Pu(IV) sorption to Callovo-Oxfordian argillite found that after seven days' desorption, Pu K_d values were of the same order of magnitude as they were following a seventy four day adsorption period, indicating sorption reversibility (Latrille et al., 2006). Similarly, Lu et al. (2003) investigated Pu interaction with montmorillonite and found that with a 20 day adsorption period and a 32 day desorption period, similar K_d values were obtained for both adsorption and desorption steps.

The aim of the current work is two-fold: to provide information on Pu sorption/desorption to/from industrial grade FEBEX bentonite, a potential repository backfill material, and to determine if the linearity observed for Pu(V) sorption to a pure Na-montmorillonite (Begg et al., 2013) extends to Pu(IV) sorption to a multi-component clay rock material. We investigate the sorption behavior of Pu(IV) to FEBEX bentonite across a wide range of initial concentrations (10^{-7}–10^{-16} M) over a 120 d period. In addition, we perform long term (10 month) sorption experiments with Pu(V) to compare with the slow apparent rates of reduction previously observed for Pu(V) on

montmorillonite (Begg et al., 2013). The results of these experiments demonstrate the apparent control that the montmorillonite component in bentonite exerts on the sorption behavior of Pu, provides long term sorption data for industrial grade FEBEX bentonite, and validates the extrapolation of Pu(IV) experiments performed at concentrations of 10^{-9}–10^{-11} M Pu to much lower concentrations typically found in the environment at timescales relevant for groundwater transport.

4.3 Materials and Methods

4.3.1 Bentonite Preparation

Unless stated otherwise, all solutions were prepared using ultrapure water (Milli-Q Gradient System, >18 MΩ·cm) and ACS grade chemicals without further purification. The FEBEX bentonite was ground in a mortar and pestle and sieved to <63 μm to minimize clay heterogeneity. The clay was then homo-ionized in 1 M NaCl solution for 7 days and dialyzed in MQ H_2O to remove excess salts. As experiments were performed to characterize the behavior of Pu in the presence of bulk bentonite, no further treatment was performed. A portion of the bentonite suspension was dried, the clay lightly ground, and its surface area measured (N_2(g)-BET Quadrasorb SI). The surface area of the prepared bentonite was 25.2 ± 1.0 m^2 g^{-1}.

The solids were re-suspended in a 0.7 mM $NaHCO_3$/5 mM NaCl buffer solution (pH 8) to make a suspension with a bentonite concentration of ~ 5 g L^{-1}. This buffer solution was chosen so as to allow comparison with previous experiments performed with SWy-1 Na-montmorillonite (Begg et al., 2013). Gravimetric analysis of the dried mass of the solid in triplicate 5 mL aliquots of the suspension returned a standard error of 1.2%, indicating homogeneity in the stock suspension and providing confidence in the amount of solid added to experiments. The stock suspension was allowed to equilibrate under aerobic conditions for several days prior to the start of sorption experiments.

4.3.2 Pu Stock Solutions

Three different Pu stock solutions were used in the sorption experiments in order to facilitate measurement over the wide range of Pu concentrations investigated. A ^{242}Pu stock (15.8% ^{238}Pu, 5.1% $^{239+240}$Pu, 79.1% ^{242}Pu by activity) and a ^{238}Pu stock (98.8% ^{238}Pu, 0.11% ^{241}Pu, and 0.1% ^{239}Pu by activity) were used in experiments with initial concentrations of 10^{-7}–10^{-11} M. A New Brunswick Laboratory (NBL) Pu reference material CRM-137 (33.5% ^{238}Pu, 35.3% ^{239}Pu, 31.3% ^{240}Pu by activity) was used in experiments with initial Pu concentrations ≤ 10^{-11} M. A table of the different stocks used, including their oxidation state, where measured, is given in the Appendix Table A1.

The Pu stock solutions were purified using anion exchange resin (BioRad AG 1 × 8, 100-200 mesh) pre-conditioned with 8 M HNO_3. Prior to loading on the resin, Pu was reacted with $NaNO_2$ to reduce it to Pu(IV). The Pu was loaded on the resin in 8 M HNO_3, washed with 3 column volumes of 8 M HNO_3, and then eluted in 1 M or 0.1 M HCl (Powell et al., 2011). For experiments using Pu(IV), the oxidation state of the Pu stocks was checked with a LaF_3 precipitation method (Kobashi and Choppin, 1988) and found to be > 92% Pu(III)/(IV) (Table A1). Subsequent stock dilutions were made using 0.1 M HCl, with select analysis indicating that this did not significantly alter the oxidation state of the Pu. For experiments starting with Pu(V), the Pu(IV) stripped from the columns was converted to Pu(VI) either electrochemically (^{242}Pu stocks) or by heating in HNO_3 (^{238}Pu stocks), adjusting to pH 3 with NaOH, spiking with 0.05 M hydrogen peroxide and gently heating to produce Pu(V). To remove any Pu(VI) remaining in

solution, the stocks were diluted in 0.7 mM $NaHCO_3$/5 mM NaCl buffer solution to achieve a circumneutral pH and contacted with 10 g/L high surface area SiO_2, which will preferentially adsorb Pu(VI), before being phase separated for use in experiments (Orlandini et al., 1986). Pu(V) stocks were <3% Pu(III)/(IV) by LaF_3 precipitation. Final Pu concentration in the stock solutions was determined by liquid scintillation counting (LSC; Packard Tri-Carb TR2900 LSA and Ultima Gold cocktail).

4.3.3 Plutonium Batch Sorption Experiments

Sorption experiments were performed over a wide range of initial Pu(IV) concentrations (10^{-7}–10^{-16} M). In the following description we use the nominal terms *high concentration* to refer to experiments initially spiked to Pu concentrations of 10^{-7}–10^{-11} M and *low concentration* for experiments initially spiked to Pu concentrations of 10^{-11}–10^{-16} M. The two types of experiments were performed in separate laboratories in order to minimize any potential contamination of the *low concentration* samples.

All Pu(IV) and Pu(V) batch sorption experiments were performed under air in 0.7 mM $NaHCO_3$/5 mM NaCl buffer solution (pH 8) with 1 g L^{-1} FEBEX bentonite. These experimental conditions were chosen to achieve consistency with previous experiments using SWy-1 Na-montmorillonite (Begg et al., 2013). Pu(IV) and Pu(V) aqueous speciation for initial Pu concentrations of 10^{-10} M in the buffer solution were calculated using the Geochemist's Workbench family of codes and thermodynamic data from Guillaumont et al. (2003a). The results are shown in Appendix Figure A1. Batch experiments were conducted in either 50 mL Nalgene Oak Ridge polycarbonate centrifuge tubes (*high concentration*) or 500 mL Nalgene bottles (*low concentration*). Higher volumes were required in *low concentration* experiments to achieve the low detection limits afforded by accelerator mass spectrometry (AMS). Pu(IV) sorption experiments were performed at *low concentrations* and *high concentrations*, while Pu(V) experiments were performed only at *high concentrations*. For Pu(IV) experiments, where the Pu stock was in 0.1 M HCl, dilute NaOH was added to the samples immediately prior to spiking in order to neutralize the acidity associated with the Pu(IV) spike. This was not necessary for Pu(V) experiments where the pH of the stock was circumneutral. Bentonite blanks (with no Pu) and Pu spiked blanks (with no bentonite; select concentrations) were run in parallel. The results of the mineral free experiments are included in the Appendix. The pH of each experiment was checked (Orion 920A with calibrated electrode) and adjusted to pH 8.0 ± 0.2 using dilute NaOH or HCl within 10 minutes of spiking. Measurement of pH over the course of the experiments indicated that the drift in pH was less than 0.2 pH units. Samples were placed on an orbital shaker at 125 rpm at room temperature for the duration of the experiment. Experiments were kept in the dark in order to minimize photo-catalyzed reactions that may directly or indirectly affect the redox speciation of Pu (Mccubbin and Leonard, 1996; Powell et al., 2005).

At each time point, samples were centrifuged to achieve a 50 nm size cut off. No further attempts at size fractionation were made. We note that centrifugation can potentially remove not only Pu sorbed on bentonite but also any Pu precipitates with a particle size greater than 50 nm. Thus, the apparent sorption determined based on centrifugation could, in fact, represent a combination of Pu sorption, Pu precipitation, as well as Pu surface precipitation on the bentonite particle surfaces. However, in the *low concentration* experiments, we consider the formation of Pu precipitates/polymers to be thermodynamically unfavorable. For *high concentration* samples, aliquots of both the suspension and the supernatant were removed and counted via LSC. In *low concentration* experiments, aliquots of supernatant were acidified to 2% HNO_3 and analyzed using AMS (10-MeV tandem accelerator at the Center for Accelerator Mass Spectrometry

(CAMS), Lawrence Livermore National Laboratory, CA). AMS is an ultra-sensitive analytical technique that can quantify long-lived radionuclides at ultra-low concentrations and routinely achieves instrumental backgrounds of 10^5 atoms for actinide elements (Marchetti et al., 2005). AMS analysis has been reported previously and included isotope dilution using a non-isobarically interfering isotope of ^{242}Pu (99.99% ^{242}Pu) (Marchetti et al., 2005).

4.3.4 Plutonium Desorption Flow Cell Experiments

A stirred flow cell experiment was performed at pH 8 to examine the desorption of Pu(IV) from bentonite. The flow cell set up was similar to that described previously for Np(V) and goethite and Pu(IV) and goethite (Begg et al., 2014; Tinnacher et al., 2011). The flow cell was made of Teflon®, with a 20 mL hemispherical chamber and fitted with a 100 nm pore size Millipore polycarbonate filter. A diagram of the flow cell is shown in Appendix Figure A2. Prior to use, the cell was washed with 10% HCl and MQ water. To sorb Pu on the clay, Pu(IV) at 3×10^{-10} M was equilibrated with 1 g L^{-1} bentonite for 21 days. After this equilibration period, an aliquot of the spiked suspension was centrifuged (25 000 × *g*, 2 h; 50 nm cut-off) and the concentration of the Pu in the supernatant measured. A 20 mL aliquot of bentonite suspension was loaded into the flow cell with a stir bar included to ensure ideal mixing conditions. In previous flow cell work with SWy-1 Na-montmorillonite, ^{3}H was used as a conservative tracer to test if ideal mixing conditions existed. A plot of the decline in ^{3}H concentration and a theoretical non-reactive species is shown in Appendix Figure A3. The similarity between the calculated and observed curves demonstrates that the flow cell experiment is ideally mixed when the stir bar is operational.

Atmosphere-equilibrated, Pu free, 0.7 mM $NaHCO_3$/5 mM NaCl buffer solution at pH 8 was flowed through the cell at an initial rate of 0.4 mL min^{-1} (average retention time of ~ 50 minutes). Effluent fractions were collected on a Spectra/Chrom CF-1 fraction collector and the volumes determined gravimetrically. Periodic pH measurements of the effluent were performed to ensure that the experiment remained at pH 8. Collected fractions were acidified with 2% HNO_3 prior to Pu analysis. Pu concentration in the effluent fractions was determined via liquid scintillation counting. The total timescale of the flow cell experiment was 12 days.

4.4 Results and Discussion

4.4.1 Pu(IV) Sorption to Bentonite

The sorption of Pu(IV) to bentonite was studied over an initial Pu concentration range of 10^{-7}–10^{-16} M. The resulting sorption isotherm after 120 d equilibration is shown in Figure 17. To determine if sorption equilibrium was achieved in the experiment, samples at 10^{-10} and 10^{-7} M were sampled after 67 d, 100 d and 120 d. The results of this sampling are shown in the inset in Figure 17. The similarity in the aqueous Pu concentrations at 100 d and 120 d versus 67 d indicate that sorption equilibrium was reached by 120 d. The slow approach to sorption equilibrium is consistent with previous studies on Pu(IV) sorption to clay and may reflect the presence of small amounts of Pu(V) in the initial stock solution, although we cannot discount other aging processes such as Pu polymerization/precipitation reactions, particularly in the higher concentration sample (Begg et al., 2013; Nagra, 2006). Furthermore, unintended changes in Pu oxidation state may be exacerbated when an acidic Pu(IV) stock is spiked into a circumneutral pH solution under oxic conditions. In the Appendix, Figure A4 shows oxidation state analysis of a parallel experiment where a mineral-free, pH 8 solution was spiked with a >97% Pu(III)/(IV) stock solution (4.48×10^{-7} M) to a concentration of 3×10^{-10} M. Both LaF_3 and solvent extraction analysis of the aqueous Pu indicate that 1 h after spiking, approximately 30% of the Pu(III)/(IV) had been oxidized to Pu(V)/(VI). LaF_3 analysis over 6 d showed no appreciable change in Pu

oxidation state from the 1 h values while no significant Pu was lost from solution over this short time period.

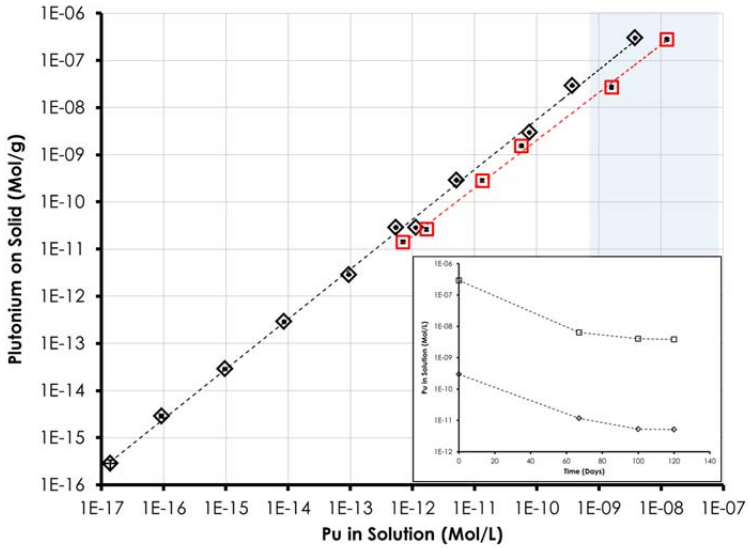

Figure 17. 120 d Pu(IV) sorption isotherm for FEBEX bentonite (1 g L^{-1}) in 0.7 mM $NaHCO_3$, 5 mM NaCl buffer solution at pH 8 (black diamonds). Inset shows time series data for experiments at 10^{-7} and 10^{-10} M initial Pu(IV) to indicate apparent adsorption equilibrium at 120 d. Also shown are data for 30 d Pu(IV) adsorption isotherm for SWy-1 Na-montmorillonite (1 g L^{-1}) in 0.7 mM $NaHCO_3$, 5 mM NaCl buffer solution at pH 8 (red squares) (Begg et al., 2013). Lines are shown to guide the eye only. Blue shaded area represents expected concentration for Pu(IV) colloid formation (Neck et al., 2007c). Error bars based on LSC counting uncertainties (1σ) for bentonite experiments and 1σ for quadruplicate montmorillonite experiments are within range of the symbols used.

After 120 d equilibration, the sorption of Pu(IV) to bentonite was broadly linear over the ten orders of magnitude concentration range tested (Figure 17). Our result shows that on timescales of months, Pu(IV) exhibits similar apparent sorption behavior to bentonite at the higher concentrations used in typical laboratory experiments (10^{-7}–10^{-11} M) as it does at concentrations typically found in contaminated environments (≤10^{-12} M). This result complements previously published linear sorption behavior observed for Pu(V) on SWy-1 Na-montmorillonite over a similar Pu concentration range (Begg et al., 2013). A log-log slope for Pu(IV) sorption to bentonite was calculated and found to be 1.06 ± 0.01 (1 S.E.). A value greater than 1 suggests that surface precipitation (or, indeed, bulk precipitation in our case) of Pu may be occurring (Dzombak and Morel, 1993). The expected concentration range for Pu(IV) intrinsic colloid formation at pH 8 is highlighted in blue in Figure 1 (Neck et al., 2007c). The highest two concentrations used in the current isotherm experiment fall within the expected range for Pu(IV) colloid formation (Neck et al., 2007c). Thus the isotherm slope, in combination with the known solubility of Pu(IV) suggest that surface polymerization/precipitation/surface precipitation processes are occurring in the two highest Pu concentration samples (initial Pu(IV) 10^{-7} and 10^{-8} M) (Neck et al., 2007c). This is consistent with Pu-goethite sorption data of Kersting et al. (2011) that exhibited substantial Pu precipitation effects only above 10^{-8} M Pu. Although the effects of precipitation/polymerization appear to be relatively small when examined across 10 orders of magnitude in Pu concentration and on a log scale, they may nonetheless affect the

sorption behavior of Pu. Accordingly, we recommend that future experiments investigating Pu(IV) environmental *ad*sorption behavior are performed at concentrations $<10^{-9}$ M.

As the isotherm slope is close to unity, sorption can be considered Langmuirian in behavior. However, unlike traditional Langmuir plots which exhibit a flattening of the isotherm as mineral surface sites become saturated, the data remain largely linear at higher concentrations. Previously, Missana and Garcia-Gutierrez (2007) calculated the strong site concentration on bentonite colloids to be 6.1×10^{-8} mol m^{-2}. Given that the experiments were performed with 1 g L^{-1} clay with a surface area of 25 m^2 g^{-1} this would suggest a strong site concentration of 1.54×10^{-6} mol L^{-1} which exceeds the highest Pu concentration used (10^{-7} M). As a result, strong site saturation effects are not expected or observed in our experiments. Indeed, we suggest that polymerization/precipitation/surface precipitation effects will become prominent before saturation of strong sites occurs.

Previous work with Pu(IV) and hematite has identified a concentration dependence to the rate of Pu(IV) sorption over a 2 d period (Romanchuk et al., 2011). A one-step, fast adsorption was seen in experiments with 10^{-14} M Pu compared to a two-step adsorption (fast initial sorption followed by slower uptake) at 10^{-10} M Pu. The fast sorption step was attributed to the adsorption of monomeric Pu(IV) while the slower step was hypothesized to be caused either by diffusion to micropores in the mineral or by the formation of polymeric Pu(IV) species (Romanchuk et al., 2011). Our current work with clays indicates that regardless of initial sorption rates, the apparent extent of Pu(IV) sorption to bentonite appears broadly independent of initial concentration for the 10^{-7}–10^{-16} M range on timescales relevant to groundwater transport scenarios. However, some small signs of Pu precipitation are present in our highest concentration samples and the importance of such reactions is acknowledged.

Log K_d values from the Pu(IV) bentonite sorption isotherm at 120 d range from 4.3 – 4.9 mL/g. There was a slight increase in calculated log K_d values as a function of Pu(IV) concentration. We attribute this to Pu(IV) intrinsic colloid formation and/or other precipitation processes at the higher concentrations, as discussed previously, rather than the result of concentration-dependent, high sorption affinity sites on the clay (that would exhibit an inverse relationship between K_d and Pu(IV) concentration). The log K_d values observed in this experiment are lower than values for Pu(IV) sorption to bentonite colloids of 5-5.9 measured by Geckeis et al. (2004) and 5.39 ± 0.18 measured by Missana et al. (2008). However, these previous experiments were performed at pH 9.5 – 9.6, used bentonite colloids of ~200 - 280 nm (which are expected to be entirely composed of montmorillonite) and were performed under anaerobic conditions (Huber et al., 2011). The K_d values observed here likely reflect the contribution of Pu(V), which sorbs weakly to montmorillonite and reduces slowly to Pu(IV) under aerobic conditions (Zavarin et al., 2012). Anaerobic conditions expected in certain repository scenarios are likely to promote greater Pu(IV) stability relative to the aerobic conditions examined herein.

Also shown in Figure 17 is the 30 d sorption isotherm for Pu(IV) on SWy-1 Na-montmorillonite previously reported in Begg et al. (1982). Comparison of the Pu(IV) sorption isotherms for montmorillonite and bentonite shows they are very similar in terms of slope and the extent of Pu sorption. These results show that Pu sorption by a bulk bentonite (92% montmorillonite) is comparable to sorption to pure montmorillonite. However, a slightly higher sorption affinity of Pu(IV) for bentonite than montmorillonite is observed and is more marked at the two highest Pu concentrations. Given that the current work suggests that sorption equilibrium is not achieved until after 67 d (Figure 17 inset), we suggest that this difference is in part due to the different equilibration period in the two experiments: 30 d for montmorillonite and 120 d for bentonite.

Indeed, interpolation of bentonite K_d values for the experiment at 10^{-10} M Pu(IV) suggests a 30 d log K_d of 4.1 compared to 4.3 in the equivalent montmorillonite experiment.

4.4.2 Pu(V) Sorption to Bentonite

The sorption rate of Pu(V) to FEBEX bentonite was studied in triplicate over a 30 day period using an initial concentration of 10^{-10} M (Figure 18). Also plotted in Figure 18 is the sorption of Pu(V) to SWy-1 Na-montmorillonite at an initial concentration of 10^{-9} M reported previously (Begg et al., 2013). Both sorption plots show a similar time dependence, suggesting that the montmorillonite component of the bentonite controls the sorption of Pu(V). The sorption of Pu(V) by bentonite shows an initial rapid uptake with 49.5% ± 0.7 % removed in the first 48 h. This is followed by a slower uptake over the rest of the experiment with 13.4 ± 1.6 % Pu remaining in solution at 30 d. Applying the first order rate model previously used to describe Pu(V) sorption to SWy-1 montmorillonite to the bentonite-Pu(V) sorption data leads to a surface area normalized sorption rate of $10^{-3.5}$ L m^{-2} h^{-1} which compares quite favorably with $10^{-2.8}$ L m^{-2} h^{-1} calculated for montmorillonite (Begg et al., 2013).

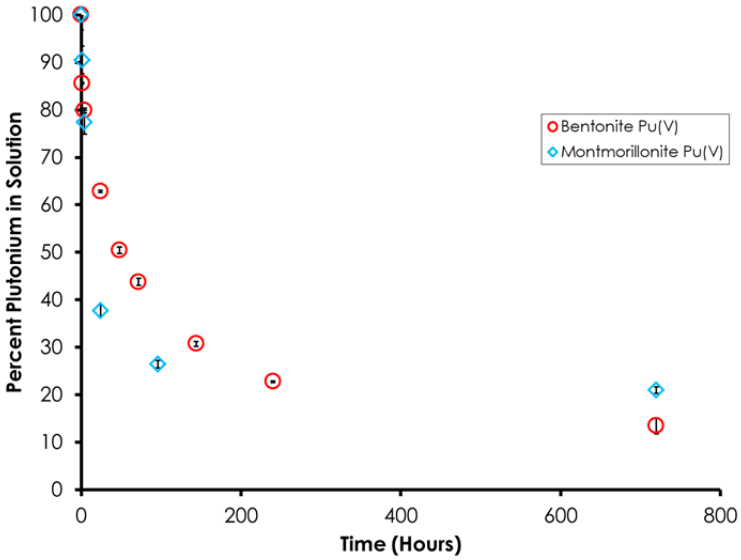

Figure 18. Sorption of Pu(V) to FEBEX bentonite (1 g L^{-1}; red circles) and SWy-1 Na-montmorillonite (1 g L^{-1}; blue diamonds) plotted as percentage of Pu removed from solution vs time. Initial Pu concentrations were 10^{-10} M for bentonite and 10^{-9} M for montmorillonite. Error bars based on 1σ for triplicate bentonite experiments and 1σ for quadruplicate montmorillonite experiments.

The long-term (greater than 30 d) sorption of Pu(V) to bentonite was also studied over an initial concentration range of 10^{-7}–10^{-11} M Pu. Samples were analyzed after 30, 120 and 300 d. At 30 days, the isotherm appears linear on a log-log plot with slope of 0.92 ± 0.03 (Figure 19). However, the slope of 0.92 indicates that sorption is, in fact, non-linear and appears to exhibit a Freundlich behavior (i.e. $S = K_f C^n$ with n = 0.92). However, as these data do not reflect an equilibrium state and sorption is affected by surface mediated reduction rates, the apparent non-linearity most likely reflects a concentration dependence on the surface mediated reduction of Pu(V). This is consistent with the findings of Hixon and Powell (2014) who observed a concentration rate dependence for Pu(V) reduction on hematite between 10^{-8} and 10^{-6} M. At 120

d, the isotherm is truly linear with a log-log slope of 1.03 ± 0.03. Further, the position of the isotherm has shifted between the two time points, indicating that sorption of Pu from the aqueous phase has continued over the time period between 30 d and 120 d. At 300 d, the isotherm is linear (1.02 ± 0.001), with a further small shift in position relative to the 120 d isotherm.

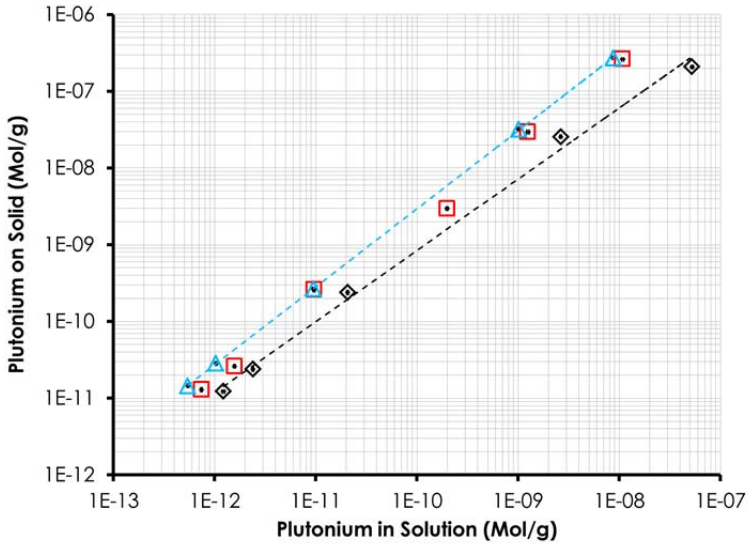

Figure 19. Pu(V) sorption isotherm for FEBEX bentonite (1 g L^{-1}) in 0.7 mM $NaHCO_3$, 5 mM NaCl buffer solution at pH 8. Different symbols represent sampling at different time points: 30 d (black diamonds), 120 d (red squares), 300 d (blue triangles). Lines are to guide the eye only. Error bars based on LSC counting uncertainties (1σ) are within range of symbols used.

The Pu(V) sorption data for 30 d and 300 d is compared to the 120 d Pu(IV) sorption data in Figure 20. Over the course of the experiment, the position of the Pu(V) sorption data moves towards the 120 d Pu(IV) sorption data. This observation is consistent with the idea that kinetically limited reduction of Pu(V) on the mineral surface is responsible for the slow, continued uptake of Pu(V) (Begg et al., 2013). Log K_d values for Pu(V) sorption to bentonite after 300 days were 4.42 ± 0.03. The similarity of the K_d values of both Pu(IV) and Pu(V) over these long timescales demonstrates a convergence of the sorption behavior of Pu on bentonite regardless of initial oxidation state.

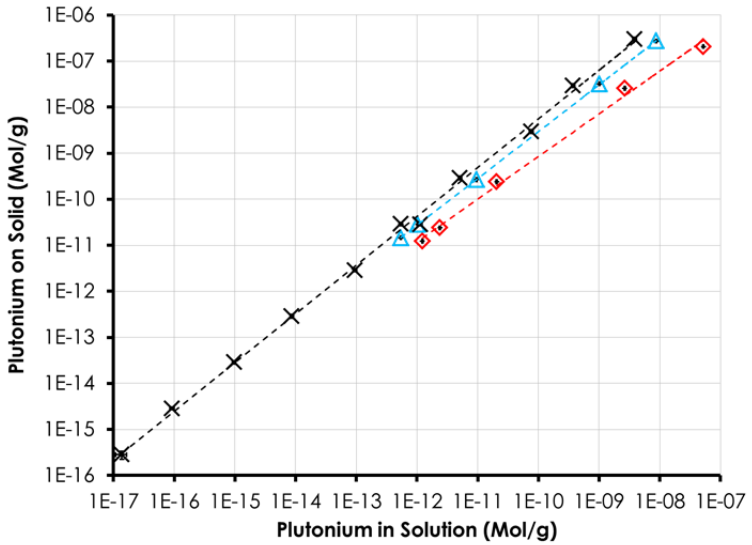

Figure 20. Sorption of Pu(V) to FEBEX bentonite (1 g L^{-1}, pH 8) at 30 d (red diamonds) and 300 d (blue triangles), compared with Pu(IV) sorption to FEBEX bentonite (1 g L^{-1}, pH 8) at 120 d (black crosses). Lines are to guide the eye only. Error bars based on LSC counting uncertainties (1σ) are within range of symbols used.

By assuming that the slow uptake of Pu from solution seen in the Pu(V) isotherm was due to the slow reduction of Pu(V) on the clay surface, the data from the 30 d, 120 d, and 300 d time points were used to estimate the apparent reduction rate. By using these last three data points, we hope to better isolate the reduction process from the early time sorption of Pu(V) (Begg et al., 2013). Apparent first order reduction rates were calculated from the slope of the plot of ln(C) versus time. The average surface normalized apparent reduction rate for these experiments was $10^{-5.3\pm1.3}$ L m^{-2} h^{-1}. Interestingly, when the same calculation was applied to the Pu(IV) data collected at 10^{-10} M for 67, 100 and 120 d, the calculated rate was $10^{-4.6\pm0.7}$ L m^{-2} h^{-1}. The similarity between the values further suggests that the long term uptake observed in Pu(IV) experiments was due to reduction of residual Pu(V) in solution.

The oxidation state of Pu in solution was monitored for bentonite experiments performed at 10^{-10} M and 10^{-8} M Pu(V) using LaF_3 precipitation (Appendix Figure A5). In both experiments, the percentage of Pu(V)/(VI) in solution declined between 30 and 120 days. At 300 d, the percent Pu(V)/(VI) in solution was ~33 at both 10^{-10} M and 10^{-8} M, respectively. In contrast, in mineral free Pu(V) experiments, LaF_3 analysis showed that the Pu remaining in solution after 300 days was dominated by Pu(V)/(VI) (96 ± 10% and 75 ± 18% for experiments at 10^{-10} and 10^{-8} M, respectively). This difference in oxidation state indicates that interaction of Pu(V) with mineral surfaces results not only in surface mediated reduction of Pu(V) but also leads to a difference in oxidation state distribution in solution. This change in the oxidation state of solution Pu in the presence of bentonite indicates that a solid:solution sorption equilibrium is established with respect to both Pu(V) and Pu(IV) under the present experimental conditions. This is in accordance with the recently proposed model for Pu(V) oxidation state distribution in the solid/aqueous phase following sorption on Savannah River sediments (Powell et al., 2014).

4.4.3 Desorption of Pu From Bentonite

A flow cell experiment was performed to investigate the desorption of Pu from bentonite. Prior to desorption, Pu(IV) at an initial concentration of 3×10^{-10} M was equilibrated with 1 g L^{-1} bentonite in 0.7 mM $NaHCO_3$/5 mM NaCl buffer solution at pH 8 for 21 days under aerobic conditions. After this period, the calculated log K_d for Pu(IV) sorption was 4.1, which is consistent with the sorption behavior of the Pu(IV) isotherm experiment performed at 10^{-10} M (4.4 at 67 d, 4.8 at 120 d).

The desorption of Pu from bentonite is plotted in terms of the cumulative fraction of total Pu desorbed in Figure 21. Also included in this plot are the data from a parallel experiment at pH 8 performed with SWy-1 Na-montmorillonite. Much (but not all) of the sharp increase in the cumulative desorbed Pu between 0 and ~ 2.5 chamber volumes (cv) in both plots represents removal of aqueous Pu remaining in solution following the sorption period. This Pu is displaced from the flow cell over the course of several cv (i.e. tailing). Comparison of a theoretical non-reactive tracer dilution curve under the initial flow conditions with the observed Pu concentrations in the bentonite experiment shows that the two curves begin to deviate within 1.2 cv (Appendix Figure A6). The deviation demonstrates an excess of Pu in the effluent from that which would be expected by dilution alone, indicating that Pu desorption from bentonite contributes significantly to the overall Pu breakthrough after just one chamber volume.

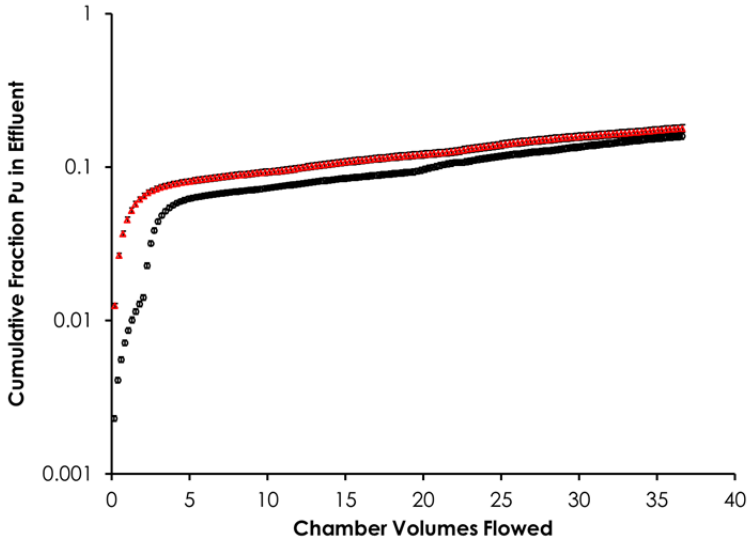

Figure 21. Cumulative fraction of Pu removed from bentonite (black circles) and montmorillonite (red triangles) flow cell experiments. Error bars based on LSC counting uncertainties (1σ) are within range of symbols used.

Both the shape of the plots and the final amounts of Pu desorbed are very similar for FEBEX bentonite and SWy-1 montmorillonite. This behavior is not unexpected in the context of the similarity of Pu sorption behavior between bentonite and montmorillonite. This plot further suggests that it is the montmorillonite component of the FEBEX bentonite that is controlling the desorption behavior of Pu in this experiment. The slope of the cumulative desorption plot for both

bentonite and montmorillonite continues to rise over the duration of the experiment, indicating that Pu is still being desorbed from the mineral surfaces at the termination of the flow period.

We calculated an apparent log K_d at the end of the flow cell experiment of 6.0 based on the Pu concentration in the final collected effluent fraction, accounting for the net removal of 16.5 % of the Pu from the system (Figure 21), and assuming no change in solid: solution ratio. This K_d value is much larger than the values in the Pu(IV) sorption experiments after 120 d equilibration (4.3 – 4.9). This indicates that on the timescale of the flow portion of the experiment (chamber residence time < 1 d) desorption of Pu appears to be rate limited. Following the cessation of the 12 d flow cell desorption experiment, the Pu-bentonite suspension was allowed to equilibrate under no-flow conditions (0.0 mL min^{-1}) for two months. After 60 d, the log K_d was calculated to be 4.8, which is in good agreement with the 120 d sorption K_d values. This similarity indicates Pu-bentonite sorption reversibility over extended time periods. The slow approach to apparent desorption equilibrium in these experiments (i.e. on timescales greater than 1 d) is consistent with previous work looking at Pu desorption from montmorillonite, bentonite colloids and argillites (Huber et al., 2011; Latrille et al., 2006; Lu et al., 2003). The slow desorption kinetics observed here highlight the need to consider both desorption rates and desorption equilibrium conditions when predicting Pu transport.

Oxidation state analysis using LaF_3 precipitation was performed on flow cell effluent during the flow period, after remnant aqueous Pu from the sorption step had been removed from the cell. The analysis indicated that the desorbed Pu was predominantly in the Pu(V)/(VI) oxidation state (90 ± 10%). This would suggest that in the short term, desorption of Pu(V) from the mineral surface is favored over Pu(IV). Further, given that Pu(IV) was initially adsorbed on the bentonite and is expected to be favored on the mineral surface, this result also suggests that the oxidation of Pu(IV) to Pu(V) is important for the desorption of Pu. However we cannot verify this without direct oxidation state analysis of Pu on the mineral surface. If Pu(IV) oxidation is involved in the desorption reaction, Pu desorption rates may be substantially lower under anoxic conditions where Pu(IV) oxidation is inhibited. Such an inhibition may further exacerbate mineral-colloid facilitated transport under anoxic repository conditions. Interestingly, oxidation state analysis of the Pu supernatant after the 2 month post flow cell equilibration period indicated that the aqueous Pu was predominantly Pu(IV). This suggests that changes in Pu oxidation state are responsible for differences in short term and long term desorption behavior of Pu from bentonite.

4.5 Conclusions

We investigated the sorption behavior of Pu(IV) to FEBEX bentonite over the concentration range 10^{-7}–10^{-16} M to determine if Pu sorption behavior at concentrations used in typical laboratory experiments (10^{-7}–10^{-11} M) was comparable to typical environmental concentrations ($\leq 10^{-12}$ M). On the timescale of months, the affinity of Pu(IV) for bentonite appears to be independent of concentration. However, slight non-linear behavior suggests that polymerization/precipitation reactions contribute to the apparent sorption at Pu(IV) concentrations $\geq 10^{-8}$ M. The sorption behavior of Pu(IV) to FEBEX bentonite is very similar to that previously observed for Pu(IV) sorption to colloidal SWy-1 Na-montmorillonite.

Pu(V) sorption to bentonite is also linear. However, Pu(V) sorption exhibits a much more significant time-dependence. The time-dependence is indicative of rate limited reduction of Pu(V) on clay minerals. The reduction rate constants determined based on these data agree with previously published reduction rates of Pu(V) on SWy-1 montmorillonite. The favorable comparison between Pu(IV) and Pu(V) behavior in the presence of FEBEX bentonite and SWy-1

Na-montmorillonite highlights the dominant role of montorillonite phases in controlling Pu sorption/desorption reactions on FEBEX bentonite.

The kinetics of desorption will be of key importance for predicting the mobility of Pu in groundwater environments, especially if Pu is associated with colloidal mineral phases. Pu oxidation state changes appear to influence the differences in desorption behavior observed at short and long timescales. The observation that after 2 months of desorption the K_d value was similar to the K_d value observed after 21 d sorption indicates rate-limited yet truly reversible Pu sorption under these experimental conditions.

These experiments were performed under aerobic conditions and Pu(IV) reoxidation appears to play an important role in the observed desorption behavior. Aerobic conditions may not be present in all nuclear waste repository scenarios (e.g. Duro et al., 2014). As a result, future work should build on these results by examining Pu sorption/desorption behavior across a wider range of geochemical conditions.

4.6 Acknowledgements

We thank P. Reimus (LANL) for providing the bentonite used in this work. This work was supported by the Used Fuel Disposition Campaign of the Department of Energy's Nuclear Energy Program and the Subsurface Biogeochemical Research Program of the U.S. Department of Energy's Office of Biological and Environmental Research. Prepared by LLNL under Contract DE-AC52-07NA27344.

4.7 Appendix

Table A1.

Name	**Isotopic composition**		
238	98.8% ^{238}Pu 0.11% ^{241}Pu 0.1% ^{239}Pu		
Stock Concentration (M)	**Medium**	**% Pu(III)/(IV) ± 10%**	**Experiment**
1.05E-06	1 N HCl	92	Pu(IV) Isotherm 10^{-9}
1.09E-07	0.1 N HCl	n.d.*	Pu(IV) Isotherm 10^{-10}
1.04E-08	0.1 N HCl	100	Pu(IV) Isotherm 10^{-11}
4.48E-08	0.1 N HCl	99	Flow Cell 10^{-10}
1.15E-08	0.7 mM $NaHCO_3$, 5 mM NaCl	2	Pu(V) isotherm 10^{-9}-10^{-11}
Name	**Isotopic composition**		
242	15.8% ^{238}Pu 5.1% $^{239+240}$Pu 79.1% ^{242}Pu		
Stock Concentration (M)	**Medium**	**% Pu(III)/(IV) ± 10%**	**Experiment**
2.67E-05	0.1 N HCl	100	Pu(IV) Isotherm 10^{-7}-10^{-8}
2.29E-06	0.7 mM $NaHCO_3$, 5 mM NaCl	3	Pu(V) isotherm 10^{-7}-10^{-8}
Name	**Isotopic composition**		
CRM	33.5% ^{238}Pu 35.3% ^{239}Pu 31.3% ^{240}Pu		
Stock Concentration (M)	**Medium**	**% Pu(III)/(IV) ± 10%**	**Experiment**
2.81E-07	0.1 N HCl	97	Top stock only
3.75E-08	0.1 N HCl	98	Pu(IV) Isotherm 10^{-11}-10^{-12}
3.60E-10	0.1 N HCl	n.d	Pu(IV) Isotherm 10^{-13}-10^{-14}
3.65E-12	0.1 N HCl	n.d.	Pu(IV) Isotherm 10^{-15}-10^{-16}

*** n.d. = not determined**

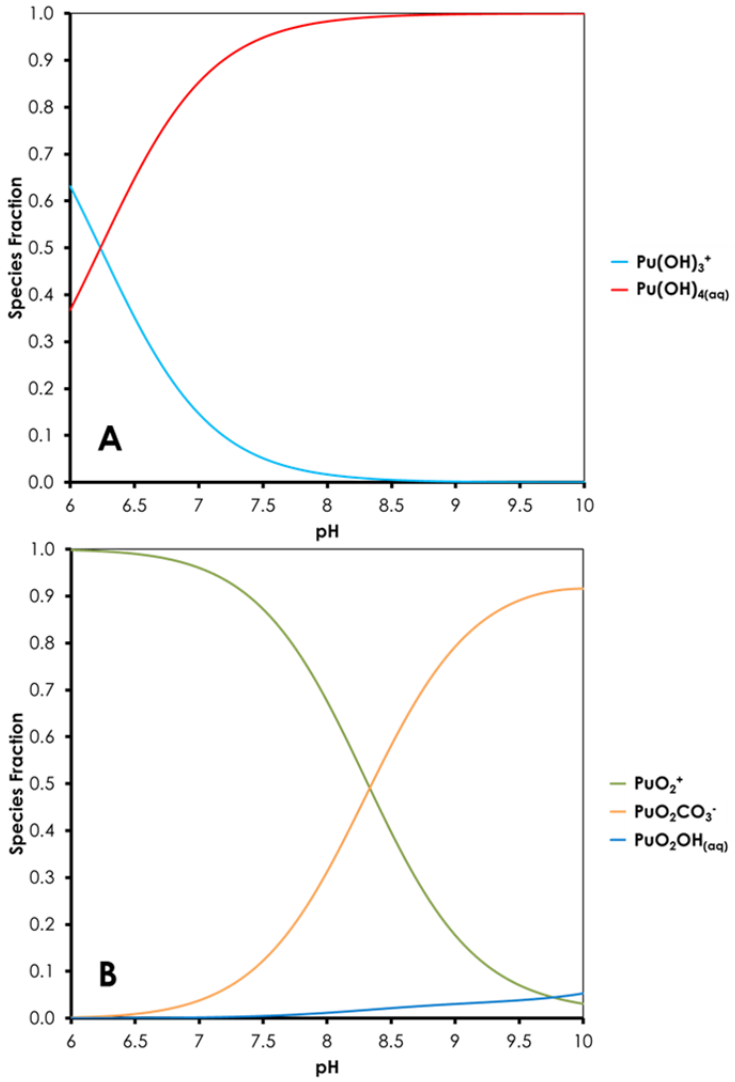

Figure A1. Predicted speciation of Pu(IV) (A) and Pu(V) (B) in experimental systems used in this study ([Pu] 10^{-10} M; 0.7 mM $NaHCO_3$, 5 mM NaCl buffer solution at pH 8). Calculations performed using thermodynamic constants from Guillaumont et al. (2003a). Other species which were accounted for but were not significant over this pH range were $Pu(CO_3)^{4-}$, $Pu(CO_3)_5^{6-}$, $Pu(OH)^{2+}$, $Pu(OH)_3^+$, Pu^{4+}, $PuCl^{3+}$ and $PuOH^{3+}$ for Pu(IV) and $PuO_2(CO_3)_3^{5-}$ for Pu(V). Figure modified from Figure S1 in Begg et al. (1982).

Mineral Free Experiments

Mineral free experiments were performed with initial Pu(IV) concentrations of 10^{-8}, 10^{-9} and 10^{-11} M Pu(IV). Measurement of the aqueous phase (i.e. with no centrifuging) within 1 d of spiking and again after 120 d showed that 60-75 % of Pu was lost from the bulk solution over this time period. Interestingly, LaF_3 analysis of the 10^{-10} M Pu(IV) mineral free experiment performed after 120 d indicated that the dominant oxidation state in the solution was Pu(V)/(VI). These results indicate that either precipitation of Pu(IV) colloids followed by sorption to container walls or sorption of monomeric Pu(IV) to container walls will occur in the absence of a mineral surface under the experimental conditions investigated. However, in the *high concentration* experiments performed with bentonite measurement of the bulk suspension phase indicated that Pu sorption to

container walls was insignificant in the presence of the mineral and that container wall sorption will not affect our measurement of Pu sorption by bentonite.

Mineral free Pu(V) experiments were performed at initial concentrations of 10^{-10} and 10^{-8} M. A loss of Pu from solution was observed in both experiments with 73% and 36% remaining in solution in the 10^{-10} M and 10^{-8} M Pu(V) experiments, respectively, after 300 d. It is likely that Pu precipitation/sorption to the container walls is responsible for this loss of Pu from solution. This is consistent with previous work that has shown the solubility of Pu(V) in natural waters at circumneutral pH to be in the range of 10^{-6} – 10^{-9} M. Further, previous work in our lab has observed similar differences in the behavior of aqueous Pu(V) in mineral free experiments at concentrations of 10^{-6} and 10^{-9} M.(Begg et al., 2013; Neck et al., 2007c; Nitsche and Edelstein, 1985; Runde et al., 2002a)

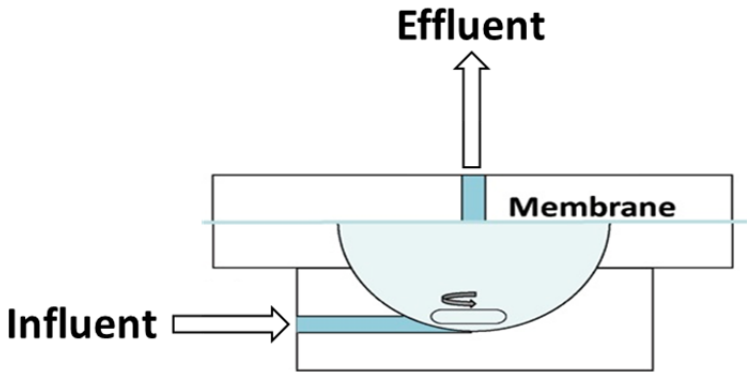

Figure A2. Flow cell set up. Cell provided by Dr Brian Powell (Environmental Engineering and Earth Sciences, Clemson University). Figure modified from Begg et al. (2014).

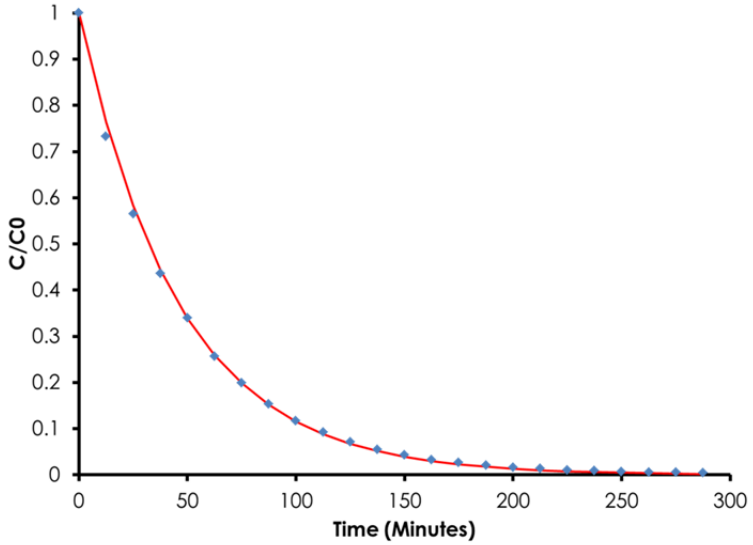

Figure A3. ^{3}H effluent profile from flow-cell experiment performed with montmorillonite. Data points represent measured fraction of ^{3}H in effluent. Solid line represents theoretical non-reactive tracer . Flow rate = 0.4 mL min^{-1}, cell volume = 20 mL.

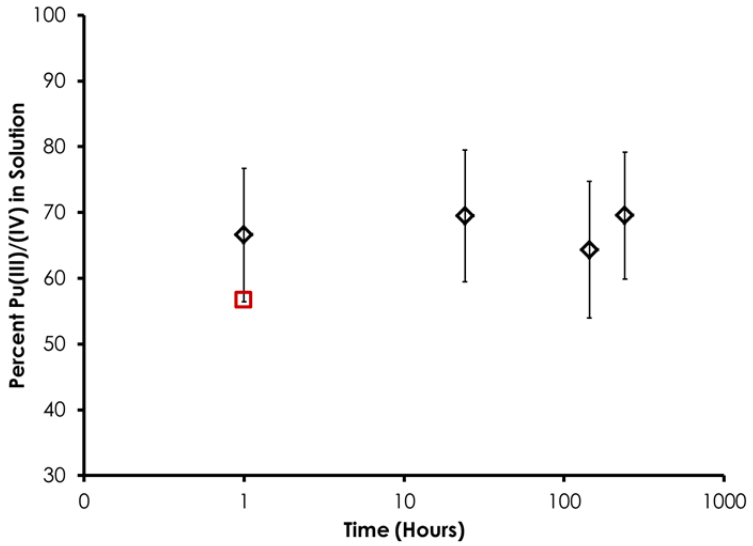

Figure A4. Percent Pu(III)/(IV) of solution Pu (3×10^{-10} M) in 0.7 mM $NaHCO_3$, 5 mM NaCl buffer (pH 8) as measured by LaF_3 precipitation (diamonds). Also shown is percent Pu(IV) in solution as measured by solvent extraction at 1 h (square). Original Pu(IV) stock solution was > 97% Pu(III)/(IV) (LaF_3). Error bars are an estimated absolute 10% value and are intended to reflect the difference between the solvent extraction and LaF_3 precipitation techniques. Note y-axis starts at 30%.

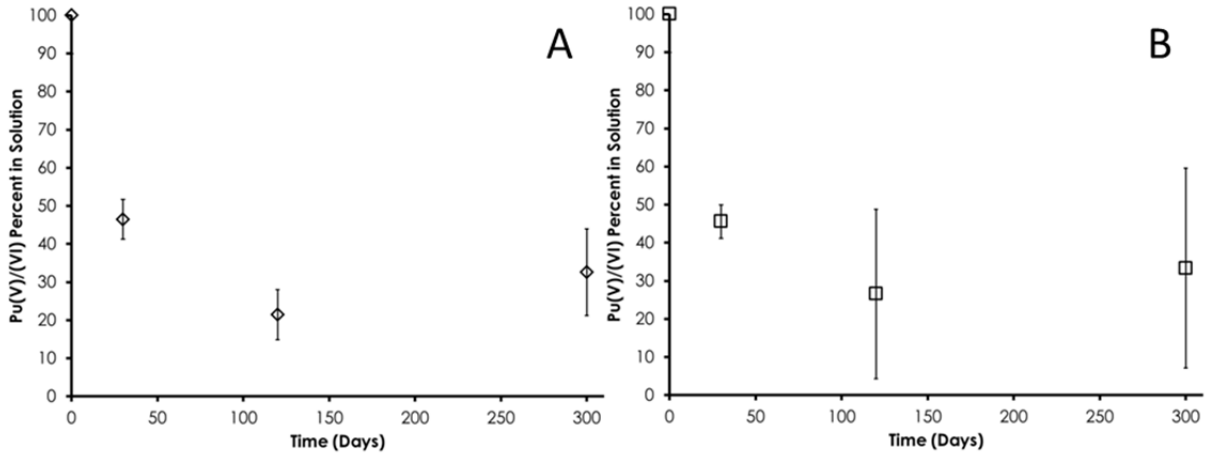

Figure A5. Changes in percent Pu(V)/(VI) in solution for Pu(V) isotherm experiments performed at initial concentrations of 10^{-10} M (A) and 10^{-8}M (B). Error bars based on LSC counting uncertainties (1σ).

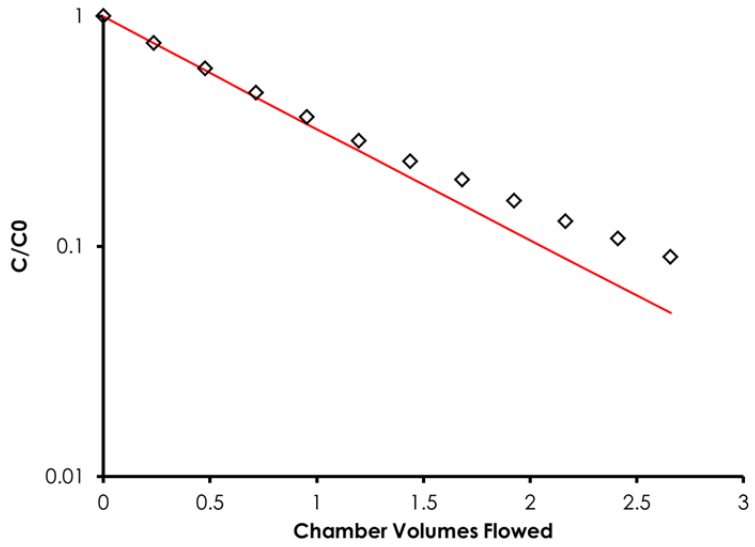

Figure A6 Comparison of expected effluent concentration of a theoretical non-reactive tracer expressed as a fraction of total tracer (red line) versus measured effluent concentration of Pu in bentonite flow cell experiment expressed as a fraction of total Pu.

5. REFERENCES

Afonso, M. D. and Stumm, W., 1992. Reductive Dissolution of Iron(Iii) (Hydr)Oxides by Hydrogen-Sulfide. *Langmuir* **8**, 1671-1675.

Akob, D. M., Mills, H. J., and Kostka, J. E., 2007. Metabolically active microbial communities in uranium-contaminated subsurface sediments. *Fems Microbiology Ecology* **59**, 95-107.

Allard, B., Olofsson, U., Torstenfelt, B., Kipatsi, H., and Andersson, K., 1982. Sorption of actinides in well-defined oxidation states on geologic media. *Mater. Res. Soc. Symp. Proc.* **11**, 775-82.

Altmaier, M., Gaona, X., and Fanghaenel, T., 2013. Recent Advances in Aqueous Actinide Chemistry and Thermodynamics. *Chem Rev* **113**, 901-943.

Artinger, R., Schuessler, W., Schaefer, T., and Kim, J. I., 2002. A kinetic study of Am(III)/humic colloid interactions. *Environ Sci Technol* **36**, 4358-4363.

Barns, S. M., Cain, E. C., Sommerville, L., and Kuske, C. R., 2007. Acidobactetia phylum sequences in uranium-contaminated subsurface sediments greatly expand the known diversity within the phylum. *Applied and Environmental Microbiology* **73**, 3113-3116.

Begg, J. D., Zavarin, M., and Kersting, A. B., 2014. Plutonium Desorption from Mineral Surfaces at Environmental Concentrations of Hydrogen Peroxide. *Environ Sci Technol* **48**, 6201-6210.

Begg, J. D., Zavarin, M., Tumey, S. J., and Kersting, A. B., 2015. Plutonium sorption and desorption behavior on bentonite. *Journal of Environmental Radioactivity* **141**, 106-114.

Begg, J. D., Zavarin, M., Zhao, P. H., Tumey, S. J., Powell, B., and Kersting, A. B., 2013. Pu(V) and Pu(IV) Sorption to Montmorillonite. *Environ Sci Technol* **47**, 5146-5153.

Berner, R. A., 1978. RATE CONTROL OF MINERAL DISSOLUTION UNDER EARTH SURFACE CONDITIONS. *American Journal of Science* **278**, 1235-1252.

Berner, R. A., 1981. Kinetics of Weathering and Diagenesis. In: Lasaga, A. C. and Kirkpatrick, R. J. Eds.), *Kinetics of Geochemical Processes*. BookCrafters, Inc., Chelsea, Michigan

Bernhard, G., Geipel, G., Reich, T., Brendler, V., Amayri, S., and Nitsche, H., 2001. Uranyl(VI) carbonate complex formation: Validation of the $Ca_2UO_2(CO_3)_3$(aq.) species. *Radiochim Acta* **89**, 511-518.

Bertetti, F. P., Pabalan, R. T., and Almendarez, M. G., 1998. Studies on neptunium(V) sorption on quartz, clinoptilolite, montmorillonite, and a-alumina. In: Jenne, E. A. (Ed.), *Adsorption of Metals by Geomedia*. Academic Press, San Diego.

Bethke, C. M. and Yeakel, S., 2010. The Geochemist's Workbench®. Hydrogeology Program, University of Illinois, Urbana, Illinois.

Boving, T. B. and Grathwohl, P., 2001. Tracer diffusion coefficients in sedimentary rocks: correlation to porosity and hydraulic conductivity. *Journal of Contaminant Hydrology* **53**, 85-100.

Bradbury, M. H. and Baeyens, B., 2002. Porewater chemistry in compacted re-saturated MX-80 bentonite: Physico-chemical characterisation and geochemical modelling*PSI Bericht Nr. 02-10*. Paul Scherrer Institute, Villigen PSI.

Bradbury, M. H. and Baeyens, B., 2003a. A comparison of apparent diffusion coefficients measured in compacted Kunigel V1 bentonite with those calculated from batch sorption measurements and D_e(HTO) data: a case study for Cs(I), Ni(II), Sm(III), Am(III), Zr(IV) and Np(V)*PSI Report 03-02*. Paul Scherrer Institut, Laboratory for Waste Management, Villigen PSI.

Bradbury, M. H. and Baeyens, B., 2003b. Porewater chemistry in compacted re-saturated MX-80 bentonite. *Journal of Contaminant Hydrology* **61**, 329-338.

Bradbury, M. H. and Baeyens, B., 2011. Physico-chemical characterisation data and sorption measurements of Cs, Ni, Eu, Th, U, Cl, I and Se on MX-80 bentonite*Technical Report 09-08*. Nagra, Wettingen.

Brockmann, S., 2006. Migration of caesium in bentonite: Influence of the pore water composition. Practical Report, Hochschule für Technik und Wirtschaft & Forschungszentrum Rossendorf.

Bruno, J., Arcos, D., Cera, E., Duro, L., and Grivé, M., 2004. Modelling near- and far-field processes in nuclear waste management. In: Grieré, R. and Stille, P. Eds.), *Energy, waste, and the environment: a geochemical perspective*. Geological Society, London.

Choppin, G. R., 1991. Redox speciation of plutonium in natural waters. *J Radioan Nucl Ch Ar* **147**, 109-116.

Choppin, G. R., 2007. Actinide speciation in the environment. *Journal of Radioanalytical and Nuclear Chemistry* **273**, 695-703.

Cleveland, J. M., 1979. The Chemistry of Plutonium. American Nuclear Society, La Grange Park.

COMSOL, 2014. COMSOL Multiphysics®. COMSOL, Inc., Burlington.

Crank, J., 1975. *The mathematics of diffusion*. Oxford University Press Inc., New York.

Dai, M. H., Buesseler, K., and Pike, S. M., 2005. Plutonium in groundwater at the 100K-Area of the US DOE Hanford site. *Journal of Contaminant Hydrology* **76**, 167-189.

Doherty, J., 2003. PEST*Model-independent parameter estimation and uncertainty analysis*. Watermark Numerical Computing, Brisbane.

Dong, W. M. and Brooks, S. C., 2006. Determination of the formation constants of ternary complexes of uranyl and carbonate with alkaline earth metals (Mg^{2+}, Ca^{2+}, Sr^{2+}, and Ba^{2+}) using anion exchange method. *Environ Sci Technol* **40**, 4689-4695.

Dozol, M., Hagemann, R., Hoffman, D. C., Adloff, J. P., Vongunten, H. R., Foos, J., Kasprzak, K. S., Liu, Y. F., Zvara, I., Ache, H. J., Das, H. A., Hagemann, R. J. C., Herrmann, G., Karol, P., Maenhaut, W., Nakahara, H., Sakanoue, M., Tetlow, J. A., Baro, G. B., Fardy, J. J., Benes, P., Roessler, K., Roth, E., Burger, K., Steinnes, E., Kostanski, M. J., Peisach, M., Liljenzin, J. O., Aras, N. K., Myasoedov, B. F., and Holden, N. E., 1993. Radionuclide migration in groundwaters - Review of the behavior of actinides (Technical report) *Pure and Applied Chemistry* **65**, 1081-1102.

Duro, L., Domènech, C., Grivé, M., Roman-Ross, G., Bruno, J., and Källström, K., 2014. Assessment of the evolution of the redox conditions in a low and intermediate level nuclear waste repository (SFR1, Sweden). *Applied Geochemistry* **49**, 192-205.

Dzombak, D. A. and Morel, F. M. M., 1993. Surface complexation modeling: hydrous ferric oxide. Wiley-Interscience, New York.

Efurd, D. W., Runde, W., Banar, J. C., Janecky, D. R., Kaszuba, J. P., Palmer, P. D., Roensch, F. R., and Tait, C. D., 1998. Neptunium and plutonium solubilities in a Yucca Mountain groundwater. *Environ Sci Technol* **32**, 3893-3900.

Fernandez, A. M., Baeyens, B., Bradbury, M., and Rivas, P., 2004. Analysis of the porewater chemical composition of a Spanish compacted bentonite used in an engineered barrier. *Physics and Chemistry of the Earth* **29**, 105-118.

Field, E. K., D'Imperio, S., Miller, A. R., VanEngelen, M. R., Gerlach, R., Lee, B. D., Apel, W. A., and Peyton, B. M., 2010. Application of molecular techniques to elucidate the influence of cellulosic waste on the bacterial community structure at a simulated low-level-radioactive-waste site. *Applied and Environmental Microbiology* **76**, 3106-3115.

Garcia-Gutierrez, M., Cormenzana, J. L., Missana, T., Mingarro, M., and Alonso, U., 2004. Analysis of uranium diffusion coefficients in compacted FEBEX bentonite. *Mater. Res. Soc. Symp. Proc.* **807**, 603-608.

Geckeis, H., Schafer, T., Hauser, W., Rabung, T., Missana, T., Degueldre, C., Mori, A., Eikenberg, J., Fierz, T., and Alexander, W. R., 2004. Results of the colloid and radionuclide retention experiment (CRR) at the Grimsel Test Site (GTS), Switzerland -

impact of reaction kinetics and speciation on radionuclide migration. *Radiochim Acta* **92**, 765-774.

Glaus, M. A., Frick, S., Rosse, R., and Van Loon, L. R., 2010. Comparative study of tracer diffusion of HTO, $^{22}Na^{+}$ and $^{36}Cl^{-}$ in compacted kaolinite, illite and montmorillonite. *Geochimica et Cosmochimica Acta* **74**, 1999-2010.

Glaus, M. A., Rossé, R., Van Loon, L. R., and Yaroshchuk, A. E., 2008. Tracer diffusion in sintered stainless steel filters: measurement of effective diffusion coefficients and implications for diffusion studies with compacted clays. *Clays and Clay Minerals* **56**, 677-685.

Glaus, M. A. and Van Loon, L. R., 2012. Diffusive behaviour of charged uranyl complexes in compacted montmorilloniteClays in Natural & Engineered Barriers for Radioactive Waste Confinement - 5th International Meeting. Andra, Montpellier.

Golubev, S. V., Bauer, A., and Pokrovsky, O. S., 2006. Effect of pH and organic ligands on the kinetics of smectite dissolution at 25 °C. *Geochimica Et Cosmochimica Acta* **70**, 4436-4451.

Grauer, R., 1986. Bentonite as a backfill material in the high-level waste repository: Chemical aspects*EIR Bericht Nr. 576, Nagra Technical Report NTB 86-12E*. Paul Scherrer Institut, Villigen, Switzerland and Nagra, Wettingen, Switzerland.

Grim, R. E., 1968. *Clay mineralogy*. McGraw Hill.

Guillaumont, R., Fanghanel, T., Neck, V., Fuger, J., Palmer, D. A., Grenthe, I., and Rand, M. H., 2003a. Update on the chemical thermodynamics of uranium, neptunium, plutonium, americium, and technetium. In: Mompean, F. J., Illemassene, M., Domenech-Orti, C., and Said, K. B. Eds.)*Chemical Thermodynamics*. Elsevier, Amsterdam.

Guillaumont, R., Fanghänel, T., Neck, V., Fuger, J., Palmer, D. A., Grenthe, I., and Rand, M. H., 2003b. *Update on the Chemical Thermodynamics of Uranium, Neptunium, Plutonium, Americium and Technetium (OECD/NEA, ed.)*. Elsevier, Amsterdam.

Guven, N., 1988. Smectites. *Reviews in Mineralogy and Geochemistry* **19**, 497-559.

Guven, N., 1990. Longevity of bentonite as buffer material in a nuclear-waste repository. *Engineering Geology* **28**, 233-247.

Herbert, H.-J. and Moog, H. C., 2002. Untersuchungen zur Quellung von Bentoniten in hochsalinaren Lösungen-Abschlussbericht*GRS-179*. Gesellschaft für Anlagen- und Reaktorsicherheit.

Hixon, A. E. and Powell, B. A., 2014. Observed changes in the mechanism and rates of Pu(V) reduction on hematite as a function of total plutonium concentration. *Environ Sci Technol* **48**, 9255-9262.

Hocsman, A., Di Nezo, S., Charlet, L., and Avena, M., 2006. On the mechanisms of dissolution of montroydite [HgO(s)]: Dependence of the dissolution rate on pH, temperature, and stirring rate. *Journal of Colloid and Interface Science* **297**, 696-704.

Huber, F., Kunze, P., Geckeis, H., and Schafer, T., 2011. Sorption reversibility kinetics in the ternary system radionuclide-bentonite colloids/nanoparticles-granite fracture filling material. *Applied Geochemistry* **26**, 2226-2237.

Huertas, F. J., Caballero, E., Jiménez de Cisneros, C., Huertas, F., and Linares, J., 2001. Kinetics of montmorillonite dissolution in granitic solutions. *Applied Geochemistry* **16**, 397-407.

IAEA, 1995. Principles of Radioactive Waste Management*Safety Series* IAEA, Vienna.

Icopini, G. A., Lack, J. G., Hersman, L. E., Neu, M. P., and Boukhalfa, H., 2009. Plutonium(V/VI) reduction by the metal-reducing Bacteria Geobacter metallireducens GS-15 and Shewanella oneidensis MR-1. *Applied and Environmental Microbiology* **75**, 3641-3647.

Idemitsu, K., Tachi, Y., Furuya, H., Inagaki, Y., and Arima, T., 1996. Diffusion of uranium in compacted bentonites in the reducing condition with corrosion products of iron. *Mater. Res. Soc. Symp. Proc.* **412**, 683-90.

Jasrotia, P., Green, S. J., Canion, A., Overholt, W. A., Prakash, O., Wafula, D., Hubbard, D., Watson, D. B., Schadt, C. W., Brooks, S. C., and Kostka, J. E., 2014. Watershed-scale fungal community characterization along a pH gradient in a subsurface environment cocontaminated with uranium and nitrate. *Applied and Environmental Microbiology* **80**, 1810-1820.

Joseph, C., Schmeide, K., Sachs, S., Brendler, V., Geipel, G., and Bernhard, G., 2011. Sorption of uranium(VI) onto Opalinus Clay in the absence and presence of humic acid in Opalinus Clay pore water. *Chemical Geology* **284**, 240-250.

Joseph, C., Stockmann, M., Schmeide, K., Sachs, S., Brendler, V., and Bernhard, G., 2013a. Sorption of U(VI) onto Opalinus Clay: Effects of pH and humic acid. *Applied Geochemistry* **36**, 104-117.

Joseph, C., Van Loon, L. R., Jakob, A., Steudtner, R., Schmeide, K., Sachs, S., and Bernhard, G., 2013b. Diffusion of U(VI) in Opalinus Clay: Influence of temperature and humic acid. *Geochimica et Cosmochimica Acta* **109**, 74-89.

Kaplan, D. I., Powell, B. A., Duff, M. C., Demirkanli, D. I., Denham, M., Fjeld, R. A., and Molz, F. J., 2007. Influence of sources on plutonium mobility and oxidation state transformations in vadose zone sediments. *Environ Sci Technol* **41**, 7417-7423.

Kaszuba, J. P. and Runde, W. H., 1999. The aqueous geochemistry of neptunium: Dynamic control of soluble concentrations with applications to nuclear waste disposal. *Environ Sci Technol* **33**, 4427-4433.

Keeney-Kennicutt, W. L. and Morse, J. W., 1985. The redox chemistry of Pu(V)O2+ interaction with common mineral surfaces in dilute solutions and seawater. *Geochimica Et Cosmochimica Acta* **49**, 2577-2588.

Keller, L. M., Holzer, L., Gasser, P., Erni, R., and Rossell, M. D., 2015. Intergranular pore space evolution in MX80 bentonite during a long-term experiment. *Applied Clay Science* **104**, 150-159.

Keren, R. and Shainberg, I., 1975. Water-vapor isotherms and heat of immersion of Na/Ca-montmorillonite systems - I: Homoionic clay. *Clays and Clay Minerals* **23**, 193-200.

Kerisit, S. and Liu, C. X., 2010. Molecular simulation of the diffusion of uranyl carbonate species in aqueous solution. *Geochimica et Cosmochimica Acta* **74**, 4937-4952.

Kersting, A. B., 2013. Plutonium Transport in the Environment. *Inorganic Chemistry* **52**, 3533-3546.

Kersting, A. B., Efurd, D. W., Finnegan, D. L., Rokop, D. J., Smith, D. K., and Thompson, J. L., 1999. Migration of plutonium in ground water at the Nevada Test Site. *Nature* **397**, 56-59.

Kersting, A. B., Zavarin, M., Powell, B. A., Moser, D., Carroll, S. A., Maxwell, R., Dai, Z., Williams, R., Tumey, S., Zhao, P., Tinnacher, R., Huang, P., Kips, R., Mason, H., Begg, J., Fisher, J., Simpkins, L., Zimmerman, T., Jablonski, J., and Snow, M., 2011. LLNL SFA FY11 Program Management and Performance Report: Environmental Transport of Plutonium.

Keto, P., Gunnarsson, D., Johannesson, L.-E., and Hansen, J., 2007. Assessment of backfilling materials and methods for deposition tunnels*Clays in Natural & Engineered Barriers for Radioactive Waste Confinement*. Andra, Lille.

Kim, H. T., Suk, T. W., Park, S. H., and Lee, C. S., 1993. Diffusivities for ions through compacted sodium-bentonite with varying dry bulk density. *Waste Manage. (N. Y.)* **13**, 303-8.

Kobashi, A. and Choppin, G. R., 1988. A study of techniques for separating plutonium in different oxidation states. *Radiochim. Acta* **43**, 211-215.

Kohler, S. J., Dufaud, F., and Oelkers, E. H., 2003. An experimental study of illite dissolution kinetics as a function of pH from 1.4 to 12.4 and temperature from 5 to 50 degrees C. *Geochimica Et Cosmochimica Acta* **67**, 3583-3594.

Kozai, N., Inada, K., Kozaki, T., Sato, S., Ohashi, H., and Banba, T., 2001. Apparent diffusion coefficients and chemical species of neptunium(V) in compacted Na-montmorillonite. *Journal of Contaminant Hydrology* **47**, 149-158.

Kozai, N., Ohnuko, T., Matsumoto, J., Banba, T., and Ito, Y., 1996. A study of the specific sorption of neptunium(V) on smectite in low pH solution. *Radiochim. Acta* **75**, 149-158.

Kozai, N., Ohnuky, T., and Muraoka, S., 1993. Sorption characteristics of neptunium by sodium-smectite. *J. Nuclear Sci. Tech.* **30**, 1153-1159.

Křepelová, A., Sachs, S., and Bernhard, G., 2006. Uranium(VI) sorption onto kaolinite in the presence and absence of humic acid. *Radiochim Acta* **94**, 825-833.

Lasaga, A. C., 1981. Transition State Theory. In: Lasaga, A. C. and Kirkpatrick, R. J. Eds.), *Kinetics of Geochemical Processes*. BookCrafters, Inc., Chelsea, Michigan

Lasaga, A. C., 1998. *Kinetic Theory in the Earth Sciences*. Princeton University Press, Princeton, NJ.

Lasaga, A. C. and Gibbs, G. V., 1990. ABINITIO QUANTUM-MECHANICAL CALCULATIONS OF WATER-ROCK INTERACTIONS - ADSORPTION AND HYDROLYSIS REACTIONS. *American Journal of Science* **290**, 263-295.

Lasaga, A. C. and Luttge, A., 2004. Mineralogical approaches to fundamental crystal dissolution kinetics. *American Mineralogist* **89**, 527-540.

Latrille, C., Ly, J., and Herbette, M., 2006. Retention of Sn(IV) and Pu(IV) onto four argillites from the Callovo-Oxfordian level at Bure (France) from eight equilibrated sedimentary waters. *Radiochim Acta* **94**, 421-427.

Lee, J. O., Lim, J. G., Kang, I. M., and Kwon, S., 2012. Swelling pressures of compacted Ca-bentonite. *Engineering Geology* **129–130**, 20-26.

Lu, N. P., Reimus, P. W., Parker, G. R., Conca, J. L., and Triay, I. R., 2003. Sorption kinetics and impact of temperature, ionic strength and colloid concentration on the adsorption of plutonium-239 by inorganic colloids. *Radiochim Acta* **91**, 713-720.

Lujaniene, G., Motiejunas, S., and Sapolaite, J., 2007. Sorption of Cs, Pu and Am on clay minerals. *Journal of Radioanalytical and Nuclear Chemistry* **274**, 345-353.

Maher, K., Steefel, C. I., DePaolo, D. J., and Viani, B. E., 2006. The mineral dissolution rate conundrum: Insights from reactive transport modeling of U isotopes and pore fluid chemistry in marine sediments. *Geochimica Et Cosmochimica Acta* **70**, 337-363.

Management, O. o. C. R. W., 2002. Yucca Mountain Science and Engineering Report: Technical Information Supporting Site Recommendation Consideration. U.S. Department of Energy.

Marchetti, A. A., Brown, T. A., Cox, C. C., Hamilton, T. F., and Martinelli, R. E., 2005. Accelerator mass spectrometry of actinides. *Journal of Radioanalytical and Nuclear Chemistry* **263**, 483-487.

McCubbin, D. and Leonard, K. S., 1996. Photochemical dissolution of radionuclides from marine sediments. *Mar Chem* **55**, 399-408.

Missana, T., Alonso, U., Garcia-Gutierrez, M., and Mingarro, M., 2008. Role of bentonite colloids on europium and plutonium migration in a granite fracture. *Applied Geochemistry* **23**, 1484-1497.

Missana, T. and Garcia-Gutierrez, M., 2007. Adsorption of bivalent ions (Ca(II), Sr(II) and Co(II)) onto FEBEX bentonite. *Physics and Chemistry of the Earth* **32**, 559-567.

Missana, T., Garcia-Gutierrez, M., and Alonso, U., 2004. Kinetics and irreversibility of cesium and uranium sorption onto bentonite colloids in a deep granitic environment. *Applied Clay Science* **26**, 137-150.

Muyzer, G., Teske, A., Wirsen, C. O., and Jannasch, H. W., 1995. Phylogenetic relationships of *Thiomicrospira* species and their identification in deep-sea hydrothermal vent samples by denaturing gradient gel electrophoresis of 16S rDNA fragments. *Archives of Microbiology* **164**, 165-172.

NAGRA, 2006. The CRR Final Project Report Series II: Supporting Laboratory Experiments with Radionuclides and Bentonite Colloids. Technical Report 03-02. In: Missana, T. and Geckeis, H. Eds.). Nagra, Wettingen, Switzerland

Nebelung, C. and Brendler, V., 2009. Uranium(VI) sorption on montmorillonite and bentonite: Prediction and experiments. In: Bernhard, G. (Ed.),*Annual Report 2008, FZD-511*. Forschungszentrum Dresden-Rossendorf, Institut für Radiochemie, Dresden.

Neck, V., Altmaier, M., and Fanghaenel, T., 2007a. Thermodynamic data for hydrous and anhydrous PuO2+x(S). *Journal of Alloys and Compounds* **444**, 464-469.

Neck, V., Altmaier, M., and Fanghanel, T., 2007b. Solubility of plutonium hydroxides/hydrous oxides under reducing conditions and in the presence of oxygen. *Cr Chim* **10**, 959-977.

Neck, V., Altmaier, M., Seibert, A., Yun, J. I., Marquardt, C. M., and Fanghanel, T., 2007c. Solubility and redox reactions of Pu(IV) hydrous oxide: Evidence for the formation of PuO(2+x)(s, hyd). *Radiochim Acta* **95**, 193-207.

Neck, V. and Kim, J. I., 2001. Solubility and hydrolysis of tetravalent actinides. *Radiochim Acta* **89**, 1-16.

Nitsche, H. and Edelstein, N. M., 1985. Solubilities and speciation of selected transuranium ions. A comparison of a non-complexing solution with a groundwater from the Nevada Tuff Site. *Radiochim Acta* **39**, 23-33.

Nitsche, H., Gatti, R. C., Standifer, E. M., Lee, S. C., Muller, A., Prussin, T., Deinhammer, R. S., Maurer, H., Becraft, K., Leung, S., and Carpenter, S. A., 1993. Measured solubilites and speciations of neptunium, plutonium, and americium in a typical groundwater (J-13) from the Yucca Mountain region. Los Alamos National Laboratory, Los Alamos, NM.

Nitsche, H., Roberts, K., Prussin, T., Muller, A., Becraft, K., Keeney, D., Carpenter, S. A., and Gatti, R. C., 1994. Measured solubilities and speciations from oversaturation experiments of neptunium, plutonium, and americium in UE-25p #1 well from the Yucca Mountain region. Los Alamos National Laboratory, Los Alamos.

Novikov, A. P., Kalmykov, S. N., Utsunomiya, S., Ewing, R. C., Horreard, F., Merkulov, A., Clark, S. B., Tkachev, V. V., and Myasoedov, B. F., 2006. Colloid transport of plutonium in the far-field of the Mayak Production Association, Russia. *Science* **314**, 638-641.

Orlandini, K. A., Penrose, W. R., and Nelson, D. M., 1986. Pu(V) as the stable form of oxidized plutonium in natural waters. *Mar Chem* **18**, 49-57.

Pabalan, R. T. and Turner, D. R., 1997. Uranium(VI) sorption on montmorillonite: Experimental and surface complexation modeling study. *Aquatic Geochemistry* **2**, 203-226.

Pabalan, R. T., Turner, D. R., Bertetti, F. P., and Prikryl, J. D., 1998. Uranium(VI) sorption onto selected mineral surfaces. In: Jenne, E. A. (Ed.), *Adsorption of metals by geomedia: Variables, mechanisms, and model applications*. Academic Press, San Diego.

Payne, T. E., Brendler, V., Comarmond, M. J., and Nebelung, C., 2011. Assessment of surface area normalisation for interpreting distribution coefficients (K_d) for uranium sorption. *Journal of Environmental Radioactivity* **102**, 888-895.

Penrose, W. R., Polzer, W. L., Essington, E. H., Nelson, D. M., and Orlandini, K. A., 1990. Mobility of plutonium and americium through a shallow aquifer in a semiarid region. *Environ Sci Technol* **24**, 228-234.

Pizzetti, I., Fuchs, B. M., Gerdts, G., Wichels, A., Wiltshire, K. H., and Amann, R., 2011. Temporal variability of coastal *Planctomycetes* clades at kabeltonne station, North Sea. *Applied and Environmental Microbiology* **77**, 5009-5017.

Powell, B. A., Dai, Z. R., Zavarin, M., Zhao, P. H., and Kersting, A. B., 2011. Stabilization of plutonium nano-colloids by epitaxial distortion on mineral surfaces. *Environ Sci Technol* **45**, 2698-2703.

Powell, B. A., Fjeld, R. A., Kaplan, D. I., Coates, J. T., and Serkiz, S. M., 2004. Pu(V)O2+ adsorption and reduction by synthetic magnetite (Fe3O4). *Environ Sci Technol* **38**, 6016-6024.

Powell, B. A., Fjeld, R. A., Kaplan, D. I., Coates, J. T., and Serkiz, S. M., 2005. Pu(V)O2+ adsorption and reduction by synthetic hematite and goethite. *Environ Sci Technol* **39**, 2107-2114.

Powell, B. A., Kaplan, D. I., Serkiz, S. M., Coates, J. T., and Fjeld, R. A., 2014. Pu(V) transport through Savannah River Site soils - an evaluation of a conceptual model of surface-mediated reduction to Pu (IV). *Journal of Environmental Radioactivity* **131**, 47-56.

Powell, B. A., Kersting, A. B., and Zavarin, M., 2008. Sorption and Desorption Rates of Neptunium and Plutonium on Goethite. In: Zavarin, M., Kersting, A. B., Lindvall, R. E., and Rose, T. P. Eds.), *Hydrologic Resources Management Program and Underground Test Area Project, FY 2006 Progress Report*. Lawrence Livermore National Laboratory, Livermore, CA.

Pruesse, E., Peplies, J., and Glöckner, F. O., 2012. SINA: Accurate high-throughput multiple sequence alignment of ribosomal RNA genes. *Bioinformatics* **28**, 1823-1829.

Radeva, G., Kenarova, A., Bachvarova, V., Flemming, K., Popov, I., Vassilev, D., and Selenska-Pobell, S., 2013. Bacterial diversity at abandoned uranium mining and milling sites in Bulgaria as revealed by 16S rRNA genetic diversity study. *Water Air and Soil Pollution* **224**, 1-14.

Radeva, G. and Selenska-Pobell, S., 2005. Bacterial diversity in water samples from uranium wastes as demonstrated by 16S rDNA and ribosomal intergenic spacer amplification retrievals. *Canadian Journal of Microbiology* **51**, 910-923.

Ramebäck, H., Skålberg, M., Eklund, U. B., Kjellberg, L., and Werme, L., 1998. Mobility of U, Np, Pu, Am and Cm from spent nuclear fuel into bentonite clay. *Radiochim Acta* **82**, 167-171.

Rao, L. F., Srinivasan, T. G., Garnov, A. Y., Zanonato, P. L., Di Bernardo, P., and Bismondo, A., 2004. Hydrolysis of neptunium(V) at variable temperatures (10-85 degrees C). *Geochimica Et Cosmochimica Acta* **68**, 4821-4830.

Rao, L. F., Tian, G. X., Di Bernardo, P., and Zanonato, P., 2011. Hydrolysis of Plutonium(VI) at Variable Temperatures (283-343 K). *Chem-Eur J* **17**, 10985-10993.

Romanchuk, A. Y., Kalmykov, S. N., and Aliev, R. A., 2011. Plutonium sorption onto hematite colloids at femto- and nanomolar concentrations. *Radiochim Acta* **99**, 137-144.

Ross, C. S. and Shannon, E. V., 1926. The minerals of bentonite and related clays and their physical properties. *Journal of the American Ceramic Society* **9**, 77-96.

Rozalén, M., Brady, P. V., and Huertas, F. J., 2009. Surface chemistry of K-montmorillonite: Ionic strength, temperature dependence and dissolution kinetics. *Journal of Colloid and Interface Science* **333**, 474-484.

Rozalén, M. L., Huertas, F. J., Brady, P. V., Cama, J., García-Palma, S., and Linares, J., 2008. Experimental study of the effect of pH on the kinetics of montmorillonite dissolution at 25 °C. *Geochimica Et Cosmochimica Acta* **72**, 4224-4253.

Runde, W., Conradson, S. D., Efurd, D. W., Lu, N. P., VanPelt, C. E., and Tait, C. D., 2002a. Solubility and sorption of redox-sensitive radionuclides (Np, Pu) in J-13 water from the Yucca Mountain site: comparison between experiment and theory. *Applied Geochemistry* **17**, 837-853.

Runde, W., Conradson, S. D., Wes Efurd, D., Lu, N., VanPelt, C. E., and Tait, C. D., 2002b. Solubility and sorption of redox-sensitive radionuclides (Np, Pu) in J-13 water from the Yucca Mountain site: comparison between experiment and theory. *Applied Geochemistry* **17**, 837-853.

Sabodina, M. N., Kalmykov, S. N., Sapozhnikov, Y. A., and Zakharova, E. V., 2006. Neptunium, plutonium and ^{137}Cs sorption by bentonite clays and their speciation in pore waters. *Journal of Radioanalytical and Nuclear Chemistry* **270**, 349-355.

Sachs, S., Křepelová, A., Schmeide, K., Koban, A., Günther, A., Mibus, J., Brendler, V., Geipel, G., and Bernhard, G., 2007. Joint Project: Migration of actinides in the system clay, humic substance, aquifer - Migration behavior of actinides (uranium, neptunium) in clays: Characterization and quantification of the influence of humic substances*Wissenschaftlich-Technische Berichte, FZD-460*. Forschungszentrum Dresden-Rossendorf, Dresden.

Sanchez, A. L., Murray, J. W., and Sibley, T. H., 1985. The adsorption of plutonium IV and plutonium V on goethite. *Geochimica et Cosmochimica Acta* **49**, 2297-2307.

Santschi, P. H., Roberts, K. A., and Guo, L. D., 2002. Organic mature of colloidal actinides transported in surface water environments. *Environ Sci Technol* **36**, 3711-3719.

Sato, H., Ashida, T., Kohara, Y., Yui, M., and Sasaki, N., 1992. Effect of dry density on diffusion of some radionuclides in compacted sodium bentonite. *J. Nucl. Sci. Technol.* **29**, 873-882.

Schwenk-Ferrero, A., 2013. German spent nuclear fuel legacy: Characteristics and high-level waste management issues. *Science and Technology of Nuclear Installations* **2013**, 11.

Silva, R. J. and Nitsche, H., 1995. Actinide environmental chemistry. *Radiochim Acta* **70-1**, 377-396.

Singer, D. M., Guo, H., and Davis, J. A., 2014. U(VI) and Sr(II) batch sorption and diffusion kinetics into mesoporous silica (MCM-41). *Chemical Geology* **390**, 152-163.

Snow, M. S., Zhao, P. H., Dai, Z. R., Kersting, A. B., and Zavarin, M., 2013. Neptunium(V) sorption to goethite at attomolar to micromolar concentrations using radiometric methods. *Journal of Colloid and Interface Science* **390**, 176-182.

Steefel, C., 2011. CrunchFlow*Software for modeling multicomponent reactive flow and transport*. Lawrence Berkeley National Laboratory, Berkeley, CA.

Stroes-Gascoyne, S., Sergeant, C., Schippers, A., Hamon, C. J., Nèble, S., Vesvres, M. H., Barsotti, V., Poulain, S., and Le Marrec, C., 2011. Biogeochemical processes in a clay formation *in situ* experiment: Part D – Microbial analyses – Synthesis of results. *Applied Geochemistry* **26**, 980-989.

Stumm, W., 1997. Reactivity at the mineral-water interface: dissolution and inhibition. *Colloids and Surfaces A: Physicochemical and Engineering Aspects* **120**, 143-166.

Tinnacher, R. M., Zavarin, M., Powell, B. A., and Kersting, A. B., 2011. Kinetics of neptunium(V) sorption and desorption on goethite: An experimental and modeling study. *Geochimica et Cosmochimica Acta* **75**, 6584-6599.

Torstenfelt, B. and Allard, B., 1986. Migration of fission products and actinides in compacted bentonite*SKB Technical Report 86-14*. Swedish nuclear fuel and waste management CO, Stockholm.

Trepte, P., 2004. Diffusion of tritiated water (HTO) through compacted bentonite samples: Effect of sample thickness. Practical report, Hochschule für Technik und Wirtschaft Dresden & Forschungszentrum Rossendorf.

Turner, D. R., Pabalan, R. T., and Bertetti, F. P., 1998. Neptunium(V) sorption on montmorillonite: An experimental and surface complexation modeling study. *Clays and Clay Minerals* **46**, 256-269.

Turner, D. R. and Sassman, S. A., 1996. Approaches to sorption modeling for high-level waste performance assessment. *Journal of Contaminant Hydrology* **21**, 311-332.

Urios, L., Marsal, F., Pellegrini, D., and Magot, M., 2013. Microbial diversity at iron-clay interfaces after 10 years of interaction inside a deep argillite geological formation (Tournemire, France). *Geomicrobiol. J.* **30**, 442-453.

Van Loon, L. R., 2014. Effective diffusion coefficients and porosity values for argillaceous rocks and bentonite: Measured and estimated values for the provisional safety analyses for SGT-E2*Technical Report 12-03*. Nagra, Wettingen.

Van Loon, L. R., Baeyens, B., Glaus, M. A., Bradbury, M. H., Müller, W., and Schaible, A., 2007a. NF-PRO Report, Contract Number: FI6W-CT-2003-02389, RTD Component: 2, Work Package: 2.5*Deliverable (D-N°: 2.5.20), Reporting period: 01/01/04 - 31/12/07*. European Commission - Community Research.

Van Loon, L. R. and Eikenberg, J., 2005. A high-resolution abrasive method for determining diffusion profiles of sorbing radionuclides in dense argillaceous rocks. *Applied Radiation and Isotopes* **63**, 11-21.

Van Loon, L. R., Glaus, M. A., and Müller, W., 2007b. Anion exclusion effects in compacted bentonites: Towards a better understanding of anion diffusion. *Applied Geochemistry* **22**, 2536-2552.

Van Loon, L. R. and Soler, J. M., 2004. Diffusion of HTO, $^{36}Cl^-$, $^{125}I^-$, and $^{22}Na^+$ in Opalinus Clay: Effect of Confining Pressure, Sample Orientation, Sample Depth and Temperature*PSI-Bericht 04-03*. Paul Scherrer Institute, Villigen PSI.

Van Loon, L. R., Soler, J. M., Jakob, A., and Bradbury, M. H., 2003. Effect of confining pressure on the diffusion of HTO, $^{36}Cl^-$ and $^{125}I^-$ in a layered argillaceous rock (Opalinus Clay): diffusion perpendicular to the fabric. *Applied Geochemistry* **18**, 1653-1662.

Vaniman, D., Furlano, A., Chipera, S., Thompson, J., and Triay, I., 1995. Microautoradiography in studies of Pu(V) sorption by trace and fracture minerals in tuff. *MRS Proceedings* **412**, 639-646.

Walther, C. and Denecke, M. A., 2013. Actinide Colloids and Particles of Environmental Concern. *Chem Rev* **113**, 995-1015.

Wang, X. K., Chen, C. L., Zhou, X., Tan, X. L., and Hu, W. P., 2005. Diffusion and sorption of U(VI) in compacted bentonite studied by a capillary method. *Radiochim Acta* **93**, 273-278.

White, T. J., Bruns, T., Lee, S., and Taylor, J., 1990. *Amplification and direct sequencing of fungal ribosomal RNA genes for phylogenetics*. Academic Press, San Diego, California, USA; London, England, UK.

Wu, T., Dai, W., Xiao, G. P., Shu, F. J., Yao, J., and Li, J. Y., 2012. Influence of dry density on HTO diffusion in GMZ bentonite. *J. Radioanal. Nucl. Chem.* **292**, 853-857.

Xiao, Y. T. and Lasaga, A. C., 1994. AB-INITIO QUANTUM-MECHANICAL STUDIES OF THE KINETICS AND MECHANISMS OF SILICATE DISSOLUTION - H+(H3O+) CATALYSIS. *Geochimica Et Cosmochimica Acta* **58**, 5379-5400.

Xiong, Q., Jivkov, A. P., and Yates, J. R., 2014. Discrete modelling of contaminant diffusion in porous media with sorption. *Microporous Mesoporous Mater.* **185**, 51-60.

Zavarin, M., Powell, B. A., Bourbin, M., Zhao, P. H., and Kersting, A. B., 2012. Np(V) and Pu(V) ion exchange and surface-mediated reduction mechanisms on montmorillonite. *Environ Sci Technol* **46**, 2692-2698.

Zavarin, M., Zhao, P. H., Dai, Z. R., and Kersting, A. B., 2014. Plutonium sorption and precipitation in the presence of goethite at 25 and 80 degrees C. *Radiochim Acta* **102**, 983-997.

Zhao, P. H., Zavarin, M., Leif, R. N., Powell, B. A., Singleton, M. J., Lindvall, R. E., and Kersting, A. B., 2011. Mobilization of actinides by dissolved organic compounds at the Nevada Test Site. *Applied Geochemistry* **26**, 308-318.

Zheng, Z. P., Tokunaga, T. K., and Wan, J. M., 2003. Influence of calcium carbonate on U(VI) sorption to soils. *Environ Sci Technol* **37**, 5603-5608.

Zirnstein, I., Arnold, T., Krawczyk-Bärsch, E., Jenk, U., Bernhard, G., and Röske, I., 2012. Eukaryotic life in biofilms formed in a uranium mine. *MicrobiologyOpen* **1**, 83-94.